

# R. T. HICKS CONSULTANTS, LTD.

901 Rio Grande Blvd NW ▲ Suite F-142 ▲ Albuquerque, NM 87104 ▲ 505.266.5004 ▲ Since 1996  
Artesia ▲ Carlsbad ▲ Durango ▲ Midland

December 29, 2016

Ms. Kristen Lynch  
Dr. Tomas Oberding  
NMOCD District 1  
1625 N. French  
Hobbs, NM 88240  
Via E-Mail

Ms. Shelly J. Tucker  
Bureau of Land Management  
620 E. Greene Street  
Carlsbad, NM 88220  
Via E-mail

RE: Corrective Action Plan MODIFICATION - Raging Bull Trionyx Release #1  
Devon Reported Release Name – Trionyx 6 Fed 5H  
Unit O, Sec 6, T25S R32E, Lea County, NM, 32 09 11.910, -103 42 47.039

Dr. Oberding, Ms. Lynch and Ms. Tucker:

On behalf of Raging Bull Oilfield Services, R.T. Hicks Consultants, Ltd. is pleased to submit Corrective Action Plan Modification to the approved plan dated October 13, 2016. This plan is a complete stand-alone document. The first section of this document presents the results of sampling associated with construction of the approved remedy. The second section describes the proposed revision to the approved remedy after discussions with OCD which includes a pilot testing program to measure soil flushing. The last section presents the final remediation plan based upon the recently-collected data.

The data demonstrate that precipitation events that occurred between the July 2016 and October sampling events caused salt flushing of such magnitude that diversion of storm water to accelerate the remedy provides no value. These data permit a conclusion that one week of relatively wet weather with one large precipitation event (e.g >1 inch) will complete the remediation of the soil horizon to a depth of 6-feet. The recent data and our conclusion are unexpected as the infrastructure to implement the storm water diversion remedy has been constructed at significant expense.

Appendix A presents the regional environmental setting of the area. In Appendix B are peer-reviewed publications relating to moisture flux under conditions similar to those proposed in the example remedy and in the remedy described in this submission.

All laboratory reports are included in Appendix C.

## Sampling Data, Evaluation and Conclusions

Figure 1 shows the sample locations plotted on a Google Earth image as well as the layout of the infrastructure for the soil flushing remedy and pilot test. As shown on Figure 1:

- S1-S4 are borings to 3-4 feet that collected soil samples the day after the release (6/18/15)
- B5-B8 are borings to 3-4 feet collected on 7/14/16
- B9-B13 are deep sampling trenches to 7-12 feet excavated during construction of the remedy on 11/3/16
- Post-construction sample locations to a depth of 2-feet

Table 1 presents all the pre-construction soil chloride data (See Figure 1). The top two sections present chloride concentrations over time at two locations (sample points S-1, BH-7, BH-10 and S-3, BH- 8, BH-11). The second middle section shows concentrations over time at location BH5/B13 with the nearby location B6 in the left column. The last two groups of rows present

data from four locations; the two locations in each row are proximal to each other as shown on Figure 1.

Location	Depth	Chloride	Date	Location	Depth	Chloride	Date	Location	Depth	Chloride	Date
S-1	0	23,600	6/18/15	BH-7	0	80	7/14/16	BH-10	1-2	432	11/3/16
S-1	1	8,400	6/18/15	BH-7	1	1,570	7/14/16				
S-1	2	4,320	6/18/15	BH-7	2	3,160	7/14/16				
S-1	3	480	6/18/15	BH-7	3	6,320	7/14/16	BH-10	4	1,220	11/3/16
								BH-10	6	104	11/3/16
								BH-10	8	32	11/3/16
S-3	0	16,400	6/18/15	BH-8	0	6,000	7/14/16				
S-3	1	9,100	6/18/15	BH-8	1	3,120	7/14/16	BH-11	1-2	736	11/3/16
S-3	2	7,300	6/18/15	BH-8	2	1,200	7/14/16				
S-3	3	1,760	6/18/15	BH-8	3	752	7/14/16	BH-11	4	1,520	11/3/16
								BH-11	8	48	11/3/16
								BH-11	10	736	11/3/16
BH-6	0	48	7/14/16	BH-5	0	288	7/14/16	BH-13	1-2	48	11/3/16
BH-6	1	64	7/14/16	BH-5	1	1,060	7/14/16	BH-13	4	7,200	11/3/16
BH-6	2	176	7/14/16	BH-5	2	3,640	7/14/16	BH-13	6	<16	11/3/16
BH-6	3	688	7/14/16	BH-5	3	4,560	7/14/16	BH-13	8	32	11/3/16
								BH-13	10	96	11/3/16
S-4	0	10,200	6/18/15					BH-9	2	1,040	11/3/16
S-4	1	8,300	6/18/15					BH-9	4	912	11/3/16
S-4	2	9,100	6/18/15					BH-9	6	64	11/3/16
S-4	3	7,300	6/18/15					BH-9	7	96	
S-4	3.5	11,800	6/18/15								
S-2	0	10,100	6/18/15					BH-12	1-2	48	11/3/16
S-2	1	9,100	6/18/15					BH-12	4	144	11/3/16
S-2	2	7,900	6/18/15					BH-12	6	32	11/3/16
S-2	3	528	6/18/15					BH-12	8	48	11/3/16
								BH-12	10	32	11/3/16
0-2	Average	10,318	6/18/15	0-2	Average	1,701	7/14/16	0-2	Average	461	11/3/16
3-4	Average	3,759	6/18/15	3-4	average	3,080	7/14/16	3-4	Average	2,199	11/3/16
								5-10	Average	132	11/3/16

Because chloride analyses can vary significantly between samples, even two samples from the same 4-oz jar, the examination of the average values on the bottom of Table 1 are most illustrative. During the period of record (June 2015 to November 2016), salt concentrations in the uppermost two feet of the sandy soil decreased by about 80% during the first 13 months of observation and 70% between July and November of 2016. In the soil horizon 3-4 feet below grade, salt concentrations declined by 20% between the first two sampling events and 30% between July and November 2016.

Figure 2 is a graphical display of precipitation data for several nearby weather stations. We chose the stations based upon the available data. Note the following observations:

1. Stations Carlsbad, Ochoa, Monument and WIPP surround the Trionyx release site
2. The 2016 dataset of Ochoa is corrupt and the 2016 WIPP data end in June.
3. All of the charts shown in Figure 2 exhibit 3 days within a 10-day period with measured precipitation of about one inch (red circles).
4. The events do not occur at the same time, which is typical of the monsoon thunderstorm events.

Our field observations and experience modelling of unsaturated flow in the Permian Basin of New Mexico allow us to conclude that relatively large precipitation events over a relatively short period will cause significant recharge and the attendant flushing of salt from sandy soil that has been denuded of vegetation by produced water releases. Examination of the CDU 292H spill

data (see forthcoming report to District 2) supports these observations and simulations regarding flushing caused by closely-spaced, large precipitation events.

### Revised Remediation Plan

Using natural precipitation and diverted storm water run-on to flush salt (measured by chloride concentration) from the soil horizon is an effective remedy that provides a higher net environmental benefit than most alternative actions if certain conditions are met. These conditions are:

1. The hydrogeologic nature of the unsaturated zone must be known with a reasonable degree of certainty and based upon field data. The hydrogeology of the area is described in Appendix A.
2. The designers of any flushing remedy must understand unsaturated flow in general and be able to apply this understanding to the specific release site. Background information relating to unsaturated flow in arid and semi-arid environments is presented in Appendix B.
3. The designers of the remedy must examine the soil horizon and the impact of the release to the soil then determine if clay minerals are present in sufficient quantity to require the use of soil amendments (e.g. agricultural gypsum).
4. The remedy designers must propose
  - a. a reasonable sampling/monitoring plan that will determine when salt flushing is sufficiently complete to allow vegetation and
  - b. a post-flushing, permanent soil cap that will significantly reduce continued salt flushing beneath the spill footprint and,
  - c. if possible, cause enhanced infiltration (recharge) of fresh water to mitigate or offset the deleterious environmental impact caused by the release

OCD requested that the Trionyx 6 Federal 5H release site and the CDU 292H undergo a pilot testing program to provide data relating to the volume of fresh water required to flush salt below the root zone in the sandy soil environment that characterizes these two site. Of particular interest is evaluation of the efficacy of the soil flushing using three different techniques

1. Natural rainfall with no addition of fresh water to accelerate flushing
2. Natural rainfall plus ponding of diverted storm water to accelerate flushing due to rainfall and
3. The importation and ponding of known volumes of fresh water to over a portion of the release footprint

Comparison of salt flushing after implementation of these remedies would provide OCD, surface owners and operators with a better understanding of salt flushing as a remedy for produced water releases. Thus, the approved plan for the Trionyx 6 Federal 5H site was revised as shown below as ~~strike-out~~ and insertions.

Under contract to Devon, Raging Bull will:

- Identify the root cause of the release
- Repair or replace the infrastructure or operational practice that caused the release

The Remediation Contractor under the direction of Hicks Consultants will has:

1. Placed d one-call for utility location-~~r~~
2. Used d the backhoe that will implement this remedy to collect samples for chloride analysis at depths of 1-2 feet, 4 feet, 6 feet and 8 feet at locations ~~S-1, S-2, S-3 and S-4~~ shown on Figure 1.
3. Tilled, loosened and disaggregated d the top 18-inches of soil within the release footprint (as outlined by Hicks Consultants representative)

4. Tilled in organic amendments (~~, such as~~ rotted hay); to increase the permeability of the soil and the thin zone of hardpan.
5. Built ~~d 8-12~~ 24 inch berms that are reinforced with silt fence, moistened and compacted in and around the release footprint in a manner that
  - a. Captures precipitation and prevents runoff on in areas identified in Figure 1 and ~~eCreates ponding within the footprint~~
  - b. Prevents overland transport of any salt or hydrocarbons from the spill footprint
  - c. Diverts storm water ~~onto the spill footprint~~ from clean areas (~~e.g.~~ lease roads) onto selected areas of the spill footprint shown in Figure 1
  - d. Used ~~s~~ only clean soil for the berms from outside of the spill footprint, thereby creating a trench or depression (if possible), which will become part of the post salt flushing remedy.
6. During the final inspection by Hicks Consultants, ~~take~~ took photographs and collect the data required to provide an as-built drawing of the remedy with relative elevations of
  - a. Nearby roads, production pads and other man-made features
  - b. At least 7 locations of the surface of the spill footprint after tilling
  - c. At least 7 locations along the top of berms
  - d. At least 5 locations within storm water diversions.
7. Provide a good estimate of the type and amount of soil amendment added to the area of the spill footprint

After the construction of the remedy Hicks Consultants will

- Provide as-built drawings and a short report to OCD (this submission)
- ~~Take~~ photographs of the site every 60-90 days and check on erosion, volunteer vegetation, overall condition of the berms and remedy
- Provide OCD with a plan to conduct a second sampling event when volunteer vegetation is observed and a third sampling event prior to final grading. The second sampling program will consist of the same number of borings at the same locations as the event described above, providing characterization to a depth of 4 feet. The final sampling event will provide characterization at the same four locations to a depth of 8-10 feet.
- When sampling and observations show that salt has moved downward out of the soil horizon (4 ft), cause a contractor to prepare the site for seeding by:
  - Moving the clean soil that comprises the berms onto the spill footprint, creating a small mound that will shed precipitation
  - Re-working the stormwater diversion such that runoff will pond in the trench or in depressions ~~that were created when the berms were built~~
- Provide photo documentation and a final C-141 when a uniform vegetative cover of at least seventy percent (70%) of pre-disturbance levels, excluding noxious weeds is observed within the spill footprint
- Install tipping-bucket data logging rain gauge at the location

As discussed in the introduction, the data no longer support the need to divert storm water to accelerate flushing or the controlled application of fresh water as a pilot-test plot to measure the rate of chloride flushing v. water application. We recommend implementing such a pilot test on a “fresh” release if additional testing of this protocol is required.

December 29, 2016

Page 5

Please contact me if you have any questions relating to this modification. Raging Bull will like to implement this remedy as soon as possible.

Sincerely,  
R.T. Hicks Consultants

A handwritten signature in black ink, appearing to read "Randall Hicks", written in a cursive style.

Randall Hicks  
Principal

Copy: Raging Bull Oilfield Services  
BLM Carlsbad



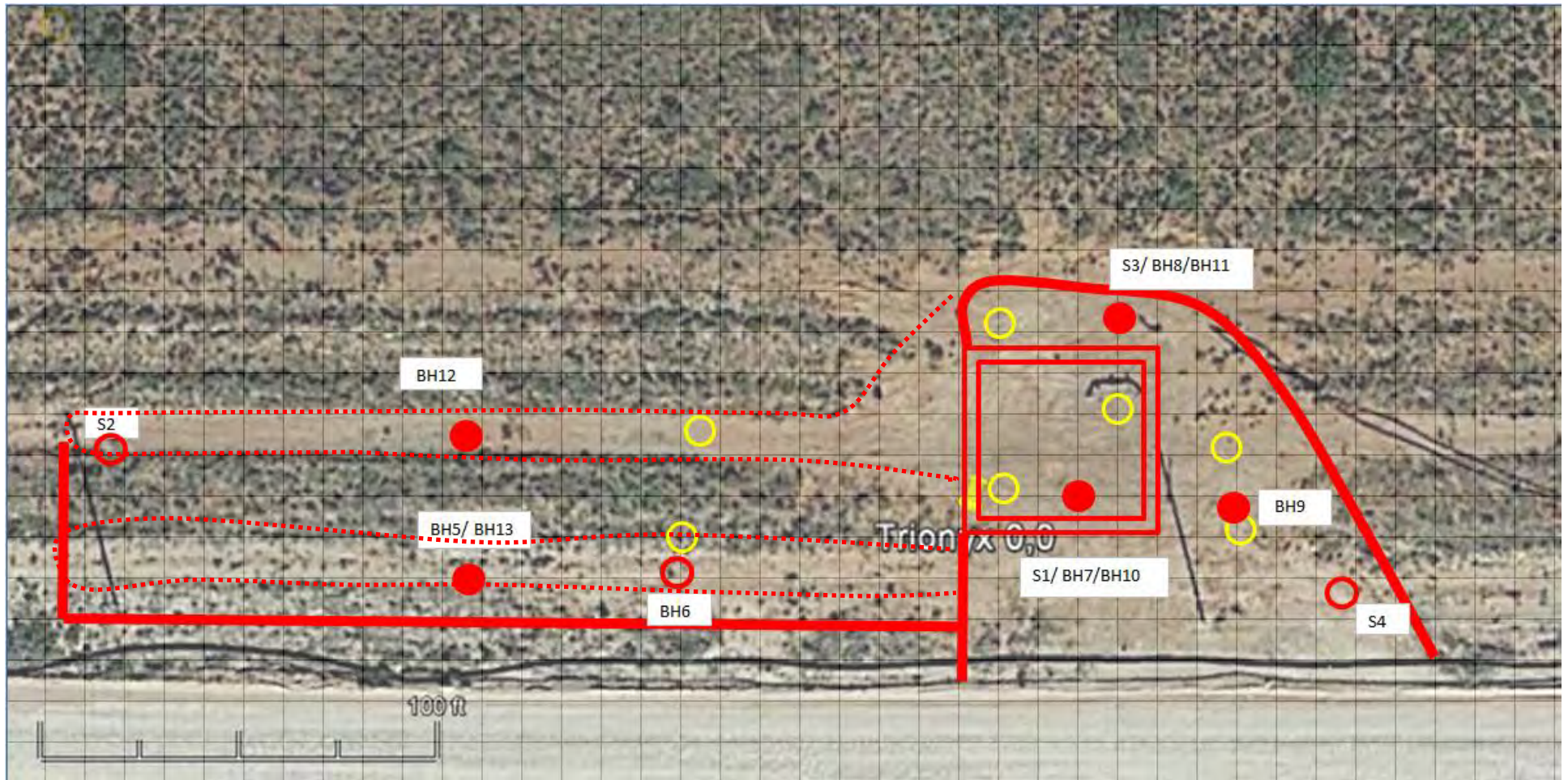




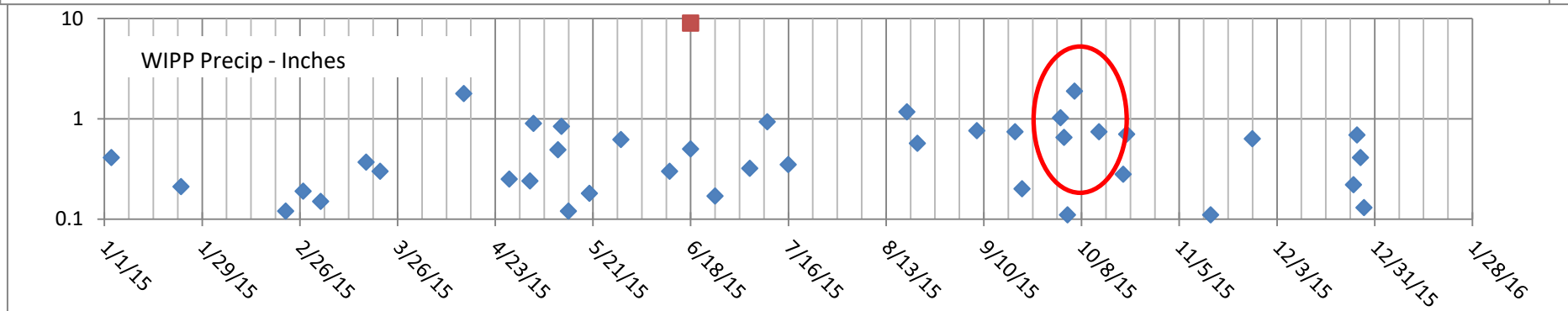
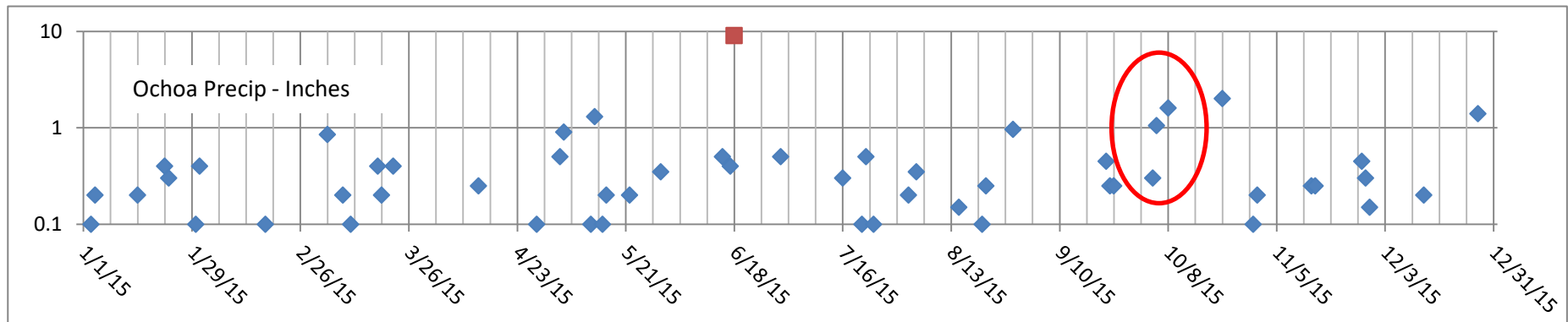
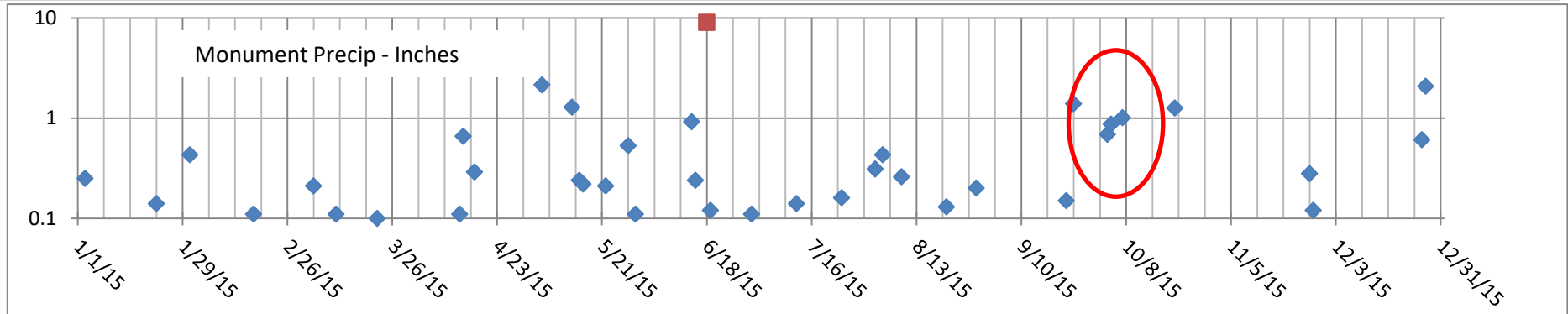
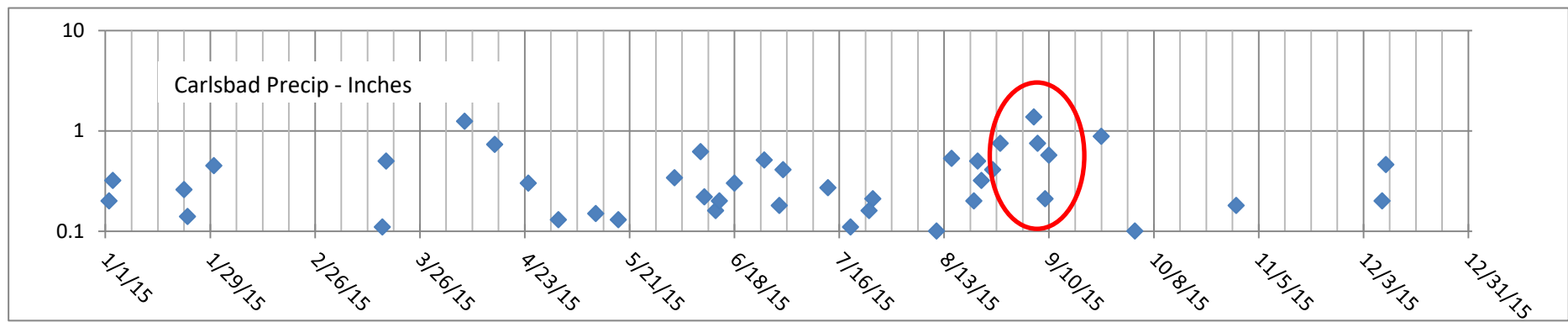


Figure 1 – Google Earth image showing the sampling locations and remedy infrastructure. Dashed red lines define the western half of spill footprint and reinforced berms define the spill footprint on the eastern half of the site.

-  Borings conducted to total depth of 4-feet. Borings S1 through S4 occurred on 6/18/15, one day after the release. Borings B-5 through B8 were installed on 7/14/16.
-  Locations B9 through B13 are sample trenches excavated to 8-12 feet on 11/3/16. These six deep sampling locations consist of three that are co-located with earlier locations and three locations to provide additional characterization.
-  Locations of post-construction soil samples to 2 feet below grade (data to be supplied when available).
-  Reinforced berms to exclude or contain storm water run on.



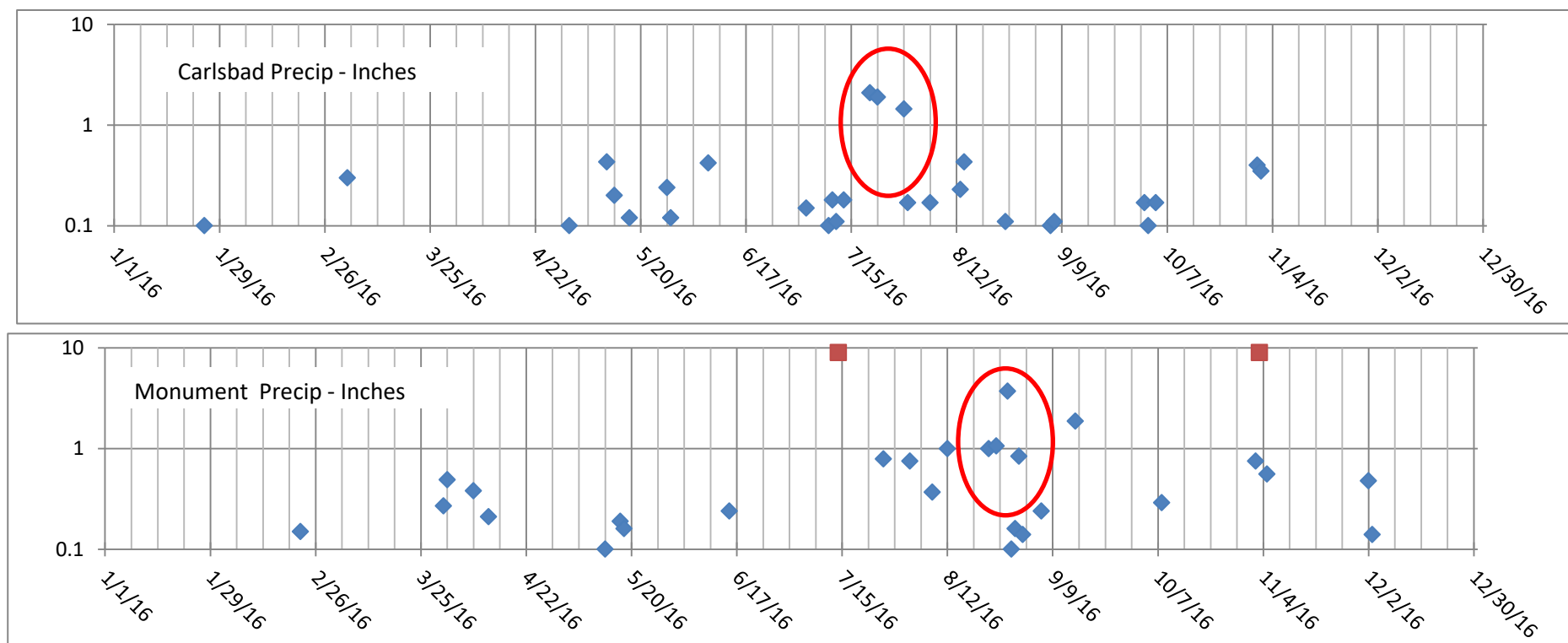


Figure 2 - Precipitation data for weather stations near release site  
Red squares at top of each chart represent sampling dates  
Red circles show multiple, large precipitation events within a 10-14 day period



## Environmental Setting

Figure 1 is a groundwater elevation map of the area and surrounding environs where Raging Bull provides services to Devon Energy wells (red rectangle). This map shows the highest groundwater potentiometric surface elevation in the service area of Raging Bull is less than 3290 feet above sea level and the lowest is about 2950 feet. Because the area spans a surface elevation of about 3350 to 3570, the depth to the groundwater surface is  $(3570-3250=)$  320 feet in the northeast and  $(3350-2950=)$  400 feet in the southwest of the Raging Bull service area.

Figure 1 also shows the locations of all known water wells in the area of Raging Bull's activities. One water well, Misc- 143 (Keyhole Windmill), exists within the area. We examined the area using Google Earth and found no evidence of other wells in the service area.

Wells outside of the service area that tap the regional aquifer were used to construct the potentiometric surface of Figure 1. Data from two shallow wells that draw from perched groundwater in the alluvium were not included. These wells (Misc- 163 and Misc-145) lie within a closed depression near the aptly named Twin Wells Ranch, shown in Figure 2 below. A wetland and surface water body are mapped adjacent to the wells and provide sufficient recharge to create the localized groundwater zone the alluvium.

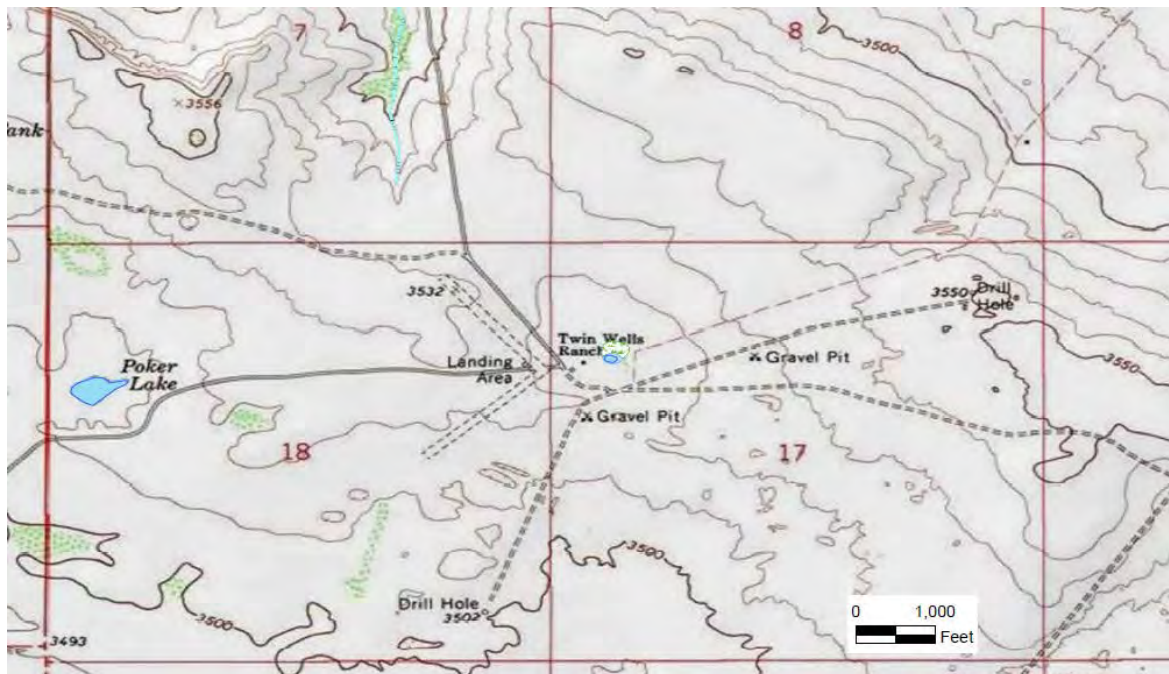


*Figure 2 – Topographic map of Twin Wells Ranch area of shallow groundwater*

Figure 3 is a map of mapped surface water and mapped wetlands in and near Raging Bull's service area. Surface water features are rare in the service area. There are no mapped watercourses and small freshwater ponds are found only in

the southern portion of the map. Unmapped watercourses in this area of stabilized sand dunes were not observed during the ground inspection. Nevertheless, a ground survey of a release site is an important step in evaluating areas of potential erosion near release sites.

We examined other environmental databases and found the area is mapped as low karst potential by the BLM and subsurface mines are not present in the area of Figure 1. However, in the center of the area is the Potash District South Island.

Releases from in the Trionyx area shown in Figure 1 cannot, with reasonable probability, impact groundwater in the reasonably foreseeable future. The 300+ foot depth to the groundwater surface is only one reason. The geology of the area is the second and more important reason.

A soil boring at the Devon Energy Trionyx Containment is, in our opinion, representative of the general area beneath the 1-4 foot veneer of dune sand. The driller's log is attached to this plan and shows

Depth	Driller's Description	Hicks Interpretation
0-20	Silty Clayey Sand with Gravel – white, very dense, carbonate indurations	Caliche
20-53 (TD)	Silty Sand – light brown to red, very dense, carbonate indurations	Dewey Lake Formation

We know that the 0-20 foot interval is caliche because we inspected nearby caliche pits and the driller's description is consistent with caliche. However, the thickness of the caliche is probably less than 20 feet and is underlain by alluvium.

The dense brown to red silty sand description is consistent with that of the Dewey Lake redbed. Although there are few bedrock exposures in the area, we believe the boring penetrated the Dewey Lake rather than the Dockum Group redbed because the basal unit of the Dockum Group, the Santa Rosa Sandstone, is exposed about 15 miles north<sup>1</sup> and in the Paduca Breaks area<sup>2</sup> which is southeast of the area shown in Figure 1. The silty sand description is not consistent with the Santa Rosa sandstone. The stratigraphy of the Santa Rosa Sandstone relative to the underlying Dewey Lake is illustrated in a cross section from another USGS study of the area<sup>3</sup> that cuts through the service area of Raging Bull (Figure 4, below). The area of Raging Bull's activity lies on the left side (south-southeast terminus) of the cross section. It shows that the Dewey Lake redbed are at/near the surface. The driller's log does not describe penetration of groundwater perched upon the redbed.

The Dewey Lake lithology is described in a USGS publication<sup>4</sup> as thin bedded siltstone with red clay comprising 15-25% of the rock as the principal cement. In

<sup>1</sup> see <https://pubs.usgs.gov/bul/1141b/report.pdf>

<sup>2</sup> see [https://nmgs.nmt.edu/publications/guidebooks/downloads/44/44\\_p0231\\_p0235.pdf](https://nmgs.nmt.edu/publications/guidebooks/downloads/44/44_p0231_p0235.pdf)

<sup>3</sup> <https://pubs.er.usgs.gov/publication/wri844077>

<sup>4</sup> <http://pubs.usgs.gov/pp/0589/report.pdf>

Raging Bull's service area shown on Figure 1, this unit does not produce groundwater and, in general, would act as a leaky aquitard over the underlying Rustler Formation, which does provide water to wells (e.g. the Keyhole Windmill). A Sandia National Laboratory report on WIPP<sup>5</sup> does state that some wells in the area of WIPP appear to draw water from the Dewey Lake redbed. There is no evidence of saturation of the Dewey Lake Formation in Raging Bull's area of service.

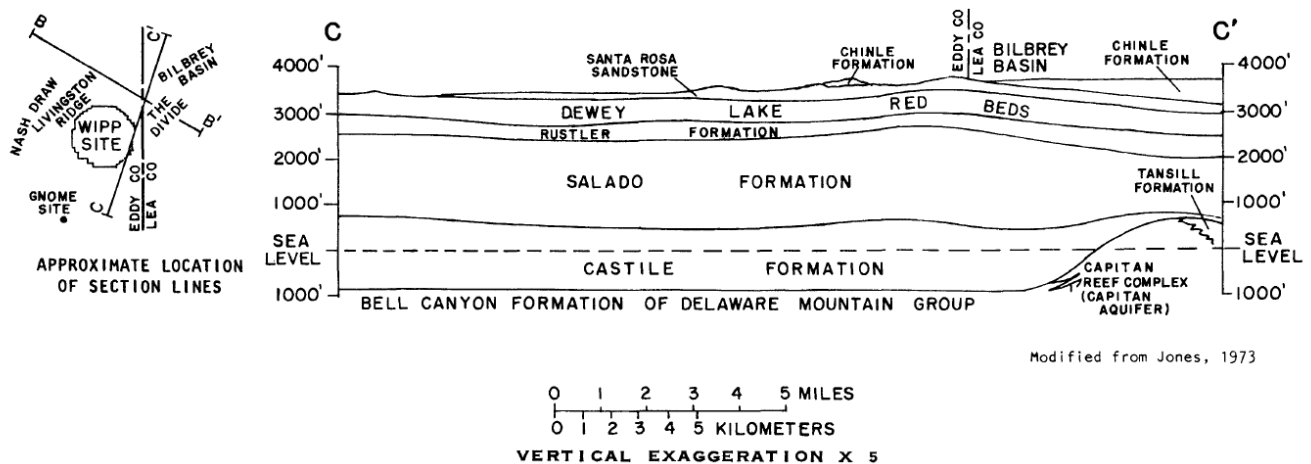


Figure 4: Stratigraphic cross section C-C' that cuts through Raging Bull's service area.

The upper Rustler Formation, which provides the water to wells in the general area, is composed of dolomite; evaporate beds and some thin sandstone. Water quality to wells can be variable but is generally acceptable for stock.

## Initial Sampling and Evaluation

Upon discovery of a release of more than 5 barrels, Hicks Consultants will

- A. Use pin flags to outline the release edges
- B. Take photographs of the release (and pin flags) with latitude/longitude georeferenced on each image:
  - a. From the point of origin looking down hill
  - b. From the end point of release looking up hill
  - c. Of the area of maximum pooling of liquid
  - d. Several additional views to help define the geometry of the release
  - e. From the highest nearby point looking over the release site
- C. Cause submission of a C-141 Form to OCD and the surface owner

Within 30 days of the initial C-141 submission, Hicks Consultants will submit the following information to support implementing a Corrective Action similar to those described later in this plan:

1. A map the release outline on Google Earth showing dimensions and an estimate of the surface area of the release
2. Photo-documentation of an inspection around the release (about 200 feet

<sup>5</sup> [www.wipp.energy.gov/library/Information\\_Repository\\_A/Supplemental\\_Information/Powers%202003b.pdf](http://www.wipp.energy.gov/library/Information_Repository_A/Supplemental_Information/Powers%202003b.pdf)

in every direction) for evidence of drainages, playa lakes or wetland vegetation

3. Field chloride titration results of samples from three-five borings
  - i. At the area of maximum pooling of liquids
  - ii. Within 20 feet of the release origin
  - iii. At 1-3 location representative of the remainder of the release
4. Each borings will collect samples from depths of
  - i. 0-12 inches
  - ii. 12-24 inches
  - iii. 36 inches (discrete sample)
5. A description of the samples for hydrocarbon staining, odor or hydrocarbon masses
6. A diagnosis of the root cause of the release with a proposed repair or improvement of the infrastructure to minimize the potential of future releases on this same footprint

### **Criteria for Closure of the Regulatory File**

Because the potential that a release will cause groundwater impairment is so small as to be nil, the Remediation Plan objectives are

- A. elimination of the root cause of the release (e.g. installation of pressure shut off switches)
- B. restoration of the soil root zone to allow for reestablishment of vegetation within the spill footprint
- C. elimination of crude or sodic clay “hard pan” that prevents moisture infiltration and impairs revegetation and
- D. establishing a surface contour and vegetation cover to minimize the potential of erosion and soil loss

Given the environmental setting of the area shown in Figure 1 and the remedial action objectives outlined above, the closure criteria for regulatory files associated with Raging Bull releases are:

- a uniform vegetative cover of at least seventy percent (70%) of pre-disturbance levels, excluding noxious weeds and
- documentation that infrastructure that should be improved to prevent future releases has been installed

### **Corrective Action #1 - Natural Restoration**

This Corrective Action Plan will be employed where the sampling described above shows

- I. The soil horizon is nearly 90-100% sand
- II. The average chloride concentration from the 0-36 inch sampling program is less than 3000 mg/kg
- III. Hydrocarbon or sodic hardpan is not present above the 36-38 inch sample and, such hardpan will not form
- IV. Implementing a mechanical remedy can create more environmental damage that allowing natural processes to restore vegetation because
  - a. the small size of the release footprint
  - b. 1-3 large precipitation events will cause restoration

- c. moving machinery to the site will damage vegetation and/or create potential erosion pathways
- d. nearby infrastructure (e.g. pipelines) could be damaged by implementation of a robust remedy and create a release.

With normal precipitation events, this natural restoration remedy should require 8-18 months from initial characterization to submission of the final C-141.

The remedy under these conditions is

1. Identify the root cause of the release
2. Repair or replace the infrastructure or operational practice that caused the release
3. Conduct a second sampling event when volunteer vegetation is observed or annually, whichever comes first. The sampling program will consist of the same number of borings at the same locations as the initial sampling, but will provide characterization to a depth of 4 feet.
4. Prepare the site for seeding using small machinery or hand techniques and broadcast seed according to the surface owner's protocols (LPC Sand/Shinnery)
5. Provide photo documentation and a final C-141 when a uniform vegetative cover of at least seventy percent (70%) of pre-disturbance levels, excluding noxious weeds is observed within the spill footprint

### **Corrective Action #2 – Tilling and Drainage/Erosion Control**

This Corrective Action Plan will be employed where the sampling described above shows

- A. The soil horizon is dominantly sand but clay is present in the samples
- B. The average chloride concentration from the 0-36 inch sampling program is greater than 3000 mg/kg or hydrocarbon/sodic hardpan is present or could form above the 36-38 inch sample
- C. Implementing a mechanical remedy will not create more environmental damage that allowing natural processes to restore vegetation

The remedy under these conditions is

1. Identify the root cause of the release
2. Repair or replace the infrastructure or operational practice that caused the release
3. Place one-call for utility location.
4. Till, loosen and disaggregate the top 18-inches of soil within the release footprint
5. If appropriate, till in organic amendments, such as rotted hay, to increase the permeability of the soil.
6. Build 4-8 inch berms in and around the release footprint in a manner that
  - a. Will capture precipitation and create ponding within the footprint
  - b. Will prevent overland transport of any salt or hydrocarbons from the spill footprint.
7. Provide photographs and as-built drawings of the remedy with elevations

- of the ground surface, berm heights and storm water diversion channels.
8. Take photographs of the site every 60-90 days and check on erosion, volunteer vegetation, overall condition of the berms and remedy
  9. Conduct a second sampling event when volunteer vegetation is observed or annually, whichever comes first. The sampling program will consist of the same number of borings at the same locations as the initial sampling, but will provide characterization to a depth of 4 feet.
  10. Prepare the site for seeding using small machinery or hand techniques and broadcast seed according to the surface owner's protocols (LPC sand/shinnery)
  11. Provide photo documentation and a final C-141 when a uniform vegetative cover of at least seventy percent (70%) of pre-disturbance levels, excluding noxious weeds is observed within the spill footprint
  12. After release by BLM and closure by OCD, remove sections of berms surrounding the spill footprint to minimize ponding of stormwater.



### **BLM Seed Mixture for LPC Sand/Shinnery Sites (LPC – Lesser Prairie Chicken)**

Holder shall seed all disturbed areas with the seed mixture listed below. The seed mixture shall be planted in the amounts specified in pounds of pure live seed (PLS)\* per acre. There shall be no primary or secondary noxious weeds in the seed mixture. Seed will be tested and the viability testing of seed shall be done in accordance with State law(s) and within nine (9) months prior to purchase. Commercial seed shall be either certified or registered seed. The seed container shall be tagged in accordance with State law(s) and available for inspection by the Authorized Officer.

Seed will be planted using a drill equipped with a depth regulator to ensure proper depth of planting where drilling is possible. The seed mixture will be evenly and uniformly planted over the disturbed area (smaller/heavier seeds have a tendency to drop the bottom of the drill and are planted first). Holder shall take appropriate measures to ensure this does not occur. Where drilling is not possible, seed will be broadcast and the area shall be raked or chained to cover the seed. When broadcasting the seed, the pounds per acre are to be doubled. Seeding shall be repeated until a satisfactory stand is established as determined by the Authorized Officer. Evaluation of growth may not be made before completion of at least one full growing season after seeding.

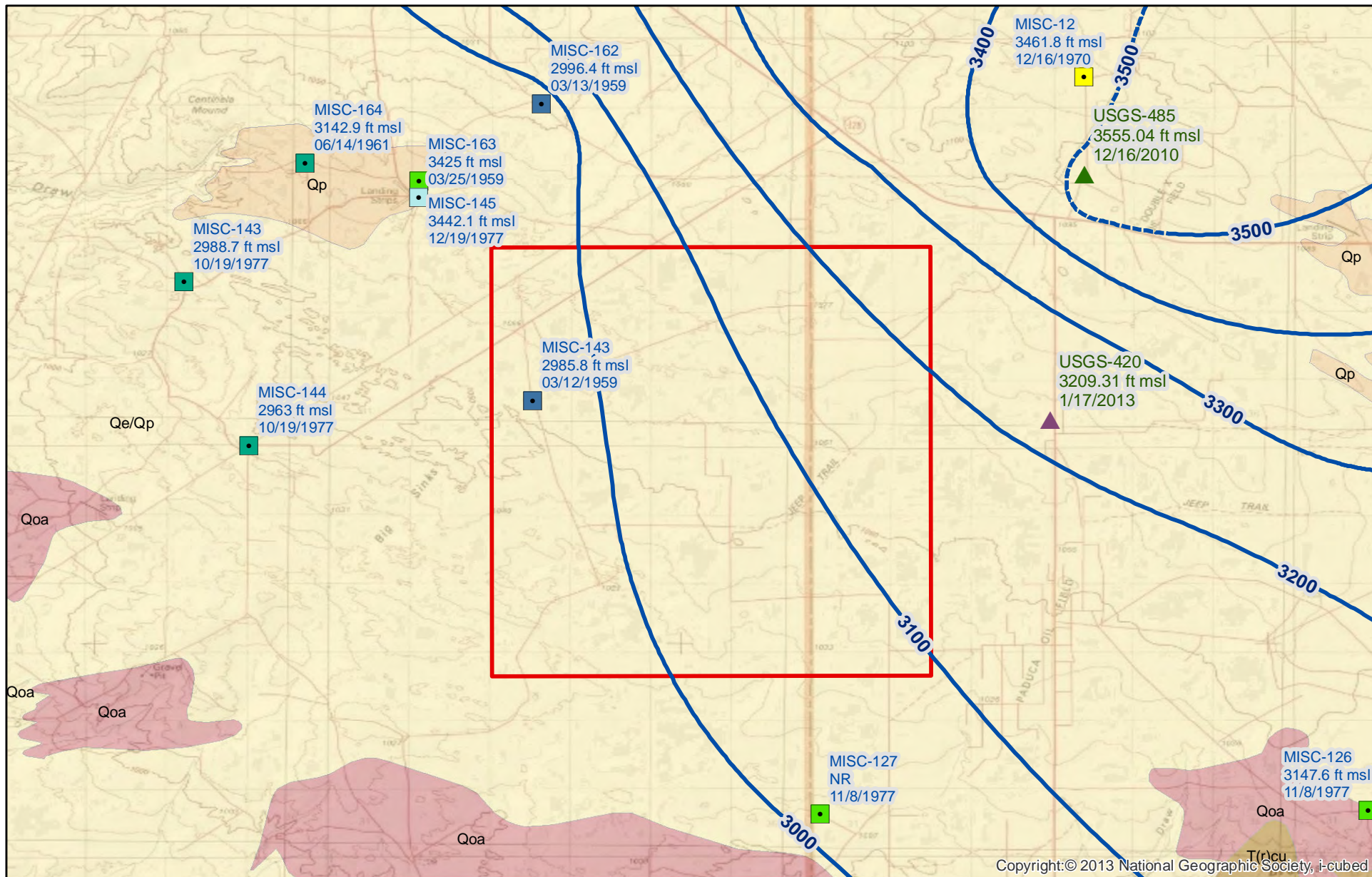
Species to be planted in pounds of pure live seed\* per acre:

Species	<u>Lbs</u> acre	Root Depth (ft)	Reference
Plains Bristlegrass	5	3.5	<a href="https://journals.uair.arizona.edu/index.php/jrm/article/viewFile/5279/4889">https://journals.uair.arizona.edu/index.php/jrm/article/viewFile/5279/4889</a>
Sand Bluestem	5	2-8	<a href="http://www.nrcs.usda.gov/.../gapmcarbigblue.pdf">www.nrcs.usda.gov/.../gapmcarbigblue.pdf</a>
Little Bluestem	3	4.5-5	<a href="http://www.fs.fed.us/database/feis/plants/graminoid/schscsco/all.html#BOTANICAL%20AND%20ECOLOGICAL%20CHARACTERISTICS">http://www.fs.fed.us/database/feis/plants/graminoid/schscsco/all.html#BOTANICAL%20AND%20ECOLOGICAL%20CHARACTERISTICS</a>
Big Bluestem	6	2-8	<a href="http://plants.usda.gov/pmpubs/pdf/gapmcarbigblue.pdf">plants.usda.gov/pmpubs/pdf/gapmcarbigblue.pdf</a>
Plains Coreopsis	2	4.7-6.5	<a href="http://www.fs.fed.us/database/feis/plants/forb/echang/all.html#BOTANICAL%20AND%20ECOLOGICAL%20CHARACTERISTICS">www.fs.fed.us/database/feis/plants/forb/echang/all.html#BOTANICAL%20AND%20ECOLOGICAL%20CHARACTERISTICS</a>
Sand Dropseed	1	8	<a href="http://plants.usda.gov/core/profile?symbol=SPCR">http://plants.usda.gov/core/profile?symbol=SPCR</a>

\*Pounds of pure live seed:

Pounds of seed x percent purity x percent germination = pounds pure live seed

(NOTE: You may substitute Plains Bristlegrass for Little Bluestem and/or Big Bluestem if needed)



Copyright:© 2013 National Geographic Society, i-cubed



0 1 2  
Miles

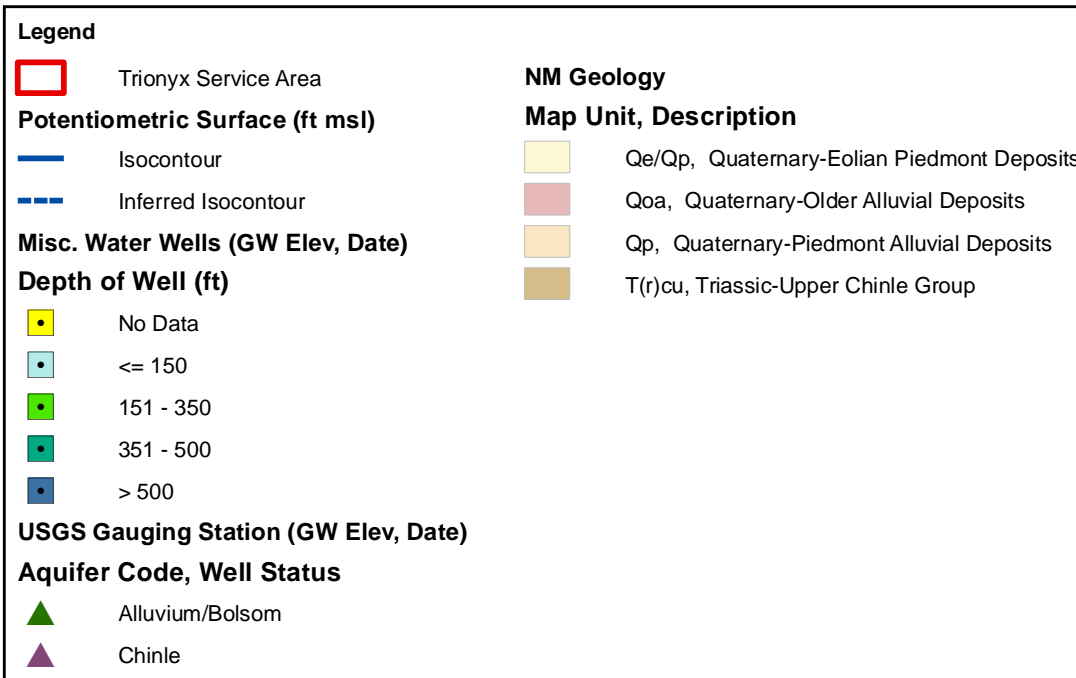
R.T. Hicks Consultants, Ltd  
901 Rio Grande Blvd NW Suite F-142  
Albuquerque, NM 87104  
Ph: 505.266.5004

Potentiometric Surface and Groundwater Elevation  
at Nearby Water Wells

Raging Bull - Trionyx Service Area

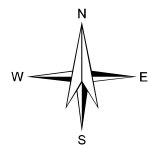
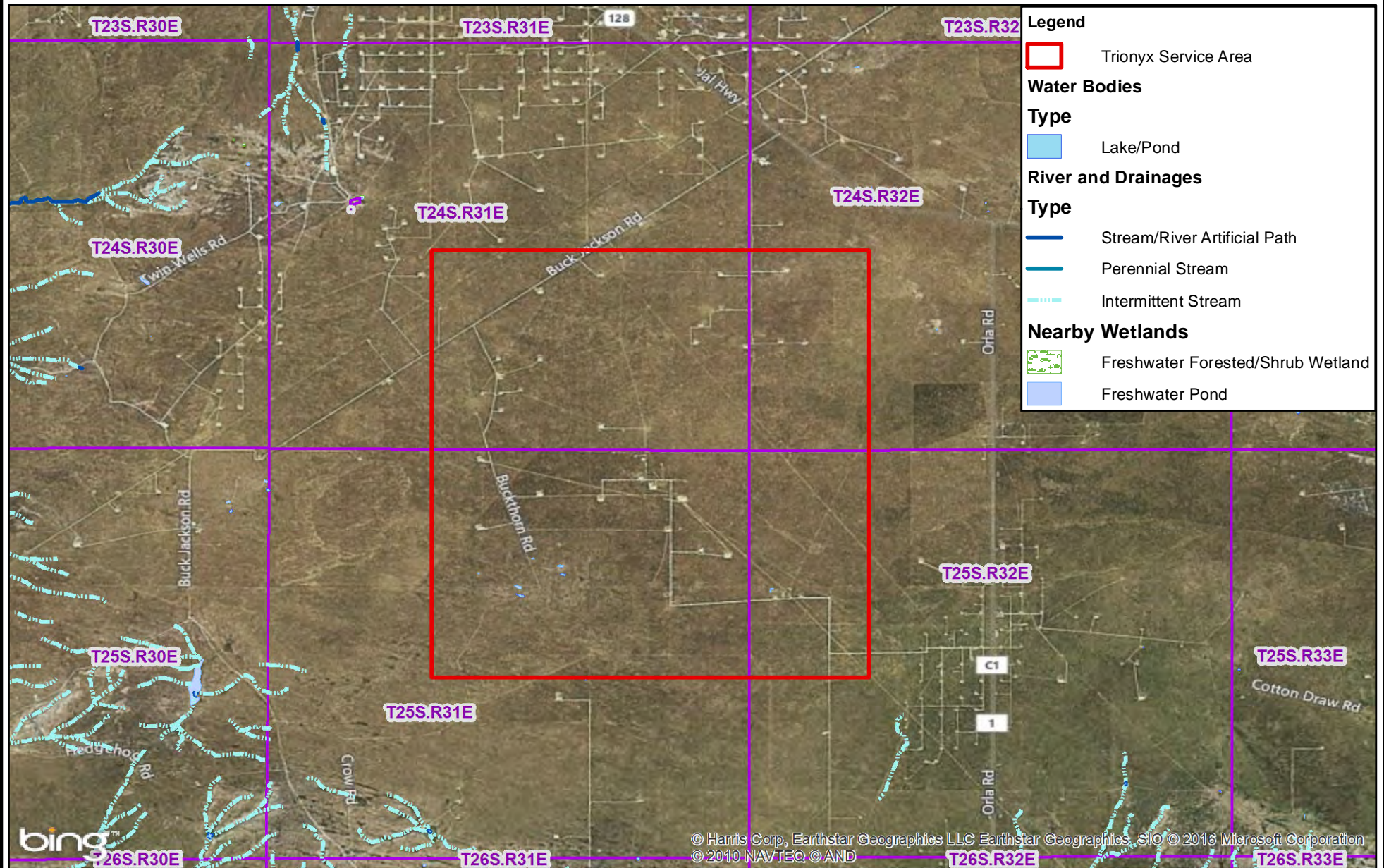
Figure 1

August  
2016



R.T. Hicks Consultants, Ltd 901 Rio Grande Blvd NW Suite F-142 Albuquerque, NM 87104 Ph: 505.266.5004	LEGEND - Potentiometric Surface and Groundwater Elevation at Nearby Water Wells	Figure 1 Legend
	Raging Bull - Trionyx Service Area	August 2016





0 1 2  
Miles

R.T. Hicks Consultants, Ltd  
901 Rio Grande Blvd NW Suite F-142  
Albuquerque, NM 87104  
Ph: 505.266.5004

Nearby Surface Water & Wetlands

Raging Bull - Trionyx Service Area

Figure 3

August  
2016



# Evaluation of Evapotranspirative Covers for Waste Containment in Arid and Semiarid Regions in the Southwestern USA

Bridget R. Scanlon,\* Robert C. Reedy, Kelley E. Keese, and Stephen F. Dwyer

## ABSTRACT

Performance evaluation of evapotranspirative (ET) covers is critical for waste containment. The purpose of this study was to evaluate ET covers at sites in Texas and New Mexico representative of arid and semiarid regions in the southwestern USA using water balance monitoring during 4- and 5-yr periods and water balance simulations using short-term (1–5 yr) and long-term (25 yr) climate forcing. Estimated drainage at the Texas site was related to irrigation while measured drainage at the New Mexico site was restricted to the first 2 yr of the 5-yr monitoring period. Evapotranspirative covers work extremely well in these regions because of the dominance of summer precipitation (62–80%) that corresponds to periods of highest ET. Strong relationships between decreases in soil water storage and vegetation productivity at both sites underscore the importance of vegetation in controlling the water balance in these systems. Simulations of the Texas site indicate that drainage can occur in response to high precipitation near the end of the growing season, but such drainage can be eliminated with a capillary barrier. Inclusion of a capillary barrier increased available water storage by a factor of about 2.5 at both sites. The capillary barrier effect of drainage lysimeters can result in underestimation of drainage and overestimation of water storage relative to covers not underlain by capillary barriers. The data from this study indicate that a 1-m-thick ET cover underlain by a capillary barrier should be adequate to minimize drainage to  $\leq 1 \text{ mm yr}^{-1}$  in these arid and semiarid regions. Comprehensive monitoring integrated with modeling is required to assess total system performance to develop a predictive understanding of ET covers.

ENGINEERED SURFACE COVERS are widely used throughout the USA to contain radioactive, hazardous, mixed, industrial, and municipal solid wastes. There are approximately 4000 active municipal solid waste and hazardous waste landfills in the USA (EPA, 1996, 1997). In addition, surface covers are commonly used alone or in combination with other remediation technologies at contaminated sites, especially those of large areal extent. The growing realization over the past decade that total cleanup of many contaminated sites is infeasible because of cost, technical difficulties, or worker safety has resulted in a shift in emphasis from contaminant removal to containment as a remediation alternative. Engineered covers may also be used as interim covers for waste containment before remediation.

Conventional engineered covers generally consist of multilayered resistive cover systems that are relatively expensive to construct and include the prescribed Re-

source Conservation and Recovery Act Subtitle C design for hazardous waste and Subtitle D design for municipal solid waste recommended by the USEPA (Koerner and Daniels, 1997). Resistive barriers rely on low hydraulic conductivity to minimize water movement into the underlying waste; however, previous studies have shown that many resistive covers, particularly compacted clay layers, leak because of desiccation, which can occur even in humid settings (Melchior, 1997; Dwyer, 2001; Albrecht and Benson, 2001; Albright et al., 2003). Increasing emphasis is being placed on optimal cover design for arid and semiarid regions because they are generally considered more suitable for waste disposal than humid regions (Reith and Thompson, 1992) and many contaminated sites are located in these regions. A variety of alternative cover designs have been proposed for waste containment in arid and semiarid regions, including monolithic ET covers, capillary barrier ET covers, and anisotropic barrier ET covers, which all rely on increased water storage rather than low hydraulic conductivity to minimize water movement into waste (Albright et al., 2003; Dwyer, 2001; Hauser et al., 2001).

Evapotranspirative covers rely on vegetation to increase the water storage capacity of the cover by removing water through ET so that deep drainage is negligible or zero. In areas where winter precipitation is dominant, the thickness of the cover is designed to store the infiltrated water until vegetation can transpire it in the spring and summer. Evapotranspirative covers generally consist of a single soil type (monolithic) and may constitute the sole barrier in a system or may form a component of more complex barrier systems that include underlying capillary or resistive barriers (Wing and Gee, 1994).

Most studies evaluating the performance of ET covers have been conducted at USDOE sites (Nyhan et al., 1990; Anderson et al., 1992; Waugh et al., 1994; Anderson, 1997; Dwyer, 2001). The Alternative Landfill Cover Demonstration project was established at Kirtland Air Force Base near Albuquerque, NM, to test four alternative cover designs (monolithic ET, capillary barrier ET, anisotropic barrier ET, and geosynthetic clay liner) relative to conventional Subtitle C and D covers (Dwyer, 2001). Long-term studies of the performance of engineered covers and comparison with the natural system were conducted at the USGS Beatty site, Nevada (Andraski, 1997). In addition, the Alternative Cover Assessment Program was established by the USEPA in 1998 to evaluate the performance of various cover designs under different climatic conditions throughout the USA (Albright et al., 2003). A total of 11 field-scale test sections were established, including conventional and alternative covers.

**Abbreviations:** AWS, available water storage; CB, capillary barrier; ET, evapotranspirative; GAB, geosynthetic clay layer overlying an asphalt barrier; GCL, geosynthetic clay liner; LAI, leaf area index; PET, potential evapotranspiration; TDR, time domain reflectometry.

B.R. Scanlon, R.C. Reedy, K.E. Keese, Jackson School of Geosciences, Bureau of Economic Geology, The University of Texas at Austin, Austin, TX 78758; S.F. Dwyer, U.S. Dep. of Energy, Sandia Natl. Lab., Albuquerque, NM 87185. Received 6 Apr. 2004. Original Research Paper. \*Corresponding author (bridget.scanlon@beg.utexas.edu).

Published in Vadose Zone Journal 4:55–71 (2005).

© Soil Science Society of America

677 S. Segoe Rd., Madison, WI 53711 USA

Monitoring approaches can be subdivided into performance and process monitoring. Performance monitoring usually focuses on a performance parameter, generally drainage in the case of engineered covers. However, natural drainage is very difficult to monitor because zero pressure (pan) lysimeters used for drainage monitoring behave like capillary barriers and require overlying soils to become almost saturated before drainage will occur. Therefore, water storage is generally overestimated and drainage underestimated relative to covers without capillary barriers. The degree to which lysimeter drainage represents actual drainage beneath a cover depends on whether the interface between the cover and the underlying waste or between the final and interim cover acts as a capillary barrier. Process monitoring includes many parameters related to flow processes in a cover and provides comprehensive information on total system performance, which is considered more robust than simply relying on a single parameter. For example, increases in water storage at the base of a cover profile could provide early warning of incipient drainage.

Numerical modeling can be used to evaluate and optimize monitoring systems, assess different cover designs, and determine critical parameters through sensitivity analyses. To increase confidence in models, it is important to compare model results with detailed field monitoring data. Many previous studies have simulated the water balance of engineered covers and compared the simulation results with the monitoring data (Fayer et al., 1992; Khire et al., 1997). A detailed evaluation of the performance of different codes for simulating the water balance of engineered covers was conducted using data from sites in Texas and Idaho (Scanlon et al., 2002). Recent advances in computer technology, more computationally efficient codes, and availability of input data on climate and hydraulic properties online make long-term simulations of the near-surface water balance much more feasible. Weather generators, such as USCLIMATE and GEM (Richardson, 2000), can be used to develop long-term climate records for simulations. Pedotransfer functions are available for estimating hydraulic parameters from information on soil texture (Schaap and Leij, 1998; Schaap et al., 1998).

The purpose of this study was to evaluate ET covers in arid and semiarid sites in Texas and New Mexico on the basis of monitoring and modeling analysis. The monitoring program provides information on performance of the covers for the duration of the monitoring (4–5 yr), whereas the modeling analysis allows us to evaluate cover performance for much longer (25 yr in this study). Unique aspects of this study include detailed instrumentation of water balance parameters at these two sites, length of monitoring record (4–5 yr), integration of monitoring and modeling analysis, and detailed knowledge of unsaturated flow processes in the natural system for comparison with the ET covers.

## MATERIALS AND METHODS

### Site Description and Cover Designs

#### Texas Site

Prototype engineered covers were installed for a proposed low-level radioactive-waste disposal site in the Chihuahuan Desert in West Texas, 10 km east of Sierra Blanca, about 150 km southeast of El Paso (31°8.773' N, 105°16.237' W; elevation, 1337 m) (Fig. 1). The potentiometric surface is at a depth of approximately 200 m. Long-term (1962–1990) mean annual precipitation is 311 mm (Sierra Blanca). Approximately 80% of precipitation occurs in June through October (Fig. 2a). Precipitation during the monitoring period was much lower in January through May (33–65%), August (47%), and September (16%) relative to the long-term (29-yr) monthly distribution. Summer precipitation generally occurs as localized convective storms with durations of a few minutes to several hours, whereas winter precipitation is generally associated with larger frontal systems of lower intensity.

Two different engineered cover designs were installed at the site in the summer of 1997: (i) a conductive or capillary barrier (CB) of sand at the 2-m depth and (ii) a resistive or geosynthetic clay layer (GCL) overlying an asphalt barrier (GAB) at the 1.3-m depth (Fig. 1). In this study, we focus on the upper portion of both covers above the barriers because water movement was generally restricted to these zones and, both covers functioned primarily as ET covers. Each cover design was 17 by 34 m (CBET, GABET) and was divided into two 17- by 17-m subplots. Both cover designs consisted of 0.3 m of topsoil (sandy clay loam, bulk density 1.5 Mg m<sup>-3</sup>)

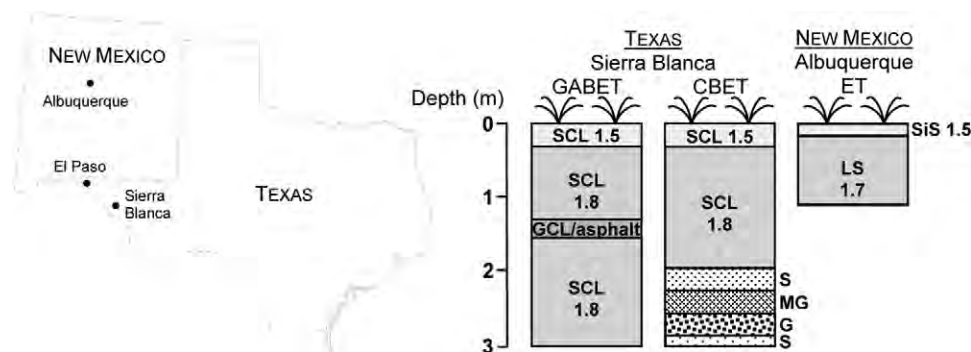


Fig. 1. Location of monitored and engineered cover sites in Texas (Sierra Blanca) and New Mexico (Albuquerque) and vertical profiles of texture and materials for the different cover designs evaluated in the study. GCL, geosynthetic clay liner; GABET, GCL/asphalt barrier ET cover; CBET, capillary barrier ET cover; SCL, sandy clay loam; S, sand; MG, muddy gravel; G, gravel; LS, loamy sand. Numbers following textures indicate soil bulk density (Mg m<sup>-3</sup>). Texas site consisted of topsoil mixed with gravel (24 wt%); New Mexico site includes a 20- to 40-mm-thick gravel surface layer.



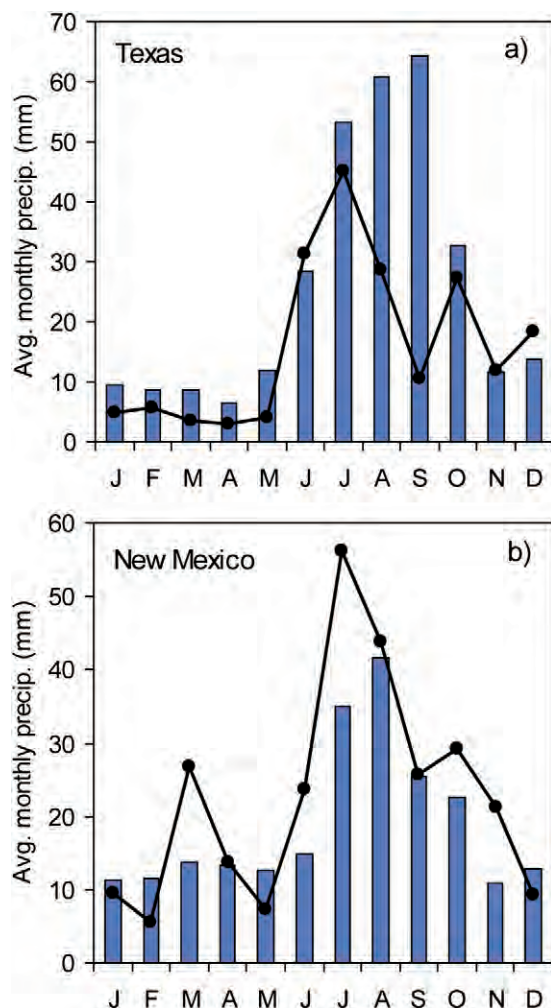


Fig. 2. Average monthly precipitation during monitoring periods (lines) and historical records (columns) for (a) Texas site (Sierra Blanca, 29-yr average annual total = 311 mm) and (b) New Mexico site (Albuquerque, 30-yr average annual total = 226 mm).

underlain by compacted soil (sandy clay loam, bulk density  $1.8 \text{ Mg m}^{-3}$ ) constructed with a 2% surface slope in all layers. Gravel (24% by weight) was added to the upper 0.3 m of the topsoil to reduce erosion.

Both covers were nonvegetated during the first year. Seedlings transplanted in August 1998 consisted of five perennial warm-season bunchgrass species, including blue grama (*Bouteloua gracilis*), plains bristlegrass (*Setaria leucopila*), sand dropseed (*Sporobolus cryptandrus*), green sprangletop (*Lepachloa dubia*), and lehmann lovegrass (*Eragrostis lehmanniana*). However, opportunistic vegetation invaded the covers at different times, including tumbleweed (russian thistle; *Salsola kali*), several salt cedar (*Tamarix ramosissima*), and one mesquite tree (*Prosopis glandulosa*). A drip irrigation system and mulch pad (20-mm-thick aspen shavings with a UV degradable mesh net) were installed before planting. The mulch pad generally degraded within 1 yr.

#### New Mexico Site

A monolithic ET cover was installed as part of the Alternative Landfill Cover Demonstration project established at Kirtland Air Force Base near Albuquerque, NM ( $34^{\circ}58.473' \text{ N}$ ,  $106^{\circ}32.396' \text{ W}$ ; elevation, 1652 m) (Dwyer, 2003). Long-term (30-yr) mean annual precipitation is 226 mm, which is based

on data from Albuquerque, 11 km northwest of the engineered covers. Approximately 62% of precipitation occurs in June through October (Fig. 2b). Monthly precipitation during the monitoring period differed from the long-term monthly distribution, particularly in March (196%), June (159%), July (161%), and November (196%) (Fig. 2b).

The ET cover was constructed between May and August 1996, and monitoring began in May 1997. The ET cover was divided into two 12.2- by 46-m subplots with east and west slope aspects. The engineered cover design consisted of 0.15 m of topsoil (loamy sand, bulk density  $1.5 \text{ Mg m}^{-3}$ ) underlain by 0.92 m of compacted soil (loamy sand, bulk density  $1.7 \text{ Mg m}^{-3}$ ) constructed with a 5% surface slope in all layers. A thin veneer of gravel (20–40 mm) was placed on the surface after the cover was seeded to enhance establishment of vegetation and minimize erosion (Reith and Thompson, 1992).

The test facility topsoil was drill seeded in fall 1996 with native rangeland vegetation that included various grasses ranging from cool-season, such as Indian ricegrass (*Oryzopsis hymenoides*) and needle-and-thread grass (*Stipa comata*), to warm-season grasses, including blue grama, galleta (*Hilaria jamesii*), and sand dropseed varieties. In addition, various opportunistic plants grew at different times, including russian thistle and fourwing saltbush (*Atriplex canescens*).

#### Monitoring Systems

Performance of the ET covers was evaluated by monitoring various components of the water balance:

$$ET = P + Irr - R_o - \Delta S - D \quad [1]$$

where  $P$  is precipitation,  $Irr$  is irrigation,  $R_o$  is runoff,  $\Delta S$  is change in soil water storage, and  $D$  is drainage. Various instruments and measurement systems were used to monitor all of the water balance parameters except ET, which was calculated by difference. Meteorological parameters monitored at both sites included precipitation, solar radiation, air temperature, relative humidity, and wind speed and direction.

#### Texas Site Monitoring Systems

The covers were irrigated in August and September 1998 to establish vegetation. Vegetation was removed in June 2001 from one of the CBET subplots using herbicide. The CBET subplots were also irrigated in late June through early August 2001. Vegetation coverage was evaluated by making notes during each site visit (approximately monthly) and by photographing the vegetation. In addition, relative variations in leaf area index (LAI, one sided green leaf area per unit ground area) were estimated from surveyed transects at selected times from October 2000 through September 2001 using an AccuPar Ceptometer (Model PAR-80, Decagon Devices, Inc., Pullman, WA).

Surface runoff was collected in trench drains at the base of each subplot and measured to  $\pm 0.004$  to  $\pm 0.06$  mm for runoff events  $\leq 2$  and  $\leq 400$  mm, respectively. Deep drainage was collected by 12- by 12-m pan lysimeters (1.5-mm [60-mil] very flexible polyethylene geomembrane) buried at a depth of 3 m and centered beneath the subplots. Lateral drainage was collected from two 15- by 15-m areas of the asphalt layer. All drainage was collected in subsurface drains located along the down-slope lysimeter edges and measured with infrared drop sensors, tipping bucket rain gauges, and a graduated cylinder in 114-L collection drums. Cumulative measurement errors per event were  $\leq 0.5\%$ .

Soil water storage was monitored on a monthly basis using a neutron probe (Model 503DR Hydroprobe, CPN, Martinez,

CA) at 0.15-m depth intervals in 20 vertical neutron probe access tubes (51-mm i.d. PVC) installed in June 1998. Water content in the upper 0.15 m was calculated using an empirical correction factor to adjust for the loss of neutrons at the soil surface (Greacen et al., 1981, after Grant, 1975). The neutron probe was calibrated with water content data from core samples ( $r^2 = 0.96$ ;  $\sigma = 0.011 \text{ m}^3 \text{ m}^{-3}$ ). Water content before June 1998 was estimated for the upper 0.3 m from matric potential measurements using heat dissipation sensors and laboratory-measured water retention functions. Electromagnetic induction was also used to monitor water storage (Reedy and Scanlon, 2003) but is not discussed in this paper.

Heat dissipation sensors (model 229, Campbell Scientific Inc., Logan, UT) were installed during site construction to monitor matric potentials that can be used to determine flow direction. These instruments were calibrated individually using pressure plate extractors ( $-0.1$  to  $-50$  m) and by equilibrating the sensors over saturated salt solutions ( $-450$  to  $-2500$  m). Temperature corrections were applied according to procedures outlined in Flint et al. (2002).

A cylindrical instrument silo (3.7-m diameter, 6.1 m high) constructed of welded steel panels was installed in the center of the installation to house data loggers and computers. Eight PVC instrument trees (0.3-m diameter) were installed 12 m from the silo to accommodate heat dissipation sensor installation. A 0.6-m-diameter, 10-mm-thick disk-shaped baffle was installed 0.45 m below the ground surface to inhibit preferential flow along the perimeter of the instrument trees. Instrument cable bundles passed through watertight fittings in the walls of the instrument trees at selected depths and were connected to data loggers in the silo. Instruments were installed in the soil during site construction at 1.0- to 1.5-m offset distances from the trees.

### New Mexico Site Monitoring Systems

The west subplot was irrigated in January and February 2002. Vegetation parameters, including plant cover percentage and species count, were measured approximately annually (fall 1997 through 2000 and spring 1998) using point frames (Dwyer, 2003). Surface runoff was collected in a gutter system located along the base of each subplot slope and routed through pipes to tanks with flow meters that quantified runoff with cumulative errors per event  $\leq 0.2\%$ . Deep drainage was measured using pan lysimeters that consisted of a geotextile underlain by a geonet, and then a geomembrane and water was routed to an underdrain collection system that included tipping buckets and measured with cumulative errors per event  $\leq 0.2\%$ .

Changes in water storage were monitored using time domain reflectometry (0.3 m long, three-wire probes; Campbell Scientific Inc. Model 610). Vertical profiles of time domain reflectometry (TDR) probes were installed in 10 locations equally spaced along the center of the plot. Time domain reflectometry probes were installed horizontally at the 0.15-m depth (base of topsoil) and 0.45- and 0.9-m depths within the compacted soil. Water content monitoring with TDR began in May 1997 and continued through September 2002.

### Numerical Modeling

The computer code UNSAT-H (Fayer, 2000) was used to simulate water balance of the engineered covers. In this study, we conducted short-term simulations (1–5 yr) of the covers at both sites for comparison with measured water balance parameters. We also conducted long-term simulations on the basis of meteorological data from 1961 through 1990, which were obtained from the GEM database for El Paso and Albu-

**Table 1. Model input parameter values.<sup>†</sup>**

Layer	Z	G, S, Si, C	$K_s$	$\theta_s$	$\theta_r$	$\alpha$	$n$
	m	— wt % —	$\text{mm d}^{-1}$	$\text{m}^3 \text{ m}^{-3}$	$\text{m}^3 \text{ m}^{-3}$	$\text{mm}^{-1}$	
<b>Texas</b>							
1	0.30	24, 43, 17, 16	410	0.45	0.00	0.0027	1.276
2	1.7	0, 55, 18, 27	199	0.35	0.00	0.0010	1.167
3	0.30	0, 89, 3, 8	6390	0.40	0.00	0.0020	1.464
<b>New Mexico</b>							
1	0.15	0, 83, 10, 7	873	0.40	0.00	0.0035	1.378
2	0.90	0, 83, 10, 7	38	0.36	0.00	0.0020	1.280
3	0.10	100, 0, 0, 0	302, 400	0.42	0.00	49.30	2.190

<sup>†</sup> Z, layer thickness; G, gravel; S, sand; Si, silt; C, clay; wt%, weight percent;  $K_s$ , saturated hydraulic conductivity;  $\theta_s$ , saturated water content;  $\theta_r$ , residual water content;  $\alpha$  and  $n$ , van Genuchten water retention function parameters.

querque (Hanson et al., 1994). Model results are reported for the last 25 yr of the 30 yr simulated to avoid the impact of initial conditions; therefore, these simulations are termed 25-yr simulations. Nodal spacing ranged from 2 mm at the top and base of the profile and increased by a factor of 1.2 to a maximum of 150 mm within the profile. This grid design resulted in negligible mass balance errors (two to three orders of magnitude less than simulated drainage).

The upper boundary for UNSAT-H was based on meteorological forcing and included daily precipitation, minimum and maximum air temperature, dew-point temperature, solar radiation, average wind speed, and average cloud cover. Daily precipitation was input to the simulations, and actual intensities were approximated by a default value of  $10 \text{ mm h}^{-1}$  (Fayer, 2000). Examination of the precipitation records during the monitoring period indicates that this intensity generally represents the median intensity of the precipitation. Plant transpiration is simulated as a sink term in UNSAT-H (Fayer, 2000). The lower boundary was simulated as a seepage face by including a 0.1-m-thick gravel layer at the base of the profile (Scanlon et al., 2002). A seepage face approximates the capillary barrier present beneath the ET cover at the Texas site and approximates the capillary barrier effect of the pan lysimeter at the base of the New Mexico cover. In additional simulations, a unit gradient lower boundary condition was used that allows free drainage at the base. Vegetation was represented using ecosystem LAI where measured transects included vegetated and bare areas, and percentage bare area was set to zero in the model. The growing season was based on visual observations of plant growth and water content and matric potential data over the monitoring period. Maximum root depths were not measured at either site, and estimates used in the models were evaluated using sensitivity analyses. Root length densities for bunchgrass were used (Rockhold et al., 1995).

### Texas Site Model Input

Most input data for the Texas site are described in Scanlon et al. (2002). Simulations were conducted of the upper 1.1 m for comparison with the New Mexico profile and of the upper 2 m to represent the CBET system. Hydraulic parameters used in the model are described in Scanlon et al. (2002) and given in Table 1. In this study, simulations were conducted through the vegetated cover for water year 2000 (October 1999–September 2000; WY00) that is generally representative of long-term conditions and provided guidance on vegetation parameters for the 25-yr simulations (Table 2). Drying that occurred in WY99 was not considered representative of long-term conditions.

Long-term (25-yr) simulations were also conducted. The short-term (1-yr) and long-term (25-yr) models were identical

**Table 2. Water balance monitoring results (mm) for the GCL/Asphalt evapotranspirative system (GABET) and capillary barrier evapotranspirative (CBET) systems and simulation results for the CBET system at the Texas site.<sup>†</sup>**

Cover	Water year	$P$	PET	Irr	$R_o$	Net $I$	0–1.1 m depth					0–2.0 m depth				
							$D$	$\Delta S$	ET	$S$	RMSE	$D$	$\Delta S$	ET	$S$	RMSE
							mm					mm				
GABET (measured)	1998	202	1644	221	56	367	0.0	59	308	246						
	1999	247	1588	0	5.5	241	0.0	−75	317	171						
	2000	130	1484	0	9.3	121	0.0	−8.7	129	163						
	2001	199	1346	0	12	187	0.0	−4.6	191	158						
	98–01	778	6062	221	83	916	0.0	−29	945	738						
CBET (measured)	1998	202	1644	226	60	368	0.9	59	309	246		0.0	61	307	448	
	1999	247	1588	0	5.7	241	0.8	−71	311	174		0.0	−73	314	374	
	2000	130	1484	0	8.2	122	0.0	−9.5	131	164		0.0	−13	135	361	
	2001	199	1346	2340	1866	673	5.0	34	630	198		0.0	43	631	404	
	98–01	778	6062	2566	1940	1404	6.7	12.5	1381	782		0.0	18	1387	1587	
SF‡	2000	130	1484	0	8.1	122	0.0	−8.5	130	165	8.4	0.0	−15	136	357	8.6
UG‡				0	8.1	122	0.2	−8.6	130	165	7.5	2.4	−17	136	359	8.6

<sup>†</sup> *P*, precipitation; PET, potential evapotranspiration; Irr, irrigation; *R<sub>o</sub>*, runoff; net *I*, net infiltration; *D*, drainage;  $\Delta S$ , water storage change; ET, evapotranspiration; *S*, water storage at end of water year; RMSE, root mean square error between simulated and measured (monthly) water storage.

<sup>‡</sup> Simulation results for SF, seepage face lower boundary for CBET; and UG, unit gradient lower boundary for CBET.

with the exception of meteorological forcing and a slight increase in ecosystem level LAI from 0.1 to 0.15 because WY00 was a dry year. The long-term simulations were based on daily meteorological data (1961–1990) from El Paso rather than Sierra Blanca because Sierra Blanca had only precipitation data and El Paso included all required meteorological parameters. During the 4-yr monitoring period (1997–2001), precipitation at El Paso was  $\pm 25\%$  of annual precipitation at Sierra Blanca and averaged within 5% during the 4 yr. The long-term monthly distributions of precipitation in El Paso and Sierra Blanca are also similar. Initial conditions for the 25-yr simulations were based on linear interpolation of water content on 1 Oct. 1999, which generally represents average conditions for the cover during the monitoring period.

### New Mexico Site Model Input

Input data for the New Mexico site are described in Dwyer (2003). Simulations were conducted for 1997 through 2002 for comparison with the measured water balance. Meteorological data for the simulations were based on daily values from the onsite meteorological station. Water retention was measured on disturbed soil samples using hanging water columns and pressure plates. The van Genuchten water retention function was fitted to the laboratory-measured water retention data (Table 1). Saturated hydraulic conductivity of the different materials was measured in the laboratory on disturbed soil samples collected from a borrow pit in the field (Dwyer, 2003). The samples (100-mm diam, 120-mm height) were recompact to bulk densities ranging from 1.5 to 1.7 Mg m<sup>–3</sup>. A falling head approach was used with a compaction mold permeameter (ASTM D5856, ASTM, 1995). Initial conditions for the simulations were based on linear interpolation of water contents monitored by TDR on 1 Oct. 1997 converted to matric potentials using water retention functions for the different materials. Long-term (25-yr) simulations were based on the monitoring period and used daily meteorological data from Albuquerque (1961–1990).

## RESULTS AND DISCUSSION

### Texas Site Monitoring

#### Precipitation, Irrigation, and Runoff

The 4-yr monitoring period was generally not representative, and precipitation ranged from 42% (WY00)

to 79% (WY99) of the long-term (29-yr) average precipitation at Sierra Blanca (311 mm yr<sup>–1</sup>) (Fig. 3, Table 2). Irrigation in August and September 1998 (221–226 mm) combined with precipitation in that year represented 140% of the long-term average precipitation. Both CBET subplots were also irrigated in summer 2001. A total of 459 mm of water was applied from 18 June through 8 Aug. 2001. Malfunction of the irrigation system in the vegetated CBET subplot resulted in continuous irrigation (1881 mm) during 9 through 11 August.

Total annual runoff ranged from 6 to 1866 mm yr<sup>–1</sup>, which represented 2 to 73% of annual precipitation + irrigation for WY98 through WY01 (Fig. 3, Table 2). Runoff was highest (1866 mm) in the CBET subplot that was irrigated with 2340 mm of water in summer 2001. Runoff was also high during WY98 (13–14% of *P* + Irr) because the covers were irrigated and not vegetated. Runoff during the remaining years (WY99 and WY00) ranged from 2 to 7% of precipitation.

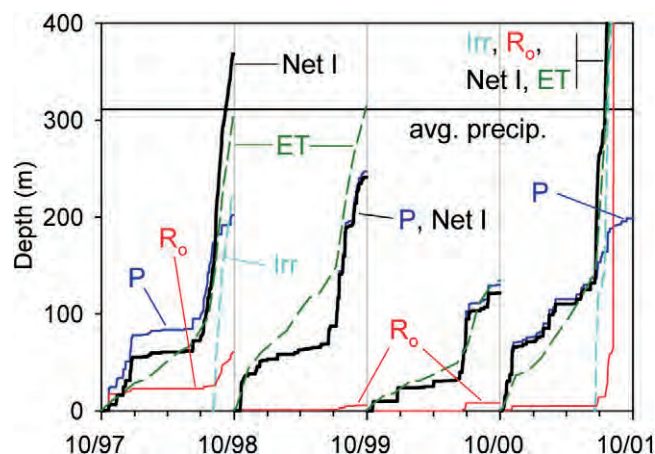


**Fig. 3.** Measured cumulative precipitation (*P*), irrigation (Irr), runoff (*R<sub>o</sub>*), and net infiltration (Net *I* = *P* + Irr – *R<sub>o</sub>*) and calculated cumulative ET for the CBET cover system for 1998 through 2001 water years at the Texas site. The long-term (1962–1990) average annual precipitation of 311 mm is shown ( $\pm 102$  mm 1 $\sigma$ ). Water year 2001 cumulative values are Irr: 2340 mm, *R<sub>o</sub>*: 1866 mm, net *I*: 673 mm, and ET: 630 mm.



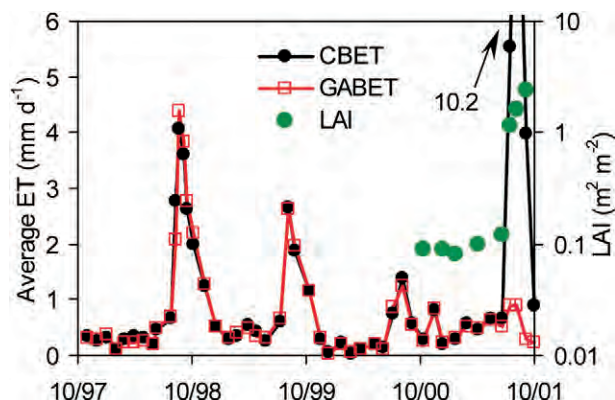


Fig. 4. Daily ET rates to the 1.1-m depth calculated from monthly average values for the GABET and CBET systems and measured leaf area index (LAI) for the CBET system at the Texas site.

### Evapotranspiration, Water Storage, and Matric Potential

The main components of the monitored water budget were ET and water storage change. Cumulative ET was less than net infiltration ( $P + Irr - R_o$ ) of water to the system in WY98 when the subplots were irrigated to establish vegetation (Fig. 3). During the following year cumulative ET exceeded net infiltration as the cover dried out. Potential evapotranspiration (PET) exceeded actual ET by factors ranging from 5 (WY 98, WY 99) to 11 (WY 00). Average daily ET rates for approximately monthly periods between water content monitoring were initially generally uniform (0.2–0.6 mm d<sup>-1</sup>; Oct. 1997–Aug. 1998) when the covers were nonvegetated and peaked ( $\leq 4.4$  mm d<sup>-1</sup>) after irrigation in September 1998 (Fig. 4). High ET rates during and after irrigation are attributed primarily to evaporation with limited transpiration from opportunistic weeds that grew on the cover. Evapotranspiration rates decreased during the 1998–1999 winter to values of 0.1 to 0.4 mm d<sup>-1</sup> and increased again in summer 1999 ( $\leq 2.6$  mm d<sup>-1</sup>), corresponding to expansion of tumbleweed growth. Highest ET rates ( $\leq 10.2$  mm d<sup>-1</sup>) were recorded in summer 2001 after irrigation of the CBET subplots. Periods of high ET generally corresponded to periods of increased water availability and vegetation productivity (Fig. 4, 5). Ecosystem level LAI measurements were low ( $\approx 0.1$  m<sup>2</sup> m<sup>-2</sup>) from Octo-

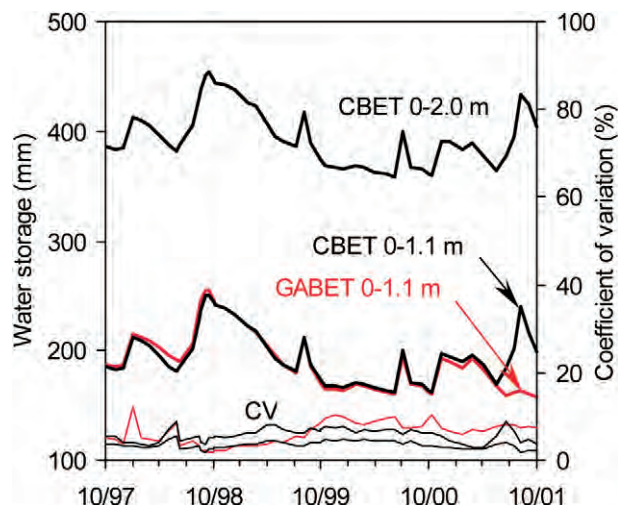


Fig. 6. Average water storage (thick lines) to the 1.1-m depth in the GABET and CBET systems and to the 2.0-m depth in the CBET system at the Texas site. Thin lines represent the coefficient of variation ( $CV = 100 \sigma/\mu$ ) of water storage from 10 neutron probe access tube measurement locations in each design.

ber 2000 through June 2001 and increased to a maximum value of 2.4 m<sup>2</sup> m<sup>-2</sup> after irrigation in summer 2001.

The importance of vegetation in controlling water balance is shown by strong relationships between vegetation productivity and soil water storage changes (Fig. 4, 6). Temporal patterns of water storage are similar for the different depth intervals considered, 0 to 1.1 m for the CBET and GABET and 0 to 2 m for the CBET. Water storage was highest after irrigation in September 1998. The large decrease in water storage from October 1998 through June 1999 can be attributed primarily to evaporation and limited transpiration related to weeds and grasses. Sharp increases in water storage (24–40 mm) during July 1999 and 2000 in response to summer monsoon precipitation were reduced rapidly in 1 to 2 mo as a result of increased ET (Fig. 4, 6). Large increases in tumbleweed occurred after high precipitation in July 1999. Monsoonal precipitation results in desert blooms as vegetation quickly responds to increased water availability. In contrast to rapid decreases in water storage in the summer, water storage in winter (e.g., October–November 2000) remained high



Fig. 5. Texas site vegetation response to (a) natural summer precipitation (Aug. 2000) and (b) irrigation (Aug. 2001).

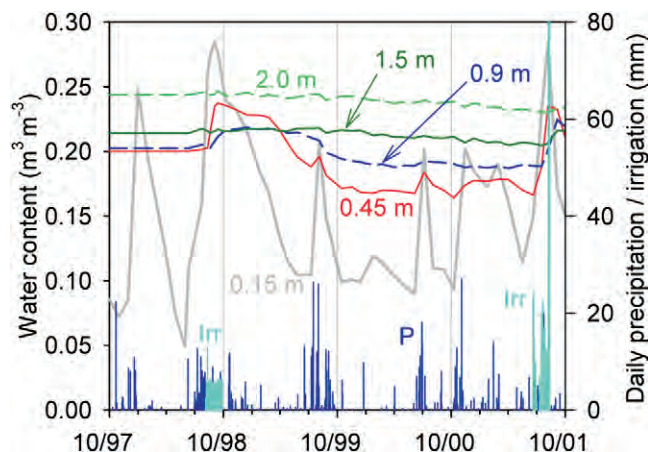


Fig. 7. Average water content based on data from 10 neutron probe access tubes at selected depths in the CBET system and daily precipitation and irrigation at the Texas site.

for several months when vegetation was dormant because evaporation was insufficient to remove the infiltrated water. Water storage was reduced in the following spring 2001 when vegetation began actively transpiring. The opportunistic response of vegetation to soil water storage is shown by the large increase in vegetation after irrigation of 422 mm (July and August 2001) and resulted in monthly ET values of 144 to 214 mm, which equaled PET in July and exceeded PET by a factor of 2 in August 2001.

Measured water content was highly variable with time at different depths in the CBET system (Fig. 7); similar patterns were seen in the GABET system (data not shown). Temporal variability in water content was greatest near the surface (0.15-m depth) and decreased with depth. Water content ranged from  $0.05 \text{ m}^3 \text{ m}^{-3}$  (May 1998) to a maximum value of  $0.28 \text{ m}^3 \text{ m}^{-3}$  (September 1998) after the plot had been irrigated to establish vegetation. Minimum water content during the remaining time was about  $0.1 \text{ m}^3 \text{ m}^{-3}$  and increased in July and August 1999 and 2000 to a maximum value of  $0.2 \text{ m}^3 \text{ m}^{-3}$ . Progressively smaller water content changes occurred with increasing depth ( $0.23 \text{ m}^3 \text{ m}^{-3}$ , 0.15 m;  $0.08 \text{ m}^3 \text{ m}^{-3}$ , 0.45 m;  $0.03 \text{ m}^3 \text{ m}^{-3}$ , 0.9 m;  $0.02 \text{ m}^3 \text{ m}^{-3}$ , 1.5 m). Increases in average water content following the 1998 irrigation penetrated to depths between 0.9 and 1.5 m, whereas the 2001 irrigation penetrated to the 1.5-m depth. Successive increases in water content with depth, as seen after the 1998 irrigation, indicate predominantly piston-type flow, as the wetting front moved progressively deeper with time. Water content generally increased with depth from a low value ( $\approx 0.10 \text{ m}^3 \text{ m}^{-3}$ ) at the 0.15-m depth when the soils were dry to a high value of  $0.24 \text{ m}^3 \text{ m}^{-3}$  at the 2-m depth. The high water content at depth is attributed to heavy precipitation during construction of the deeper parts of the cover. There was no uniform trend in average water content for the top of slope vs. the base of slope, which may reflect in part the low slope of the cover (2%). Initially, water contents were higher at the base of the slope relative to the top; however, vegetation concentrated in this region and resulted

in lower water contents at the base relative to the top of the slope.

Representative time series of monitored matric potentials indicate predominantly upward water movement, except after infiltration events, as shown by low matric potentials near the surface (0.3-m depth) and increasing with depth (Fig. 8b, 8c). Information on flow processes derived from matric potential data was similar to that from water content data: piston-type flow following irrigation, matric potential spikes to 0.3-m depth in the summer in response to monsoon precipitation followed by high ET, and persistent high matric potential in response to winter precipitation (2000–2001). Two time series representing different types of vegetation after October 1999, grasses and salt cedar (Fig. 8b) and grasses only (Fig. 8c), indicate that salt cedar was more effective in drying out the soil, as shown by lower matric potentials from summer 2000 through mid summer 2001. The matric potential data during fall 2001 following irrigation recorded progressive downward movement of a drying front. Matric potentials stopped decreasing in mid November 2001 because vegetation was dormant and started decreasing again in April and May 2002 when vegetation became active. Matric potentials at all depths started decreasing at the same time, indicating that roots at different depths were active in the spring. These data provide very valuable information on the time scales at which vegetation actively dries out the cover. The matric potential data suggest generally deeper water penetration at the locations of the heat dissipation sensors relative to the neutron probe access tubes, which showed penetration to 1.4 to 2 m at different locations. Focused flow may have occurred because of less compaction around the instrument trees where heat dissipation sensors were installed.

## Drainage

Measured drainage was zero at the base of the capillary barrier (3-m depth) (Table 2). Even after addition of 1883 mm of irrigation in August 2001, there was no measured drainage at the base of the profile in 2001 through 2002. Ideally, evaluation of the performance of the ET portion of the cover would require drainage measurements at the 2-m depth. However, the capillary break at the 2-m depth precludes drainage until the overlying material becomes almost saturated. Calculated drainage at the 1.1-m depth in the CBET profile for comparison with the New Mexico profile was based on increases in water content over time below this depth and ranged from  $0.00 \text{ mm yr}^{-1}$  (WY00) to  $5.0 \text{ mm yr}^{-1}$  (WY01). Calculated drainage at the 1.1-m depth in the CBET subplots followed 1998 and 2001 irrigations.

Measured lateral drainage from the GCL/asphalt layer in the GABET cover ranged from  $0.00 \text{ mm yr}^{-1}$  in one subplot to  $0.14 \text{ mm yr}^{-1}$  in the other for WY98 through WY01. The measured lateral drainage from one subplot may be attributed to localized fluxes because there was no evidence of increased water contents or matric potentials in any of the instrument locations.



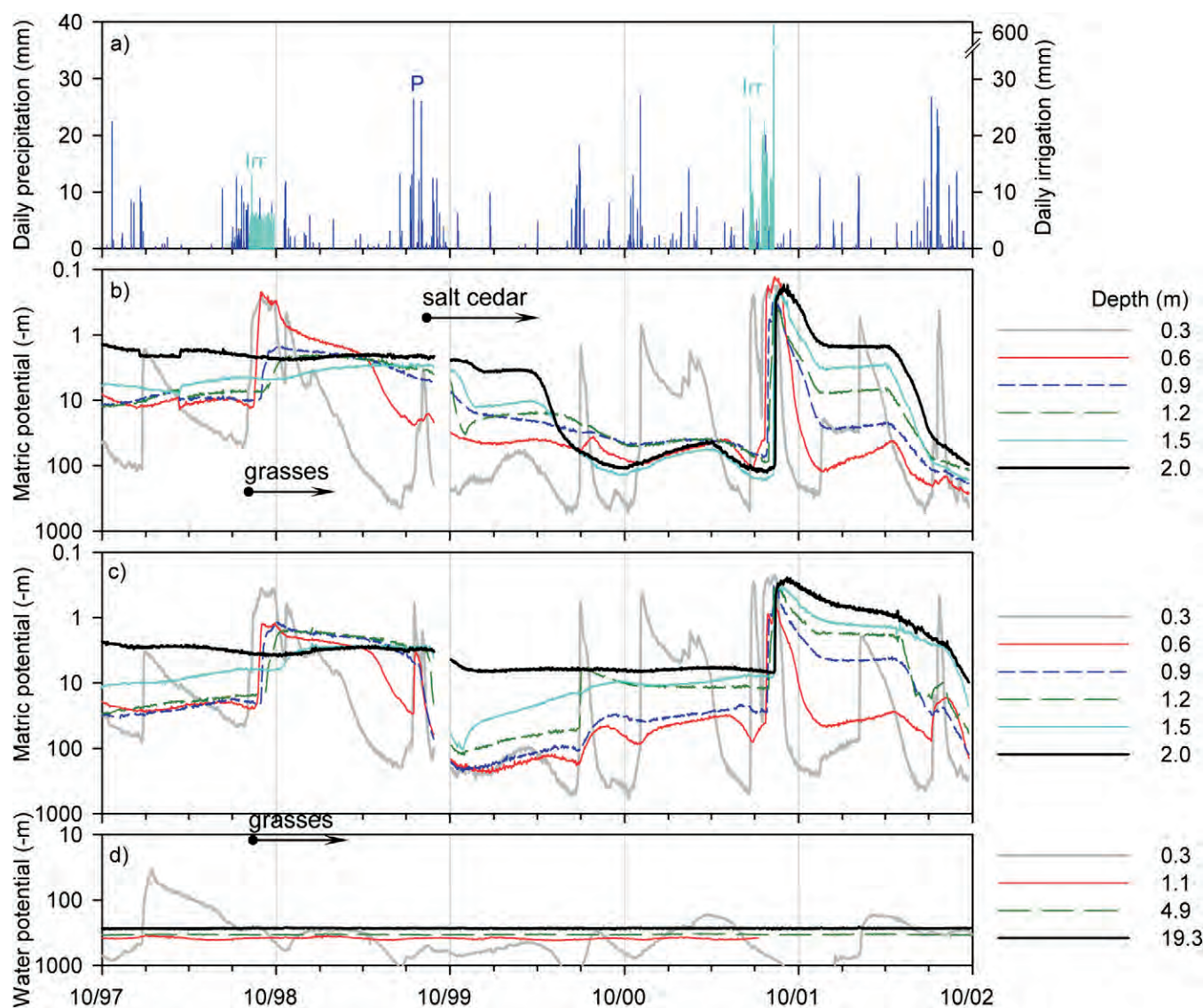


Fig. 8. (a) Daily precipitation ( $P$ ) and irrigation ( $Irr$ ) depths, (b) and (c) matric potential at selected depths at two locations in the CBET cover system at the Texas site, and (d) water potential monitored with thermocouple psychrometers in the adjacent natural setting at the Texas site.

## New Mexico Site Monitoring

### Precipitation, Irrigation, and Runoff

The monitored period was representative and precipitation ranged from 80% (WY02) to 151% (WY01) of the long-term (30-yr) average precipitation at Albuquerque ( $226 \text{ mm yr}^{-1}$ ) (Table 3, Fig. 9). The west subplot was irrigated in late January through early February 2002, with a total of 110 mm of water. Total annual runoff ranged from 0.2 to 22.0 mm. The highest runoff (14 mm on 26 July 1998) occurred in response to heavy precipitation (24.2 mm) the previous day. Runoff was also relatively high in WY97 in the west subplot ( $6.4 \text{ mm yr}^{-1}$ ). Annual runoff was generally low during the remaining time ( $0.2\text{--}0.8 \text{ mm yr}^{-1}$ ).

### Evapotranspiration, Water Storage, and Drainage

Cumulative ET was greater than net infiltration to the cover in WY98 and similar to net infiltration on an an-

nual basis during the remaining time (Fig. 9). Net infiltration generally exceeded ET during November through June in WY01. Potential evapotranspiration exceeded actual ET by factors ranging from 5 (WY01) to 11 (WY02) (Table 3).

Trends in water storage were similar in the west and east subplots; however, water storage was generally lower in the west subplot, except after irrigation in WY02 (Fig. 10). Mean water storage showed large seasonal and interannual variability. High initial water storage may be attributed to precipitation exceeding the long-term average by 70% in summer 1997 (April–September) and by 57% in winter 1997–1998 (October–March), corresponding to the strong 1997–1998 El Niño period. Large decreases in water storage in spring and summer 1998 corresponded to substantial increases in plant cover from about 1% in fall 1997 to between 30 and 60% in 1998 (Fig. 10). Interannual variability in water storage generally reflected variability in precipitation: low water



**Table 3. Water balance monitoring (west and east subplots) and simulation results (east subplot) (mm) for the New Mexico site.†**

Subplot	Water year	<i>P</i>	PET	Irr	<i>R</i> <sub>o</sub>	Net <i>I</i>	<i>D</i>	Δ <i>S</i>	ET	<i>S</i>	RMSE
mm											
West (meas.)	1997‡	227	–	0	6.4	221	0.1	–23.2	244	162	
	1998	299	1772	0	22.0	277	0.4	–66.4	343	95	
	1999	280	1851	0	0.8	279	0.0	–0.9	280	95	
	2000	189	1908	0	0.2	189	0.0	35.1	153	130	
	2001	341	1786	0	0.6	341	0.0	–44.1	385	86	
	2002	181	2012	110	0.6	290	0.0	20.3	270	106	
	1997–2002	1517	9329	110	30.6	1597	0.5	–79.2	1675	674	
East (meas.)	1997‡	227	–	0	1.5	226	0.0	31.5	194	182	
	1998	299	1772	0	0.8	298	0.0	–73.6	372	108	
	1999	280	1851	0	0.6	279	0.0	–8.6	288	99	
	2000	189	1908	0	0.2	189	0.0	16.2	172	116	
	2001	341	1786	0	0.8	340	0.0	–4.3	345	111	
	2002	181	2012	0	0.4	180	0.0	3.5	177	114	
	1997–2002	1517	9329	0	4.3	1512	0.0	–35.3	1548	730	
East (simul. SF)§	1998	299	1772	0	0.0	299	0.0	–76	375	106	37
	1999	280	1851	0	0.0	280	0.0	–14	294	94	17
	2000	189	1908	0	0.0	189	0.0	–8.2	197	91	17
	2001	341	1786	0	0.0	341	0.0	–1.6	343	115	37
	2002	181	2012	0	0.0	181	0.0	13	167	124	19
	1998–2002	1290	9329	0	0.0	1290	0.0	–86.8	1376	530	
East (simul. UG)§	1998	299	1772	0	0.0	299	0.3	–76	375	106	32
	1999	280	1851	0	0.0	280	0.1	–14	294	94	17
	2000	189	1908	0	0.0	189	0.0	–8.1	197	91	17
	2001	341	1786	0	0.0	341	0.0	–1.5	343	114	37
	2002	181	2012	0	0.0	181	0.0	13	167	124	18
	1998–2002	1290	9329	0	0.0	1290	0.4	–86.6	1376	529	

† *P*, precipitation; PET, potential evapotranspiration; Irr, irrigation; *R*<sub>o</sub>, runoff; net *I*, net infiltration; *D*, drainage; Δ*S*, water storage change; ET, evapotranspiration; *S*, water storage at end of water year; RMSE, root mean square error between simulated and measured (daily) water storage.

‡ 1 May through 30 Sept.

§ Simulation results for SF, seepage face lower boundary; and UG, unit gradient lower boundary.

storage in WY99 and WY00 when precipitation was low and higher water storage in WY01 when precipitation was higher. Temporal variability in water storage at shorter time scales generally reflected variability in precipitation and plant growth. Large increases in water storage occurred on 15 Mar. 1998, in response to high precipitation (48 mm in 2 d). Summer precipitation in 1999 was effective in increasing water storage. The large increase in water storage recorded in summer 2000 through spring 2001 was attributed to high precipitation during this time. Decreases in water storage in some years (1998 and 2002) can be related to vegetation growth and ET in the spring and summer. However, there was

no definite seasonal variability in water storage because water storage increases and decreases occurred in both winter and summer. The much larger coefficient of variation (100  $\sigma/\mu$ ) in measured water storage ( $\leq$  about 35%) relative to that for the Texas data ( $\leq$  about 10%) may reflect the smaller sampling volume of the TDR probes relative to the neutron probe and lower number of sample points in each average (15 in New Mexico vs. 70 in Texas data). The CV in water storage also reflects spatial variability in measured water content: lower water contents in the upland areas and higher water contents toward the base of the slopes (Fig. 11a).

Temporal variability in water content measured at different depths was greatest near the surface and decreased with depth (Fig. 11b). Water content was generally high at 0.15 m during winter periods, with the exception of 1999, and generally decreased in March and April of each year when vegetation became active. Water redistributed to depths of 0.45 and 0.90 m after infiltration in winter 1997–1998 and winter and spring 2000–2001. Drying also propagated with depth (e.g., for 1998: 0.15 m in March, 0.45 m in June, 0.9 m in August).

Measured drainage at the base of the ET cover was 0.0 mm yr<sup>–1</sup> in the east subplot and ranged from 0.0 to 0.4 mm yr<sup>–1</sup> in the west subplot. Drainage occurred during the first 2 yr of the 5-yr monitoring period. Low drainage during 1997 extended over several months and was attributed to wet initial conditions (average water content 0.18 m<sup>3</sup> m<sup>–3</sup>) from construction water in the profile and summer precipitation events (10 July 1997, 24.4 mm; 18 July 1997, 20.6 mm; 22 Aug. 1997, 23.6 mm; 21 Sept. 1997, 50.8 mm). Drainage in 1998 generally occurred during a short time period (0.39 mm; 18 July 1998 to 20 Sept. 1998) and was attributed to a sequence

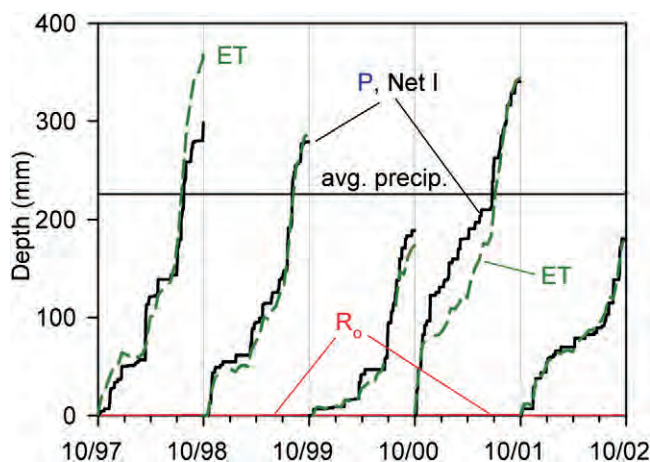


**Fig. 9. Measured cumulative precipitation (*P*), runoff (*R*<sub>o</sub>), and net infiltration (net *I* = *P* – *R*<sub>o</sub>) and calculated cumulative evapotranspiration (ET) for the ET engineered cover to the 1.1-m depth for water years 1998 through 2002 at the New Mexico site. The long-term (1961–1990) average annual precipitation of 226 mm is shown ( $\pm 55$  mm 1  $\sigma$ ).**

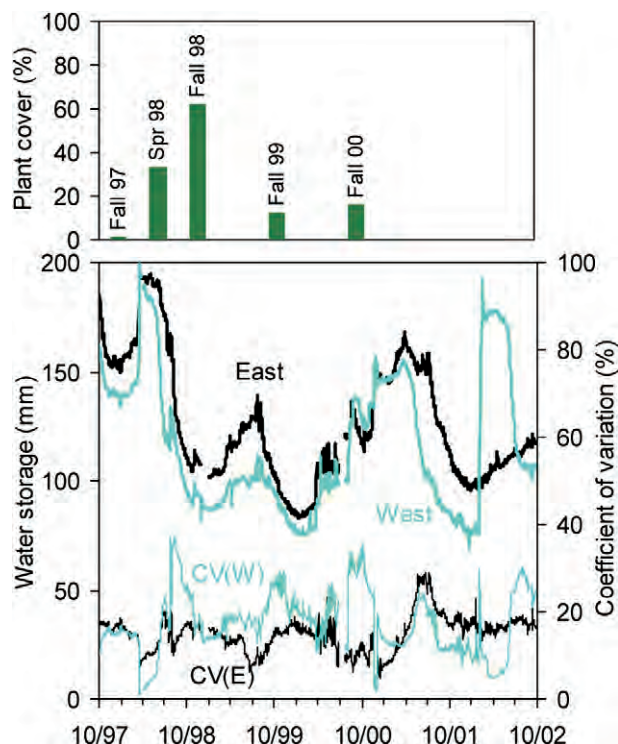


Fig. 10. Average plant cover (columns) and average water storage (thick lines) to the 1.1-m depth in the west and east subplots at the New Mexico site. Thin lines represent the coefficients of variation of five TDR measurement locations for both the west and east subplots.

of large discrete precipitation events (16 July 1998, 24.6 mm; 25 July 1998, 24.4 mm; and 1 Aug. 1998, 18.5 mm). Drainage may have been spatially focused also, as shown by lack of drainage in the east subplot.

### Comparison with the Natural System

The natural system surrounding the ET covers in West Texas was characterized for a proposed low-level radioactive waste disposal facility (Scanlon et al., 1999). Water content monitored with a neutron probe in an access tube installed 20 m from the covers did not change

below 0.6 m during the 4-yr monitoring period. Long-term water potential monitoring using thermocouple psychrometers 30 m from the covers showed that maximum depth of the wetting front was  $<0.3$  m (Fig. 8d; Scanlon et al., 2003). Water potential includes matric and osmotic potentials; however, estimated osmotic potentials from pore water  $\text{Cl}^-$  data are generally  $\leq 10\%$  of measured water potentials (Scanlon et al., 2003); therefore, water potential and matric potential can be considered approximately equivalent. Matric potentials in the engineered cover were much higher than water potentials monitored in the natural system (Fig. 8d). Wetter conditions in the engineered covers can be attributed partly to precipitation, addition of water for compaction during construction, and irrigation of the subplots to establish vegetation. Measurement and modeling of matric potential and  $\text{Cl}^-$  profiles in the natural system indicate that it has been in a long-term drying trend since the Pleistocene ( $\approx 10\,000$ – $15\,000$  yr ago) and that water has been moving upward since that time (Scanlon et al., 2003). Chloride moves into the subsurface with infiltrating precipitation and builds up in the subsurface as water is evapotranspired because  $\text{Cl}^-$  is not volatile and plant uptake is negligible. This comparison of engineered covers and the surrounding natural system indicates that the two are not directly comparable. Soils in the natural system have been developing for very long times and are characterized by thick caliche development. It is questionable whether the water balance of the covers will approach that of the natural system in the near future.

## Numerical Simulation Results

### Texas Site Water Balance Simulations

Previous studies indicate that simulated and measured water balance generally compare favorably for the first year of monitoring (WY98) when the system was non-vegetated; however, simulated runoff was underestimated (Scanlon et al., 2002). Simulated water balance of the vegetated cover for WY00 was similar to the

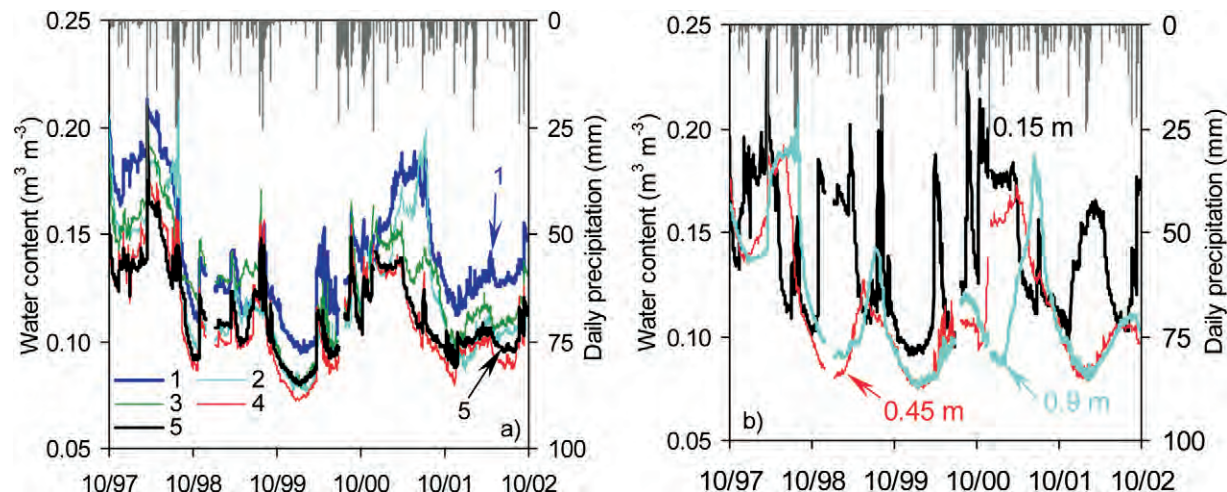


Fig. 11. Average measured water content for (a) all monitored depths within a given slope position (1: base of slope, 5: top of slope) and (b) all slope positions at a given monitored depth in the east subplot at the New Mexico site.



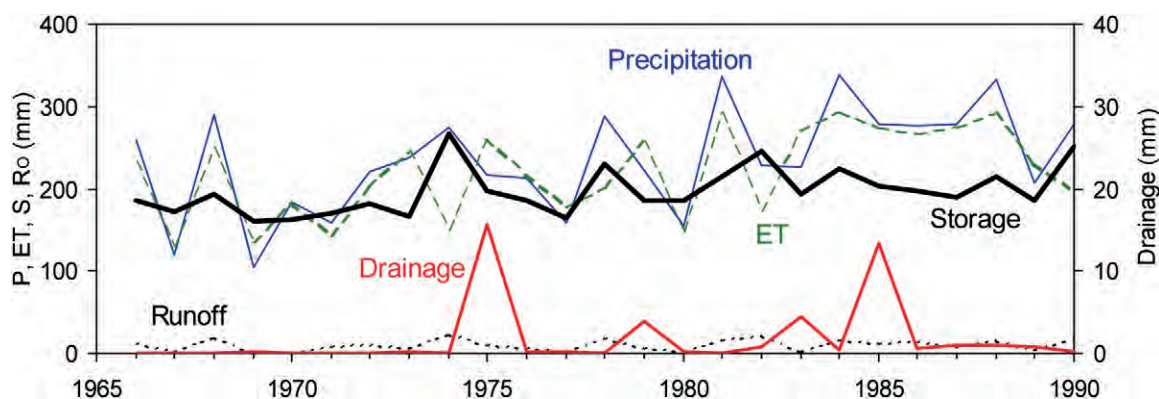


Fig. 12. Simulated annual water balance results for the 1.1-m Texas profile with a unit gradient lower boundary condition.

measured water balance also (Table 2). Vegetation parameters included maximum ecosystem level LAI of  $0.1 \text{ m}^2 \text{ m}^{-2}$ . The growing season extended from mid March to the end of September, with maximum LAI from late May through mid-August. The maximum rooting depth was set at 0.75 m and was evaluated using sensitivity analyses. To better simulate runoff, a 50-mm crust with 44% lower hydraulic conductivity was included in the simulation profile. Crusts often form in these regions. The saturated hydraulic conductivity of the crust can be considered a calibration parameter to better simulate runoff. Simulated drainage was 0.0 mm for the 2-m profile using a seepage face lower boundary condition that reflects the underlying capillary barrier. In contrast, simulations using a unit gradient lower boundary condition, which allows free drainage, resulted in 0.2 mm of drainage at the 1.1-m depth and 2.4 mm of drainage at the 2-m depth. The higher drainage at the 2-m depth reflects the wetter initial conditions between 1 and 2 m because of heavy rain during construction (Fig. 7). Simulated drainage at the 1.1-m depth is similar to zero drainage estimated at this depth.

The main components of the water balance were ET and water storage change because runoff and drainage were low. Simulated and measured annual ET values were within 1%, and water storage changes were within 12%. Calculated root mean square errors based on measured and simulated water storage were low ( $\leq 10 \text{ mm}$ ), indicating that the simulations generally reproduced the temporal variability in water storage.

Although there are no measured data for comparison with the 25-yr simulations, these simulations provide information on how the cover might perform in response to long-term climate forcing (Fig. 12). The results for the 1.1-m profile are described and are similar to those for the 2-m profile. Simulated runoff ranged from 0.0 to  $22.7 \text{ mm yr}^{-1}$  and averaged  $9.5 \text{ mm yr}^{-1}$ , which is similar to measured values during the monitoring period (Table 2). Simulated drainage was  $0.0 \text{ mm yr}^{-1}$  for the 1.1- and 2-m profiles using a seepage face lower boundary condition. In contrast, a unit gradient lower boundary resulted in simulated drainage ranging from 0.0 to  $1.0 \text{ mm yr}^{-1}$ , with the exception of 4 yr when drainage was higher: 1975 ( $16.7 \text{ mm yr}^{-1}$ ), 1979 ( $4.5 \text{ mm yr}^{-1}$ ), 1983 ( $4.9 \text{ mm yr}^{-1}$ ), and 1985 ( $14.1 \text{ mm yr}^{-1}$ ) (Fig. 12). The highest drainage occurred in 1975 after above-normal

precipitation in September 1974. A total of 163 mm of precipitation occurred in 9 d in September, with daily precipitation up to 57 mm. Precipitation during 1974 before September was low (112 mm), and low simulated ET is consistent with the low precipitation before September. High precipitation near the end of the growing season resulted in insufficient time for the vegetation to remove the infiltrated water and resulted in a large increase in water storage (100 mm) in 1974 followed by drainage in 1975 (16.7 mm) (Fig. 12). Similar processes occurred in 1984 (131 mm precipitation 4–13 Aug.; 68 mm, 23–26 Oct.) that resulted in 14.1 mm of drainage in 1985. Dominant parameters in the water balance were ET and water storage changes. Temporal variability in water storage was low. The highest water storage increase (100 mm) was recorded in 1974, which corresponded to above-normal precipitation in September. These simulations indicate that cover performance in response to long-term climatic forcing should be similar to that shown by the shorter term monitoring record; however, drainage may occur in response to intense precipitation toward the end of the growing season that can be eliminated with a capillary barrier.

### New Mexico Site Water Balance Simulations

The 5-yr water balance of the east subplot was simulated to determine how well simulations would match measured values. The vegetation parameters included maximum ecosystem level LAI of  $0.3 \text{ m}^2 \text{ m}^{-2}$  (Dwyer, 2003). The growing season extended from mid-March to the end of September, with maximum LAI from mid-May through early September. Maximum rooting depth was set at 0.75 m, and sensitivity of model results to this parameter was tested. Zero runoff was simulated, which is generally consistent with very low measured runoff values (Table 3). Simulated drainage of zero for the seepage face lower boundary condition is consistent with zero measured drainage. Replacement of the seepage face with a unit gradient resulted in small amounts of drainage that decreased with time ( $0.1\text{--}0.3 \text{ mm yr}^{-1}$ ; Table 3). Interannual trends and variability in both ET and water storage were generally reproduced by the simulations; however, magnitudes differed. Simulated and measured annual ET values were within 15%. The greatest discrepancy in simulated and measured water

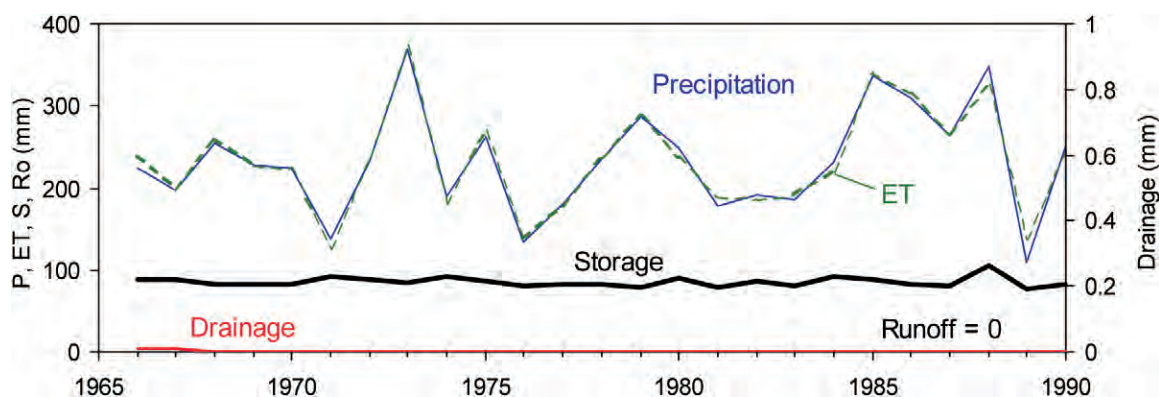


Fig. 13. Simulated annual water balance results for the 1.1-m New Mexico profile with a unit gradient lower boundary condition.

storage was for WY00, when measured storage increased and simulated storage decreased.

The 25-yr simulations resulted in zero runoff and drainage, which is consistent with the monitoring data (Fig. 13). The largest increase in water storage occurred in 1988 (24 mm) and may be attributed to precipitation being about 60 to 70% above average in April through September 1987 and October through March 1997-1998 related to El Nino. Increases in water storage of about 10 mm also occurred in 1964, 1965, 1971, 1974, 1980, and 1984. Annual precipitation and ET were highly correlated ( $r = 0.99$ ). Similar results were obtained for seepage face and unit gradient lower boundary conditions.

### Sensitivity Analysis

The simulations provide information on the sensitivity of the simulated water balance to variations in meteorological forcing, profile thickness, and lower-boundary condition. Additional simulations were conducted to assess sensitivity of simulations to variations in PET, vegetation parameters (including root depth, root-length density, vegetation type, and LAI), and hydraulic parameters (Fig. 14, Table 4). Parameters were generally varied from a factor of 0.5 to 1.5 times the values used in the base case. The sensitivity analyses were conducted on the 25-yr simulations.

Results of sensitivity analyses for the Texas site are

described for the 1.1-m-deep profiles because results from the 2-m profiles were similar (Fig. 14; Table 4). Simulations were based on a unit gradient lower boundary condition. Simulated water balance was most sensitive to the presence or absence of vegetation. Simulating the extreme case of no vegetation resulted in increased drainage by  $27.7 \text{ mm yr}^{-1}$  and was balanced by reduced ET. The model was not very sensitive to variations in individual vegetation parameters, such as LAI, root depth, or root-length density. Varying root distribution from bunchgrass (base case) to cheat grass (higher root density at shallower depths; Rockhold et al., 1995) increased drainage by  $3.6 \text{ mm yr}^{-1}$  and was generally balanced by reduced ET. Decreasing PET by a factor of 2 increased drainage by  $7.7 \text{ mm yr}^{-1}$  and was generally balanced by reduced ET, whereas increasing PET by a factor of 1.5 decreased drainage and increased ET. However, temporal variability in annual PET is low (CV 0.06-0.08), and PET is generally not highly uncertain. Simulated water balance was more sensitive to variations in hydraulic parameters than in vegetation parameters. Previous studies at the Texas site showed that laboratory and field measured  $K_s$  values underestimated the effective  $K_s$  of the cover as shown by the monitoring data (Scanlon et al., 2002). Simulations are sensitive to variations in  $K_s$ . Increasing  $K_s$  by an order of magnitude increased drainage by  $7.5 \text{ mm yr}^{-1}$  that was balanced by reduced ET, whereas

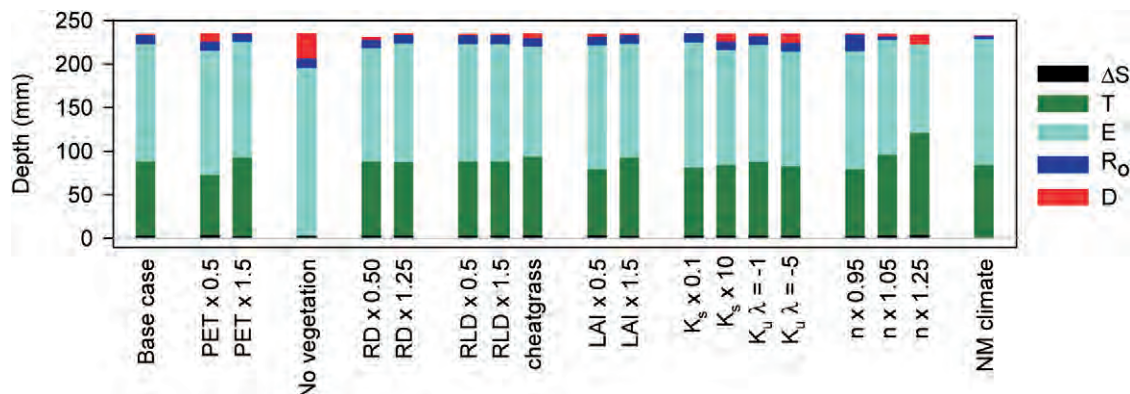


Fig. 14. Sensitivity analysis for the Texas site simulation: 25-yr average annual values are shown for the base case simulation and for simulations with a single parameter altered as indicated. PET, potential evapotranspiration; RD, root depth; RLD, root length density; LAI, leaf area index;  $K_s$ , saturated hydraulic conductivity;  $K_u \lambda$ , unsaturated hydraulic conductivity function parameter;  $n$ , van Genuchten soil water retention function parameter; NM climate, simulation using New Mexico site climate forcing. Water balance parameters are  $\Delta S$ , water storage change;  $T$ , transpiration;  $E$ , evaporation;  $R_o$ , runoff;  $D$ , drainage.

**Table 4.** Sensitivity analysis results for 25-yr simulations using a unit-gradient lower boundary condition. Base case represents the model average annual total values. All other values represent *changes* relative to the base case in average annual total values resulting from the indicated parameter modification.<sup>†</sup>

Parameter	Texas site 1.1-m profile						New Mexico site 1.1-m profile					
	<i>T</i>	<i>E</i>	ET	<i>R<sub>o</sub></i>	<i>D</i>	Δ <i>S</i>	<i>T</i>	<i>E</i>	ET	<i>R<sub>o</sub></i>	<i>D</i>	Δ <i>S</i>
	mm											
Base case	85.8	134.9	220.7	9.5	1.9	3.2	93.6	139.8	233.4	0.0	0.0	-0.8
PET × 0.5	-16.7	7.7	-9.0	0.8	7.7	0.9	-11.2	13.6	2.5	0.0	0.0	0.3
PET × 1.5	5.1	-2.7	2.3	-0.3	-1.1	-0.5	9.0	-6.7	2.3	0.0	0.0	0.5
No vegetation	-85.8	57.4	-28.4	1.0	27.7	-0.3	-93.6	90.8	-2.8	0.0	1.8	1.0
RD × 0.5	1.9	-4.3	-2.4	-0.1	2.6	0.0	16.0	-17.2	-0.3	0.0	0.1	0.2
RD × 1.25	-1.2	1.5	0.3	0.1	-0.3	0.0	0.0	0.0	0.0	0.0	0.0	0.0
RLD × 0.5	0.0	0.0	0.0	0.0	0.0	0.0	1.4	-1.3	0.0	0.0	0.0	-0.1
RLD × 1.5	-0.3	0.2	-0.1	0.1	0.0	0.0	0.0	0.0	0.0	0.0	0.0	0.0
Cheat grass	4.8	-8.5	-3.8	-0.2	3.6	0.3	21.0	-20.9	0.2	0.0	0.0	-0.2
LAI × 0.5	-9.3	7.4	-1.9	0.1	1.5	0.3	-9.6	9.3	-0.3	0.0	0.0	0.3
LAI × 1.5	4.9	-4.1	0.8	-0.1	-0.5	-0.2	6.3	-6.3	0.0	0.0	0.0	0.0
<i>K<sub>s</sub></i> × 0.1	-6.6	8.6	2.0	0.2	-1.9	-0.3	-11.5	11.4	-0.1	0.0	0.0	0.1
<i>K<sub>s</sub></i> × 10	-4.1	-3.2	-7.4	-0.1	7.5	0.0	14.6	-14.7	-0.1	0.0	0.0	0.1
<i>K<sub>u</sub></i> λ = -1	-0.1	-1.1	-1.2	0.0	1.2	0.0	7.3	-7.4	-0.1	0.0	0.0	0.1
<i>K<sub>u</sub></i> λ = -5	-6.0	-3.0	-8.9	0.1	8.9	0.0	20.6	-24.0	-3.5	0.0	3.3	0.1
<i>n</i> × 0.95	-8.5	0.3	-8.2	9.6	-0.9	-0.5	-7.5	7.5	0.0	0.0	0.0	0.0
<i>n</i> × 1.05	7.3	-3.4	3.9	-5.5	1.2	0.4	7.5	-7.5	0.0	0.0	0.0	0.0
<i>n</i> × 1.25	32.1	-34.2	-2.1	-9.5	10.7	1.0	41.3	-41.2	0.1	0.0	0.0	-0.1
Climate	-0.8	9.2	8.4	-5.7	-1.7	-3.8	0.6	-2.8	-2.2	2.1	0.0	2.9

<sup>†</sup> *T*, transpiration; *E*, evaporation; ET, evapotranspiration; *R<sub>o</sub>*, runoff; *D*, drainage; Δ*S*, water storage change; PET, potential evapotranspiration; RD, root depth; RLD, root length density; LAI, leaf area index; *K<sub>s</sub>*, saturated hydraulic conductivity; *K<sub>u</sub>* λ, unsaturated hydraulic conductivity function parameter; *n*, van Genuchten water retention function parameter; Climate, climate forcing exchanged between the Texas and New Mexico sites.

decreasing *K<sub>s</sub>* by an order of magnitude decreased drainage by 1.9 mm yr<sup>-1</sup>. The unsaturated hydraulic conductivity (*K<sub>u</sub>*) can also be varied by changing the λ parameter in the van Genuchten–Mualem *K<sub>u</sub>* function. Mualem (1976) suggested a value of 0.5 for λ. Decreasing λ to values of -1 to -5 increased the *K<sub>u</sub>* and increased drainage by 1.2 and 8.9 mm yr<sup>-1</sup>, respectively, balanced by reduced ET. The van Genuchten *n* parameter in the water retention function represents the range in pore sizes in the soil: high *n* indicates low pore-size distribution, typical of coarser material, and low *n* indicates high pore-size distribution, typical of finer material. The typical range in parameters (factor of 0.5–1.5) could not be considered for *n* because it resulted in unrealistic values (*n* ≤ 1.0). Increasing *n* by a factor of 1.25 increased drainage by 10.7 mm yr<sup>-1</sup> and was balanced by reduced runoff. Decreasing *n* by a factor of 0.95 generally reduced drainage slightly. Replacing the unit gradient lower boundary condition with a seepage face to simulate a capillary barrier resulted in zero drainage for all sensitivity cases.

Simulated water balance of the New Mexico site was much less sensitive to the parameter variations considered in the sensitivity analyses than that of the Texas site (Fig. 15, Table 4). The following results are based on a unit gradient lower boundary condition. Varying PET by factors of 0.5 and 2 changed ET by only 1%. Simulating nonvegetated conditions increased water storage by 1.0 mm yr<sup>-1</sup> and increased drainage by 1.8 mm yr<sup>-1</sup> and was balanced by reduced ET. Simulation results were insensitive to variations in vegetation parameters. Varying hydraulic parameters, such as *K<sub>s</sub>* and van Genuchten *n*, had little impact on the simulated water balance. Reducing the Mualem λ parameter to -5 increased drainage by 3.3 mm yr<sup>-1</sup> balanced by reduced ET. Results for a seepage face lower boundary condition were similar to those for unit gradient condition, except that simulated

drainage was zero for all sensitivity cases with a seepage face. The general insensitivity of simulated water balance to many of the parameters evaluated suggests that it may be difficult to estimate parameters using inverse modeling.

To evaluate causes of differences in simulated long-term water balances between Texas and New Mexico, we interchanged climate forcing between sites. Simulating Texas soils with New Mexico climate forcing resulted in reduced drainage, runoff, and water storage change, balanced by increased ET relative to the Texas base case simulation. These changes may be attributed to the lack of large precipitation events occurring near the end of the growing season (August–October) that are present in the Texas climate forcing. Simulating New Mexico soils with Texas climate forcing resulted in zero drainage (i.e., no change) and increased runoff and water storage change balanced by decreased ET relative to the New Mexico base case simulation. The changes may be attributed to the 80% lower *K<sub>s</sub>* in New Mexico subsoil relative to Texas subsoil, which reduced the impact of the late growing season precipitation events present in the Texas climate forcing. These comparisons indicate that low *K<sub>s</sub>* in New Mexico subsoil plays an important role in minimizing drainage; however, as with traditional resistive covers, it may be difficult to determine the optimal *K<sub>s</sub>* that can be achieved without developing cracks and preferential pathways. The above comparisons indicate that both climate forcing and hydraulic properties contribute to differences in simulated water balances between the sites.

### Implications for Future Studies

Monitoring and modeling results from these studies have important implications for future studies of engineered covers. Major implications for the monitoring program include (i) limitations of relying on a single param-



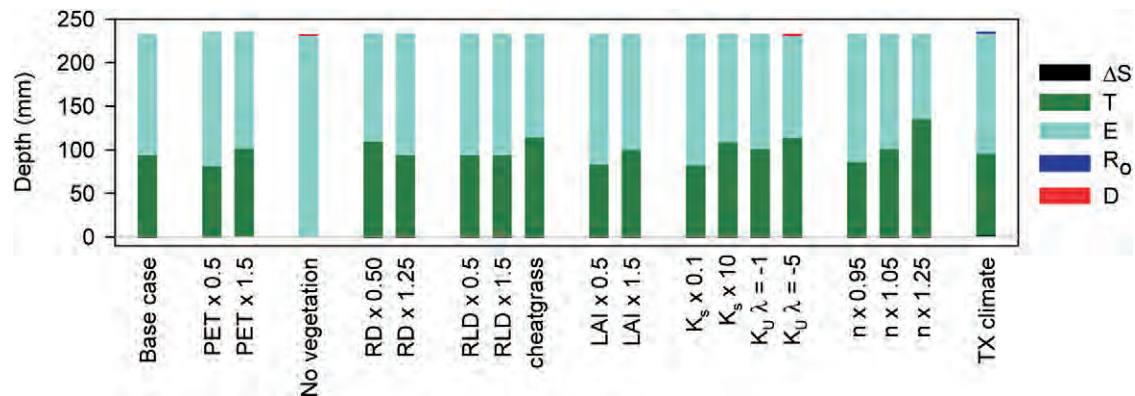


Fig. 15. Sensitivity analysis for the New Mexico site simulation: 25-yr average annual values are shown for the base case simulation and for simulations with a single parameter altered as indicated. PET, potential evapotranspiration; RD, root depth; RLD, root length density; LAI, leaf area index;  $K_s$ , saturated hydraulic conductivity;  $K_u \lambda$ , unsaturated hydraulic conductivity function parameter;  $n$ , van Genuchten soil water retention function parameter; TX climate, simulation using Texas site climate forcing. Water balance parameters are  $\Delta S$ , water storage change;  $T$ , transpiration;  $E$ , evaporation;  $R_0$ , runoff;  $D$ , drainage.

eter such as drainage, (ii) length of the monitoring record, and (iii) spatial variability in water balance parameters.

Drainage is the most critical water balance parameter for performance of engineered covers; however, it is difficult to measure natural drainage in these systems because most pan lysimeters create a capillary barrier effect. The applicability of the lysimeter drainage measurements to actual cover system performance depends on whether the interface between the cover and the underlying waste also acts as a capillary barrier. Although the measurement systems used with pan lysimeters (e.g., tipping bucket rain gauges) can precisely measure drainage, the problem is that water cannot reach these measurement devices and builds up above the lysimeter. Therefore, these systems can underestimate drainage and overestimate soil water storage relative to systems that do not contain a capillary barrier. The impact of the lower-boundary condition was shown by monitoring and modeling at the Texas site. The lack of drainage in the CBET subplot that was irrigated with 2340 mm of water in summer 2001 is attributed to the capillary barrier. In addition, simulated drainage at the Texas site was higher for the unit gradient vs. the seepage face boundary condition, indicating that measured drainage using lysimeters underestimates natural drainage and overestimates water storage for systems without a capillary barrier at this site. The low  $K_s$  subsoil in the New Mexico profile resulted in zero drainage for both seepage face and unit gradient conditions. The studies described here emphasize the importance of monitoring multiple parameters to understand total system performance, including water storage, matric potential, and plant parameters.

Engineered covers should be monitored for at least 10 to 20 yr because short-term monitoring may be dominated by construction effects and by disequilibrium between cover parameters and climate forcing. The representativeness of climate forcing during the monitoring period is also very important.

Spatial variability in water balance parameters is important in assessing cover performance. Spatial variability in water content was particularly evident in the New Mexico site (slope 5%) with lower water content in up-

land areas and higher water content at the base of the slope (Fig. 11a). Monitoring of future covers, particularly those with steeper slopes, should not rely on a single vertical profile for monitoring water storage.

Many limitations associated with modeling are described in an intercode comparison study (Scanlon et al., 2003), such as difficulties in simulating runoff, accurate representation of precipitation intensity, upper boundary condition during precipitation, and variations in simulated water balance related to hydraulic parameterization. One of the most critical parameters in ET covers is vegetation and how it controls water balance. Most models simulate vegetation by externally prescribing time series in vegetation parameters such as LAI and root depth (Simunek et al., 1998; Fayer, 2000). However, this approach precludes any feedback between soil water storage changes and vegetation and fails to simulate the dynamic two-way interaction between vegetation and water balance. The opportunistic behavior of vegetation is clearly shown in the monitoring data. Vegetative response to water storage changes should be simulated internally rather than prescribed in the input data set. All available data, including monitoring and modeling, should be combined to develop a comprehensive conceptual model of total system performance.

### Implications for Cover Design

The monitoring and modeling studies described in this work provide valuable information that can be used to optimize the design of ET covers in arid and semiarid regions. One of the basic design issues is cover thickness. A variety of approaches can be used to estimate cover thickness. Traditional approaches estimate available water storage (AWS) from water content at field capacity and wilting point. However, Meyer and Gee (1999) showed that a head-based approach for estimating AWS may not be valid because field capacity may correspond to unacceptably large water fluxes; they proposed a flux-based approach to estimate AWS. Using the Texas profile as an example, field capacity ( $h = -3.3$  m) corresponds to a flux of 67 mm yr<sup>-1</sup> under unit gradient



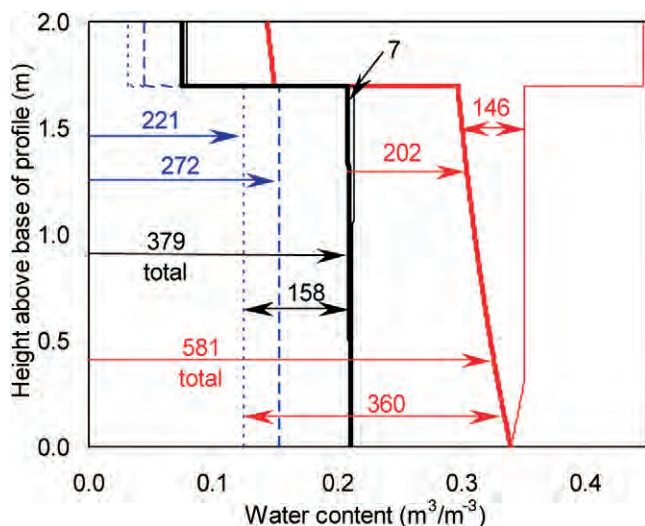


Fig. 16. Calculated water content profiles for the Texas CBET system. All values shown are in millimeters and represent total water storage values over the intervals indicated by associated arrows. Heavy and thin solid line pairs converging at the zero height represent water content profiles for zero and unit downward total head gradient conditions, respectively. The pair of lines converging at  $0.34 \text{ m}^3 \text{ m}^{-3}$  water content represent profiles with a capillary barrier located at the zero height having a breakthrough water content equating to  $-0.3 \text{ m}$  head. The two lines converging at  $0.21 \text{ m}^3 \text{ m}^{-3}$  water content represent profiles without a capillary barrier and water content at the zero height equating to a prescribed flux of  $1 \text{ mm yr}^{-1}$ . Dashed lines represent wilting point water content profiles for uniform head conditions ranging from  $-150 \text{ m}$  (long dash) to  $-500 \text{ m}$  (short dash). Abrupt shift in water content near the top of each profile indicates transition from topsoil to subsoil.

conditions (free drainage, no capillary barrier). A flux of  $67 \text{ mm yr}^{-1}$  is considered excessive. A reasonable performance goal for covers in arid and semiarid regions would be a flux of  $1 \text{ mm yr}^{-1}$  which corresponds to a head at the base of the profile of  $-21 \text{ m}$ . The maximum water that can be stored in the profile before drainage occurs corresponds to equilibrium or no flow conditions, which corresponds to a total head ( $H$ ) gradient of zero (i.e.,  $H = h + z$ , unit downward gravitational potential head,  $z$ , gradient balanced by unit upward matric potential head,  $h$ , gradient). Under equilibrium conditions, a head of  $-21 \text{ m}$  corresponds to  $379 \text{ mm}$  total water storage in a  $2\text{-m}$  profile (Fig. 16) and  $191 \text{ mm}$  in a  $1.1\text{-m}$  profile (Table 5). Under drainage conditions, a unit downward total head gradient is more appropriate, which corresponds to a zero matric potential head gra-

dient and unit downward gravitational potential head gradient. However, the difference in water storage between equilibrium and a downward gradient is small ( $7 \text{ mm}$ ) (Fig. 16). To calculate the AWS, water storage associated with the wilting point should be subtracted from storage calculated for the  $1 \text{ mm yr}^{-1}$  flux. The AWS ranges from  $158 \text{ mm}$  for a  $2\text{-m}$  profile to  $82 \text{ mm}$  for a  $1.1\text{-m}$  profile using a wilting point head of  $-500 \text{ m}$ , which is typical of arid and semiarid conditions (Table 5). The choice of wilting point head impacts the AWS estimate. Use of a wilting point head of  $-500$  vs.  $-150 \text{ m}$  (typical of more humid settings) results in 1.5 times greater AWS.

Stormont and Morris (1998) and Khire et al. (2000) assessed increased storage provided by an underlying capillary barrier. A similar approach was used in this study to evaluate the impact of a capillary barrier. The Texas profile was used as an example. Similar results were found for the New Mexico profile (Table 5). A water entry pressure of  $-0.3 \text{ m}$  was used for the capillary barrier. This analysis indicated that addition of a capillary barrier increases the AWS by  $202 \text{ mm}$  ( $2 \text{ m}$  profile) and  $121 \text{ mm}$  ( $1.1 \text{ m}$  profile) for zero total head gradient (equilibrium) and by  $348 \text{ mm}$  ( $2 \text{ m}$  profile) and  $221 \text{ mm}$  ( $1.1 \text{ m}$  profile) for unit downward total head gradient (drainage). Stormont and Morris (1998) indicated that unit downward gradients are generally observed during capillary breakthrough conditions. The calculated AWS was not very sensitive to variations in water entry pressure of the capillary break material. Varying water entry pressure from  $-1.0 \text{ m}$  to  $-3.0 \text{ m}$  only changed the AWS in the  $2\text{-m}$  profile by  $45 \text{ mm}$ . Average water storage at the Texas site exceeded water storage corresponding to the calculated  $1 \text{ mm yr}^{-1}$  downward water flux  $70\%$  of the time; therefore, a capillary barrier was required to minimize drainage in this system (Fig. 17).

The required AWS of a cover is difficult to determine. The dominance of summer precipitation in the Texas and New Mexico regions studied, which corresponds to periods of high ET, reduces the required AWS. However, critical events may result from periods of above-normal summer precipitation followed by high winter precipitation, as in the 1997–1998 El Niño period in New Mexico. Examining the long-term simulations of the Texas site using a unit gradient lower boundary condition (free drainage), total water storage increased from  $167$  to  $282 \text{ mm}$  for a  $1.1\text{-m}$  profile, and drainage

Table 5. Total water storage ( $WS_T$ ) and available water storage (AWS) estimates for the Texas and New Mexico cover systems. Both unit gradient (UG) (equivalent to free drainage) and seepage face (SF) (equivalent to capillary barrier) lower boundary conditions are shown using water content profiles corresponding to both zero total head (Equil. = equilibrium conditions) and downward ( $\downarrow$ ) UG total head conditions within the cover system profiles. AWS was estimated as the difference between  $WS_T$  and the water storage corresponding to a uniform  $-500 \text{ m}$  wilting point matric potential. Also shown is the benefit related to a capillary barrier (SF lower boundary condition) expressed as the ratio of SF to UG water storage capacity.

Profile	UG lower boundary condition				SF lower boundary condition				SF/UG ratio			
	Equil. profile		$\downarrow$ UG profile		Equil. profile		$\downarrow$ UG profile		$WS_T$		AWS	
	$WS_T$	AWS	$WS_T$	AWS	$WS_T$	AWS	$WS_T$	AWS	Equil	$\downarrow$	Equil	$\downarrow$
mm												
TX 2.0 m	379	158	386	165	581	360	727	506	1.5	1.9	2.3	3.1
TX 1.1 m	191	82	193	84	312	203	412	303	1.6	2.1	2.5	3.6
NM 1.1 m	181	130	194	143	303	252	390	339	1.7	2.0	1.9	2.4

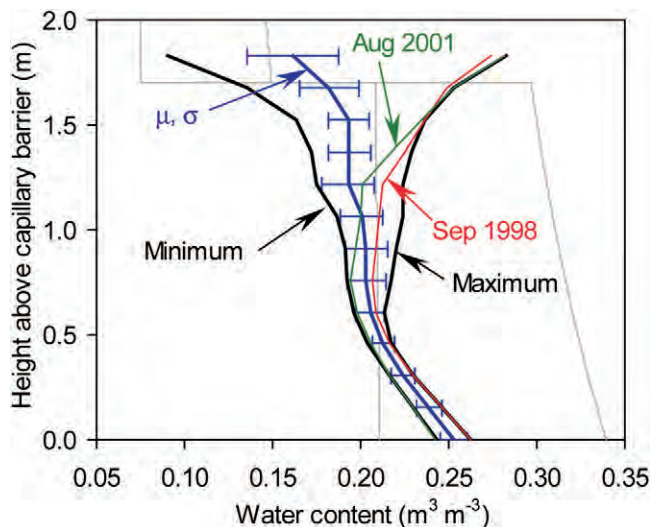


Fig. 17. Temporal variability of measured water content with depth in the Texas site CBET system. Calculated water content profiles for zero total head gradient conditions from Fig. 16 are shown in the background for reference. Average water content throughout the monitored period ( $\mu$ ) is shown with error bars, indicating the temporal standard deviation ( $\sigma$ ) at the monitored depths. Also shown are water content temporal minimum and maximum values at each depth. The two wettest measured water content profiles are shown (Sept. 1998 and Aug. 2001).

later occurred following a large precipitation event in September 1974 (Fig. 12). Simulated total water storage increased above the total water storage corresponding to  $1 \text{ mm yr}^{-1}$  flux without a capillary barrier (191 mm) but remained below that corresponding to a capillary barrier (zero total head gradient, 312 mm; unit downward total head gradient, 412 mm). Monitoring and modeling analyses indicate that a 1-m-thick ET cover underlain by a capillary barrier should be adequate to minimize drainage to  $\leq 1 \text{ mm yr}^{-1}$  in these arid and semiarid settings.

## CONCLUSIONS

- Estimated drainage from water content data at the Texas site ( $0.4\text{--}5.0 \text{ mm yr}^{-1}$ ) corresponded to irrigation (226–2340 mm). Low drainage at the New Mexico site ( $0.1\text{--}0.4 \text{ mm yr}^{-1}$ ) was restricted to the first 2 yr of the 5-yr monitoring period.
- Vegetation plays a critical role in controlling the water balance of ET covers, as shown by the correspondence between rapid water storage decreases and enhanced vegetation productivity at both sites.
- Climate at the Texas and New Mexico sites is particularly suitable for ET covers because of the dominance of monsoonal precipitation in June through October (62–80% of annual precipitation) when ET rates are highest.
- Modeling analysis indicates that the measured water balance can generally be reproduced with the models. Simulating runoff is difficult and required calibration of surface saturated hydraulic conductivity at the Texas site.
- Extension of these models to 25-yr periods indi-

cates that there were critical precipitation events toward the end of the growing season in 1974 and 1984 at the Texas site that resulted in simulated drainage.

- Differences in long-term simulations between the Texas and New Mexico sites indicate that both climate forcing and hydraulic conductivity impact the simulated water balance. Low  $K_s$  in New Mexico subsoil was important in resulting in zero simulated drainage at this site.
- Sensitivity analyses indicated that simulated water balance was most sensitive to the presence or absence of vegetation and variations in hydraulic parameters at the Texas site but was much less sensitive to all parameters considered at the New Mexico site.
- Much wetter conditions in the ET covers relative to the natural system at the Texas site are attributed to addition of water for compaction and precipitation during construction of the covers.
- Monitoring and modeling analyses indicate that capillary barrier effects of the drainage lysimeters underestimate free drainage and overestimate water storage in the covers at the Texas site relative to systems that do not contain a capillary barrier. The reliability of the drainage estimates depends on how well the lysimeter capillary barrier replicates the actual system over the waste.
- Capillary barriers increased AWS at both sites by a factor of approximately 2.5 and precluded drainage for all simulated conditions, suggesting that a capillary barrier can provide a significant safety factor and should be considered in cover designs where technically and economically feasible.
- Limitations associated with monitoring drainage in systems without a capillary barrier underscore the need to monitor multiple parameters and integrate modeling to develop a predictive understanding of total system performance.
- Various limitations associated with monitoring and modeling, particularly drainage monitoring and vegetation modeling, should be addressed in future studies. The opportunistic behavior of vegetation would be simulated more realistically using two-way feedback between soil water storage and vegetation.

## ACKNOWLEDGMENTS

We would like to acknowledge financial support for this study provided by U.S. Department of Energy, the Jackson School of Geosciences, and technical and financial support provided by U.S. EPA (David Carson, Steve Rock, and Ken Skahn) and the Texas Low-Level Radioactive Waste Disposal Authority (Ruben Alvarado and Rick Jacobi).

## REFERENCES

- Albrecht, B.A., and C.H. Benson. 2001. Effect of desiccation on compacted natural clays. *J. Geotech. Geoenviron. Eng.* 127:67–75.
- Albright, W.H., C.H. Benson, G.W. Gee, T. Abichou, A.C. Roesler, and S.A. Rock. 2003. Examining the alternatives. *Civil Eng.* 73(5): 70–74.
- Anderson, J.E. 1997. Soil-plant cover systems for final closure of solid waste landfills in arid regions. p. 27–38. *In* T.D. Reynolds and

- R.C. Morris (ed.) Landfill capping in the semi-arid west: Problems, perspectives, and solutions. Environmental Science and Research Foundation, Idaho Falls, ID.
- Anderson, J.E., R.S. Nowak, T.D. Ratzlaff, and O.D. Markham. 1992. Managing soil moisture on waste burial sites in arid regions. *J. Environ. Qual.* 22:62–69.
- Andraski, B.J. 1997. Soil-water movement under natural-site and waste-site conditions: A multi-year field study in the Mojave Desert, Nevada. *Water Resour. Res.* 33:1901–1916.
- ASTM. 1995. D5856. Standard test method for measurement of hydraulic conductivity of saturated porous materials using a rigid wall compaction mold permeameter. ASTM, Philadelphia, PA.
- Dwyer, S.F. 2001. Finding a better cover. *Civil Eng.* 71(1):58–63.
- Dwyer, S.F. 2003. Water balance measurements and computer simulations of landfill covers. Ph.D. diss. Univ. of New Mexico, Albuquerque.
- Fayer, M.J. 2000. UNSAT-H Version 3.0: Unsaturated soil water and heat flow model, theory, user manual, and examples. PNNL Rep. 13249. Pacific Northwest Natl. Lab., Richland, WA.
- Fayer, M.J., M.L. Rockhold, and M.D. Campbell. 1992. Hydrologic modeling of protective barriers: Comparison of field data and simulation results. *Soil Sci. Soc. Am. J.* 56:690–700.
- Flint, A.L., G.S. Campbell, K.M. Ellet, and C. Calissendorff. 2002. Calibration and temperature correction of heat dissipation matrix potential sensors. *Soil Sci. Soc. Am. J.* 66:1439–1445.
- Grant, D.R. 1975. Measurement of soil moisture near the surface using a moisture meter. *J. Soil Sci.* 26:124–129.
- Greacen, E.L., R.L. Correll, R.B. Cunningham, G.G. Johns, and K.D. Nicolls. 1981. Calibration. p. 50–81. *In* E.L. Greacen (ed.) Soil water assessment by the neutron method. CSIRO, Adelaide, Australia.
- Hanson, C.L., K.A. Cumming, D.A. Woolhiser, and C.W. Richardson. 1994. Microcomputer program for daily weather simulation. USDA Agric. Res. Serv. Publ. ARS-114.
- Hauser, V.L., B.L. Weand, and M.D. Gill. 2001. Natural covers for landfills and buried waste. *J. Environ. Eng.* 127:768–775.
- Khire, M.V., C.H. Benson, and P.J. Bosscher. 1997. Water balance modeling of earthen final covers. *J. Geotech. Geoenviron. Eng.* 123:744–754.
- Khire, M.V., C.H. Benson, and P.J. Bosscher. 2000. Capillary barriers: Design variables and water balance. *J. Geotech. Geoenviron. Eng.* 126:695–708.
- Koerner, R.M., and D.E. Daniels. 1997. Final covers for solid waste landfills and abandoned dumps. ASCE, New York.
- Melchior, S. 1997. In situ studies on the performance of landfill caps. *Land Contam. Reclam.* 5:209–216.
- Meyer, P.D., and G.W. Gee. 1999. Flux-based estimation of field capacity. *J. Geotech. Geoenviron. Eng.* 125:595–599.
- Mualem, Y. 1976. A new model for predicting the hydraulic conductivity of unsaturated porous media. *Water Resour. Res.* 12:513–521.
- Nyhan, J.W., T.E. Hakonson, and B.J. Drennon. 1990. A water balance study of two landfill cover designs for semiarid regions. *J. Environ. Qual.* 19:281–288.
- Reedy, R.C., and B.R. Scanlon. 2003. Soil water content monitoring using electromagnetic induction. *J. Geotech. Geoenviron. Eng.* 129:1028–1039.
- Reith, C.C., and B.M. Thompson. 1992. Deserts as dumps? The disposal of hazardous materials in arid ecosystems. Univ. New Mexico Press, Albuquerque.
- Richardson, C.W. 2000. Data requirements for estimation of weather generation parameters. *Trans. ASAE* 43:877–882.
- Rockhold, M.L., M.J. Fayer, C.T. Kincaid, and G.W. Gee. 1995. Estimation of natural ground water recharge for the performance assessment of a low-level waste disposal facility at the Hanford site. PNL-10508. Battelle Pacific Northwest Natl. Lab., Richland, WA.
- Scanlon, B.R., M. Christman, R.C. Reedy, I. Porro, J. Simunek, and G. Flerschinger. 2002. Intercode comparisons for simulating water balance of surficial sediments in semiarid regions. *Water Resour. Res.* 38:1323–1339.
- Scanlon, B.R., K. Keese, R.C. Reedy, J. Simunek, and B.J. Andraski. 2003. Variations in flow and transport in thick desert vadose zones in response to paleoclimatic forcing (0–90 kyr): Field measurements, modeling, and uncertainties. *Water Resour. Res.* 39(7):1179. doi:10.1029/2002WR001604.
- Scanlon, B.R., R.P. Langford, and R.S. Goldsmith. 1999. Relationship between geomorphic settings and unsaturated flow in an arid setting. *Water Resour. Res.* 35:983–999.
- Schaap, M.G., and F.J. Leij. 1998. Database-related accuracy and uncertainty of pedotransfer functions. *Soil Sci.* 163:765–779.
- Schaap, M.G., F.J. Leij, and M.Th. van Genuchten. 1998. Neural network analysis for hierarchical prediction of soil hydraulic properties. *Soil Sci. Soc. Am. J.* 62:847–855.
- Simunek, J., M. Sejna, and M.Th. van Genuchten. 1998. The HYDRUS-1D software package for simulating the one-dimensional movement of water, heat, and multiple solutes in variably-saturated media. Version 2.0. IGWMC-TPS-70. International Groundwater Modeling Center, Colorado School of Mines, Golden, CO.
- Stormont, J.C., and C. E. Morris. 1998. Method to estimate water storage capacity of capillary barriers. *J. Geotech. Geoenviron. Eng.* 124:297–302.
- USEPA. 1996. List of municipal solid waste landfills. EPA/530/R-96/006. EPA Office of Solid Waste and Emergency Response, Washington, DC.
- USEPA. 1997. Resource Conservation and Recovery Act Information System (RCRAIS) database, EPA National Oversight Database.
- Waugh, W.J., M.E. Thiede, D.J. Bates, L.L. Caldwell, G.W. Gee, and C.J. Kemp. 1994. Plant cover and water balance in gravel admixtures at an arid waste-burial site. *J. Environ. Qual.* 23:676–685.
- Wing, N.R., and G.W. Gee. 1994. Quest for the perfect cap. *Civil Eng.* 64:38–41.



# Uncertainties in estimating water fluxes and residence times using environmental tracers in an arid unsaturated zone

Bridget R. Scanlon

Bureau of Economic Geology, University of Texas at Austin

**Abstract.** Environmental tracers are used widely to evaluate flow processes and estimate fluxes and ages of pore water in arid regions. The purpose of this study was to evaluate uncertainties in water flux and age on the basis of data from environmental tracers, including meteoric Cl,  $^{36}\text{Cl}$ ,  $^3\text{H}$ ,  $\delta^2\text{H}$ , and  $\delta^{18}\text{O}$  in porous media. Representative profiles of environmental tracers from drainage and interdrainage areas at a site in the Chihuahuan Desert of Texas were evaluated. The chloride mass balance approach (CMB) was used to evaluate water fluxes and ages. The long residence times indicated by the Cl data in interdrainage areas (55,000 to 105,000 years to 25 m depth) were generally corroborated by residence times estimated from radioactive decay of  $^{36}\text{Cl}$  ( $39,000 \pm 13,000$  to  $59,000 \pm 14,400$  years). Uncertainties in the CMB approach include uncertainties in transport processes, Cl input, and Cl output. Although the CMB approach assumes one-dimensional, downward piston flow, water potential and stable isotope data in interdrainage areas suggest net upward water movement. Cl data indicate that drying of the profiles may have persisted throughout the Holocene ( $\sim 10,000$  years). Therefore the downward flow assumption may only be applicable in the older, deeper sections of the profiles. Cl diffusion is significant near the surface where Cl concentration gradients are steep. Anion exclusion may affect calculated water fluxes based on Cl in clay-rich zones. Although it is difficult to quantify uncertainties in diffusion and anion exclusion processes, they act in concert and result in overestimation of water flux and underestimation of age by the CMB approach. Therefore, in interdrainage areas the CMB approach provides an upper bound on actual water fluxes and a lower bound on actual ages. Error bars on these bounding estimates were evaluated on the basis of uncertainties in Cl input ( $\sim \pm 35\%$ ) and in Cl output ( $\pm 3\%$ ) that result in  $\pm 38\%$  uncertainty in water flux and  $-24$  to  $56\%$  uncertainty in water age in interdrainage areas. In drainage areas it is much more difficult to apply the CMB approach because of preferential flow, large uncertainties in Cl input as a result of run-on, reduced sensitivity of Cl to water flux, and analytical uncertainties in Cl measurements. Although preferential flow was shown by  $^3\text{H}$  data, mixing calculations suggest that  $^{36}\text{Cl}/\text{Cl}$  ratios cannot be used to evaluate preferential flow when Cl concentrations in the matrix exceed  $10$  to  $100 \text{ g m}^{-3}$ , as is found in the playa and the fissure. Neglecting Cl input from run-on results in underestimation of water flux by about an order of magnitude. Therefore the apparent CMB water flux, which ignores preferential flow and run-on, represents a lower bound on the actual water flux in contrast to an upper bound for interdrainage areas. These results have important implications for waste disposal in arid regions because they suggest that water fluxes estimated using the CMB approach are conservatively high in interdrainage areas characterized by porous media.

## 1. Introduction

Interest in water flux through thick, unsaturated zones in arid regions has increased greatly in the last couple of decades because of concerns about waste disposal, including proposed low-level and high-level radioactive waste disposal sites in the United States, and groundwater contamination, such as at the Hanford Reservation in Washington, Sandia National Laboratory in New Mexico, and other sites. With increased development of arid regions, water-resource concerns have also become important, and recharge to the underlying aquifers has become critical to maintaining current and proposed development in these regions.

Many techniques for quantifying long-term net water fluxes and residence times or ages of pore water in arid systems rely on environmental tracers [Allison *et al.*, 1994; Phillips, 1994]. There are, however, various sources of uncertainty related to estimating water fluxes and ages from tracer data. Evaluation of water fluxes and ages from tracer data is an inverse process that involves inferring or assuming the tracer input and transport processes required to produce the measured tracer output. Tracer output, which corresponds to the subsurface distribution of tracers, is generally measured. Uncertainties related to analytical measurements of tracer-output concentrations are readily evaluated. Such uncertainties generally reflect the precision of laboratory measurements and not accuracy, which is determined by how well calibrated an instrument is with respect to some absolute or defined standard. The measured tracer concentration is assumed to represent the average

Copyright 2000 by the American Geophysical Union.

Paper number 1999WR900240.  
0043-1397/00/1999WR900240\$09.00

in situ concentration of the infiltrating water at the sampled depth. Uncertainties associated with tracer input are generally more difficult to quantify. The validity of estimated transport processes will also result in uncertainties in estimated water fluxes and ages. In some cases, more than one conceptual model can result in the same tracer distribution, and we have to rely on corroborative evidence from other tracers or physical data to discriminate between different models and resolve non-unique problems.

The chloride mass balance (CMB) approach has been used in many studies to quantify water fluxes and ages [Allison and Hughes, 1978]. Water flux in the unsaturated zone can be estimated from the degree of Cl enrichment in pore water as a result of evapotranspiration relative to the Cl concentration in precipitation. Uncertainties associated with the CMB approach include uncertainties in the Cl input to the system, in transport processes, and in Cl output or Cl concentrations measured in pore water. Applications of the CMB approach assume that the transport process is approximated by one-dimensional (1-D), downward piston flow. Although the CMB approach assumes downward water movement, water-potential measurements in interdrainage areas of many basins in the southwestern United States indicate that the driving force for water movement is upward in the top 20 to 40 m [Scanlon *et al.*, 1997b]. In addition to water-potential data, stable isotope data from the Nevada Test Site also indicate upward water movement since the last glacial cycle [Tyler *et al.*, 1996]. The effect of upward flow should be examined further with respect to Cl profiles in arid settings.

Various factors may cause violation of the piston flow assumption. The term piston flow, or plug flow, refers to uniform displacement of water in the unsaturated zone by infiltrating water where hydrodynamic dispersion and preferential flow are insignificant. Hydrodynamic dispersion includes the effects of mechanical dispersion as a result of microscopic water-velocity variations and molecular diffusion. Field studies have indicated that in many cases hydrodynamic dispersion minimally affected the results of their studies [Allison and Hughes, 1978; Murphy *et al.*, 1996; Ginn and Murphy, 1997]. However, low water fluxes and long timescales in arid settings can result in diffusion being important, as shown by Peck *et al.* [1981] and Cook *et al.* [1992]. Anion exclusion occurs when Cl is excluded from water associated with the diffuse double layer and only moves in free water. Preferential flow refers to nonuniform water movement in which much of the unsaturated zone is bypassed. Preferential flow is common in fractured rocks, such as fractured tuff at Yucca Mountain [Yang *et al.*, 1996; Fabryka-Martin *et al.*, 1998] and fractured chalk in the Negev Desert [Nativ *et al.*, 1995]. In these fractured systems, preferential flow is generally inferred from deep penetration of bomb-pulse tracers such as  $^{36}\text{Cl}$  and  $^3\text{H}$  to 440-m depth at Yucca Mountain and bomb-pulse  $^3\text{H}$  to 12-m depth at the Negev site. These observations indicate that some of the assumptions associated with the Cl transport process may not be valid. This could result in greatly increased uncertainties in estimated fluxes and ages of pore water. These assumptions should be questioned and tested if necessary at all field sites. Potential problems with the CMB technique underscore the need for independent techniques for estimating water fluxes and dating pore water in arid unsaturated zones.

Several tracers have been used to evaluate flow in thick vadose zones. Chlorine 36 (half-life of 301,000 years) has been used to a limited extent to date pore water in arid unsaturated

zones over timescales ranging from decades to thousands of years and to evaluate preferential flow. Tritium (half life of 12.4 years) has also been used to date pore water up to 40 years old and to evaluate preferential flow. Natural  $^3\text{H}$  abundance ranges from about 5 to 10 tritium units (TU) in precipitation in the Northern Hemisphere. Tritium concentrations increased to  $\geq 2000$  TU during atmospheric nuclear testing [International Atomic Energy Agency, 1983] from 1952 through 1963 in the Northern Hemisphere. Stable isotopes of oxygen and hydrogen are useful in determining the direction of water movement and in estimating upward water fluxes as a result of evaporation.

The primary objective of this study was to evaluate uncertainties in estimating water fluxes and dating pore water in arid unsaturated zones, with particular emphasis on the accuracy of the CMB technique. Radioactive decay of  $^{36}\text{Cl}$  was also examined to date pore water. Uncertainties in input, transport processes, and output for meteoric Cl were evaluated using information from Cl and other tracers and hydraulic data. An in-depth analysis of transport processes was conducted by using water-potential and stable isotope data to determine flow direction, and bomb  $^3\text{H}$  and bomb  $^{36}\text{Cl}$  were used to evaluate preferential flow. In this study, representative Cl profiles from drainage and interdrainage settings in Eagle Flat basin in the Chihuahuan Desert of Texas were used.

## 2. Site Description

The Eagle Flat basin is a sediment-filled basin within the Basin and Range physiographic province [Scanlon *et al.*, 1999a, b]. The mineralogy of the sediment fill includes quartz, feldspar, amphibole, and calcite derived from Precambrian metamorphic rocks, Permian and Cretaceous sandstones and limestones, and Tertiary volcanic rocks [Jackson *et al.*, 1993]. The unsaturated zone ranges from 198 to 230 m in thickness in the basin. The regional climate is subtropical arid [Larkin and Bomar, 1983]. Mean annual precipitation is 320 mm derived from a 30-year record.

The main geomorphic features are the drainage system, including Blanca Draw and Grayton Lake playa; interdrainage areas, including basin-fill deposits and eolian sheets; and localized topographic depressions, such as a fissure in the interdrainage area [Scanlon *et al.*, 1999a, b]. Blanca Draw, the axial drainage system for Eagle Flat basin, drains into Grayton Lake playa (20 km<sup>2</sup>), an ephemeral playa that was flooded between May 1992 and October 1993. When not flooded, it is sparsely vegetated. The floor of the playa consists of clay containing mud cracks resulting from shrink/swell of the sediment. An earth fissure, found in the interdrainage area, has a surface expression of about 640 m in length. Water ponds occasionally in this fissure. The fissure, or gully, is underlain by a tension fracture. The fracture extends to a depth of at least 3.5 m; however, the maximum vertical extent is unknown because dug trenches did not reach the base of the fracture.

## 3. Methods

### 3.1. Theory

Quantitative interpretation of Cl concentrations is based on applying the continuity equation to Cl transport through the unsaturated zone, which assumes that Cl in the liquid phase does not partition into the solid or gas phases and that Cl is conservative (i.e., no subsurface sources or sinks). A simple form of the CMB approach is generally applied at most sites:

$$q_w = J_{Cl}/c_{Cluz} = P c_{Clp}/c_{Cluz}, \quad (1)$$

where  $q_w$  is the volumetric water flux below the root zone ( $L T^{-1}$ ),  $J_{Cl}$  is the Cl mass flux or Cl deposition flux at the surface (input ( $M L^{-2} T^{-1}$ )),  $c_{Cluz}$  is the pore water Cl concentration in the unsaturated zone (output ( $M L^{-3}$ )),  $P$  is precipitation ( $L T^{-1}$ ), and  $c_{Clp}$  is the Cl concentration in precipitation (assumed to include dry fallout ( $M L^{-3}$ )). The Cl mass flux at the surface includes Cl in precipitation and dry fallout. Many precipitation collectors include wet and dry fallout. According to this simplified CMB approach the transport process for Cl is assumed to be 1-D, downward piston transport, and the Cl input is assumed to be constant at the surface.

The age or residence time ( $t$ ) represented by Cl at depth  $z$  can be evaluated by dividing the cumulative total mass of Cl from the surface to that depth by the annual Cl input:

$$t = \frac{1}{J_{Cl}} \int_0^{z_i} \theta(z) c_{Cluz}(z) dz = \frac{1}{J_{Cl}} \int_0^z \rho_b(z) M_{Cluz}(z) dz, \quad (2)$$

where  $\theta$  is the volumetric water content ( $L^3 L^{-3}$ ),  $\rho_b$  is the dry bulk density ( $M L^{-3}$ ), and  $M$  is the mass of Cl per mass of dry soil ( $M M^{-1}$ ). The assumptions for estimating age are similar to those for estimating flux with the exception that flow can be upward or downward.

Chlorine 36 has been used to date pore water and to evaluate preferential flow in arid unsaturated zones. Chlorine 36 is produced naturally in the atmosphere [Bentley *et al.*, 1986]. Estimates of water residence time over three different time-scales can be calculated from chlorine 36 data. (1) Bomb-pulse  $^{36}Cl/Cl$  ratios have been used to estimate water fluxes up to 40 years old and to evaluate preferential flow [Phillips *et al.*, 1988; Scanlon, 1992; Fabryka-Martin *et al.*, 1993, 1998]. Nuclear weapon tests conducted in the Pacific between 1952 and 1958 resulted in  $^{36}Cl$  concentrations in rainfall that were up to 1000 times greater than natural fallout levels [Bentley *et al.*, 1986]. (2) Variations in  $^{36}Cl/Cl$  ratios during the past 40,000 years may also be used as a tracer of water movement [Plummer *et al.*, 1997]. The temporal variations in  $^{36}Cl/Cl$  ratios are attributed either to variations in cosmogenic production of  $^{36}Cl$ , which is inversely related to Earth's magnetic field intensity, or to a shift in the jet stream, which determines the latitude at which the peak  $^{36}Cl/Cl$  deposition rate occurs. The  $^{36}Cl/Cl$  ratios were measured in fossil urine from pack rat middens in Nevada, which were dated by  $^{14}C$  from 38,000 years to present. These data showed increases in  $^{36}Cl/Cl$  ratios up to 150 to 200% higher than modern prebomb ratios earlier than 10,000 years ago and ranged from 50 to 100% of modern prebomb ratios during the past 10,000 years. Comparison of the reconstructed  $^{36}Cl$  production with variations in  $^{36}Cl/Cl$  in pore water has been used to estimate ages of water at the Nevada Test Site [Tyler *et al.*, 1996]. (3) Radioactive decay of  $^{36}Cl$  can also be used to estimate water ages up to 1,000,000 years. The residence time of the pore water ( $t$ ) is calculated as follows:

$$t = -\frac{1}{\lambda_{36}} \ln \frac{R - R_{se}}{R_0 - R_{se}} \quad (3)$$

where  $\lambda_{36}$  is the decay constant for  $^{36}Cl$  ( $2.30 \times 10^{-6} \text{ yr}^{-1}$ ),  $R$  is the measured  $^{36}Cl/Cl$  ratio,  $R_{se}$  is the secular equilibrium  $^{36}Cl/Cl$  ratio ( $\sim 10 \times 10^{-15}$ ) [Bentley *et al.*, 1986], and  $R_0$  is the initial  $^{36}Cl/Cl$  ratio.

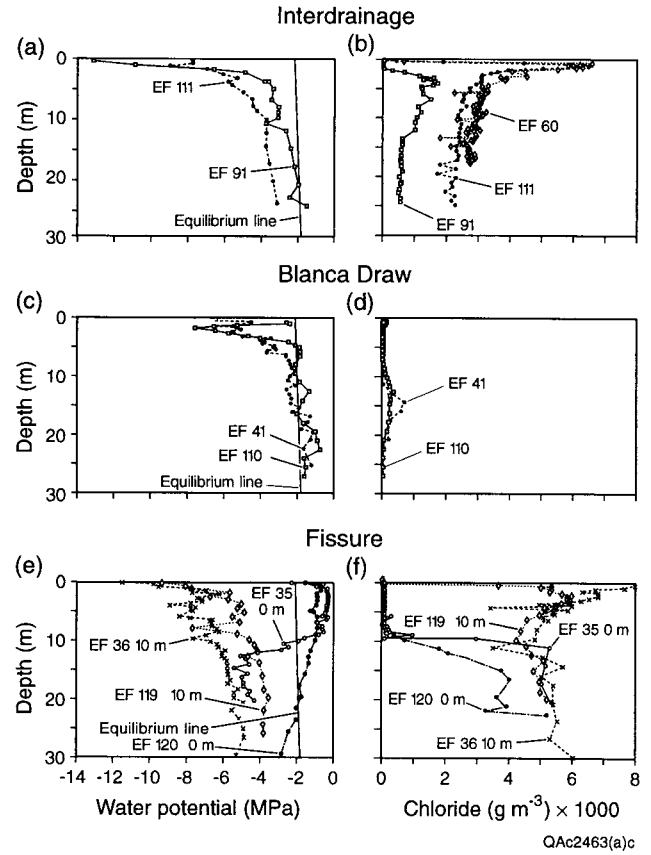


**Figure 1.** (a, c, and e) Water potential and (b, d, and f) Cl concentrations in pore water in interdrainage profiles (EF 60, EF 91, and EF 111), drainage profiles (Blanca Draw EF 41 and EF 110), and fissure (EF 35, EF 36, EF 119, and EF 120). The equilibrium line represents the no-flow line in which water potential and gravitational potential are balanced (i.e., water potential equals negative gravitational potential).

### 3.2. Field and Laboratory Procedures

Representative profiles of environmental tracers from a maximum of 50 different profiles from the Eagle Flat basin described by Scanlon *et al.* [1999a, b] were used to evaluate uncertainties in estimating water flux and dating pore water. Sediment samples from these boreholes were analyzed for water content, water potential, and Cl (Figure 1). Gravimetric water content was determined by weighing and oven drying the samples at 105°C for 24 hours. This procedure may have resulted in removal of some bound water from clays. Water potential was measured in the laboratory using a thermocouple psychrometer with sample changer (model SC-10A, Decagon Devices, Inc., Pullman, Washington). To determine Cl content, double-deionized water was added to the dried sediment sample in a 3:1 ratio by weight. Samples were agitated on a reciprocal shaker table for 4 hours. The supernatant was filtered through 0.45- $\mu m$  filters. Cl was then analyzed by ion chromatography (IC) for concentrations generally  $\leq 20 \text{ g m}^{-3}$  or by potentiometric titration for concentrations generally  $> 20 \text{ g m}^{-3}$ . Cl concentrations are expressed as grams of Cl per cubic meter of pore water (equivalent to milligrams of Cl per liter of pore water). Cl/Br ratios were measured in 14 samples from the surface to 21 m depth from borehole EF 61. Both ions were analyzed using IC by HydroGeoChem Inc. (Tucson, Arizona).



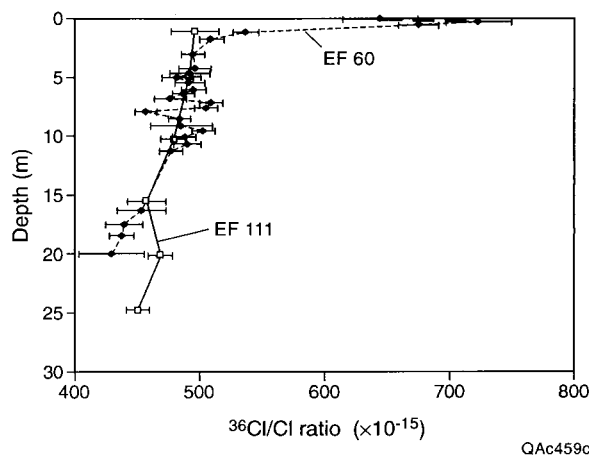


**Figure 2.** Vertical  $^{36}\text{Cl}/\text{Cl}$  profiles in interdrainage areas (EF 60 and EF 111). Error bars represent  $1\sigma$  analytical uncertainties in  $^{36}\text{Cl}/\text{Cl}$  measurements calculated according to *Elmore et al.* [1984].

Cl and Br concentrations were measured by IC by Los Alamos National Laboratory in 16 precipitation samples collected at the site approximately monthly during 1996 and 1997. Some months had no rain.

The  $^{36}\text{Cl}/\text{Cl}$  ratios were measured in samples from boreholes EF 60, EF 111 (interdrainage area), EF 92, EF 96 (beneath and 10 m from fissure), and GL 2 (Grayton Lake playa) by accelerator mass spectrometry at Lawrence Livermore National Laboratory according to procedures outlined by *Elmore et al.* [1979]. Preparation of  $^{36}\text{Cl}$  samples for analysis followed procedures outlined by *Mattick et al.* [1987].

Samples for  $^3\text{H}$  analysis were collected from boreholes EF 79, EF 117 (interdrainage area), EF 92, EF 96 (beneath and 10 m from fissure), and GL 2 (Grayton Lake playa). The water was extracted from the core samples in the laboratory by toluene azeotropic distillation. The pore water samples were electrolytically enriched and analyzed by liquid scintillation at the University of Arizona Tritium Laboratory or by gas proportional counting at the University of Miami Tritium Laboratory.

Water was analyzed for  $\delta^2\text{H}$  and  $\delta^{18}\text{O}$  by the Desert Research Institute (University of Nevada, Las Vegas) on samples from EF 64, EF 91, EF 113 (interdrainage area), GL 2 (Grayton Lake), GL 4 (adjacent to Grayton Lake), EF 92, and EF 96 (beneath and 10 m from fissure) and on 16 precipitation samples collected during 1996 and 1997. Water was extracted for analysis from approximately 100 g of sediment by toluene extraction [*Ingraham and Shadel*, 1992]. Results of isotopic analysis are reported in standard delta notation, with respect to Vienna standard mean ocean water (VSMOW).

## 4. Results and Discussion

Representative Cl profiles in interdrainage and drainage areas and beneath the fissure from the Eagle Flat basin were used to evaluate water fluxes and ages. Borehole locations and detailed results of all sampling are given by *Scanlon et al.* [1999a, b]. Residence times based on  $^{36}\text{Cl}/\text{Cl}$  ratios are discussed first, then uncertainties related to the CMB technique are evaluated, including uncertainties in Cl input and Cl output and in transport mechanisms. The effect of these uncertainties on water fluxes and ages calculated by the CMB technique is then described.

### 4.1. Residence Time Based on $^{36}\text{Cl}$ Data

Detailed sampling for  $^{36}\text{Cl}$  analysis was conducted in EF 60 to test for variations in  $^{36}\text{Cl}/\text{Cl}$  ratios (Figure 2). The CMB age for this profile is 91,000 years at 17.5 m depth (equation (2)) on the basis of a Cl input of  $87\text{ mg m}^{-2}\text{ yr}^{-1}$  that is discussed in section 4.2. This CMB age spans the time period in which secular variations in  $^{36}\text{Cl}/\text{Cl}$  were suggested by *Plummer et al.* [1997]. These variations were attributed either to variations in cosmogenic production of  $^{36}\text{Cl}$  or to a shift in the jet stream. Measured  $^{36}\text{Cl}/\text{Cl}$  ratios in the EF 60 profile were decay corrected according to the CMB age and compared with measured  $^{36}\text{Cl}/\text{Cl}$  ratios in urine from pack rat middens in Nevada and with the reconstructed  $^{36}\text{Cl}/\text{Cl}$  [*Guyodo and Valet*, 1996] and  $^{14}\text{C}$  production [*Plummer et al.*, 1997] (Figure 3). There is no systematic variation in  $^{36}\text{Cl}/\text{Cl}$  ratios over this time in the EF 60 profile. Either the deposition flux of  $^{36}\text{Cl}/\text{Cl}$  did not vary over this time at this location, or the variations were not preserved in this profile, possibly because of diffusion. The effect of diffusion is discussed in more detail in section 4.3.4. Although sampling for  $^{36}\text{Cl}$  in the EF 111 profile is less detailed than that in EF 60, decay-corrected  $^{36}\text{Cl}/\text{Cl}$  ratios from EF 111 also do not vary over time. Therefore variations in cosmogenic production of  $^{36}\text{Cl}$  could not be used to date pore water in this basin.

Use of radioactive decay of  $^{36}\text{Cl}$  to date pore water was also evaluated. High  $^{36}\text{Cl}/\text{Cl}$  ratios ( $537\text{--}723 \times 10^{-15}$ ) in the upper 1.2 m of the EF 60 profile probably reflect the tail of the bomb-pulse signal (Figure 2). Ratios of  $^{36}\text{Cl}/\text{Cl}$  do not vary systematically from 1.8- to 10.7-m depth and have a mean value of  $491 \times 10^{-15} \pm 12 \times 10^{-15}$  in this zone. Ratios of  $^{36}\text{Cl}/\text{Cl}$  decrease gradually from  $491 \times 10^{-15}$  at 10.7-m depth to  $430 \times 10^{-15}$  at 20-m depth. Assuming the decrease is due solely to radioactive decay, then the residence time of the pore water corresponding to this decay is 59,000 years. This decay age compares favorably with the CMB age of 55,000 years for the same depth interval. Propagation of errors resulting from  $1\sigma$  uncertainties in the  $^{36}\text{Cl}/\text{Cl}$  analyses results in a  $1\sigma$  uncertainty in age of 28,700 years (Appendix A). The analytical uncertainty associated with the  $^{36}\text{Cl}/\text{Cl}$  ratio at 20-m depth is unusually high at 6%, whereas that for 70% of the samples and the next shallower sample is 2%. This reduction in analytical uncertainty would reduce the uncertainty in age to 14,400 years. The  $^{36}\text{Cl}/\text{Cl}$  ratios decreased from  $491 \times 10^{-15}$  at 5-m depth in EF 111 in the interdrainage area to  $450 \times 10^{-15}$  at 25-m depth, which suggests a residence time of  $39,000 \pm 13,000$  years, based on radioactive decay. The residence time is much less than that estimated by CMB analysis (105,000 years) for the EF 111 profile. The discrepancy between decay age and CMB age for the EF 111 profile probably reflects uncertainties in both techniques.

It may be argued that the decay of  $^{36}\text{Cl}$  with depth and the calculated ages are not significant because of the large errors in the  $^{36}\text{Cl}/\text{Cl}$  ratios; however, the slopes of the lines relating  $^{36}\text{Cl}/\text{Cl}$  ratios and age to depth were significantly different from 0 in both profiles ( $\alpha = 0.05$ ) [*Taylor*, 1982]. Increases in the deposition flux of  $^{36}\text{Cl}$  by up to a factor of 2, as suggested by data from Nevada [*Plummer et al.*, 1997], or subsequent diffusion of the  $^{36}\text{Cl}$  would result in increased decay ages. The residence times based on radioactive decay of  $^{36}\text{Cl}$  ( $39,000 \pm 13,000$  to  $59,000 \pm 14,400$  years) represent the lower limit of applicability of this technique because of analytical uncertainties in the measurement of  $^{36}\text{Cl}/\text{Cl}$  ratios (Figure 4). Percent



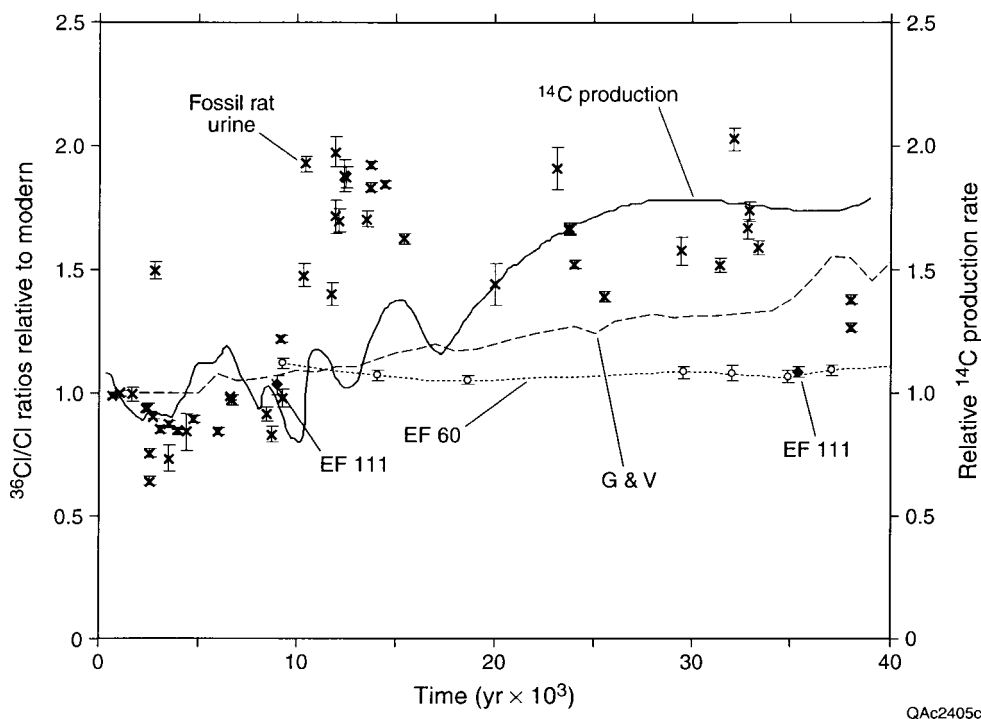


**Figure 3.** Decay-corrected  $^{36}\text{Cl}/\text{Cl}$  ratios using the chloride mass balance age relative to the modern  $^{36}\text{Cl}/\text{Cl}$  ratio at the site ( $491 \times 10^{-15}$ ) in interdrainage areas (EF 60 and EF 111);  $^{36}\text{Cl}/\text{Cl}$  ratios in urine from pack rat middens; reconstructed  $^{36}\text{Cl}/\text{Cl}$  ratios [Guyodo and Valet, 1996]; and reconstructed  $^{14}\text{C}$  production (based on Plummer *et al.* [1997]) from cosmic production as influenced by variations in the geomagnetic field intensity.

uncertainty in residence time increases sharply as residence time decreases. The  $^{36}\text{Cl}/\text{Cl}$  radioactive decay data are used only as corroborative evidence for the CMB ages in this study. Both techniques indicate long pore water residence times in interdrainage settings.

#### 4.2. Uncertainties in Cl Input and Output

Cl input or Cl mass deposition flux can be estimated from (1)  $^{36}\text{Cl}$  data or (2) direct measurements of Cl concentrations in precipitation and dry fallout multiplied by the mean annual precipitation ( $320 \text{ mm yr}^{-1}$ ). The Cl input ( $87 \text{ mg m}^{-2} \text{ yr}^{-1}$ ) was calculated by dividing the atmospheric fallout of  $^{36}\text{Cl}$  ( $^{36}\text{Cl}_a$ ) for the latitude of the site ( $23 \text{ atoms m}^{-2} \text{ s}^{-1}$  [Bentley

*et al.*, 1986]) by the measured prebomb  $^{36}\text{Cl}/\text{Cl}$  ratio (samples from 1.8 to 10.7 m in borehole EF 60 ( $491 \times 10^{-15}$ ,  $^{36}\text{Cl}/\text{Cl}_0$ )) according to the following equation:

$$J_{\text{Cl}} = \frac{^{36}\text{Cl}_a (\text{atoms m}^{-2} \text{ s}^{-1}) (31.558 \times 10^6 \text{ s yr}^{-1}) (35.5 \times 10^3 \text{ mg mol}^{-1})}{^{36}\text{Cl}/\text{Cl}_0 (6.023 \times 10^{23} \text{ atoms mol}^{-1})} \quad (4)$$

This Cl input ( $87 \text{ mg m}^{-2} \text{ yr}^{-1}$ ) is similar to values estimated by Phillips [1994] for sites in New Mexico ( $75$  to  $125 \text{ mg m}^{-2} \text{ yr}^{-1}$ ) and is equivalent to a Cl concentration in precipitation and dry fallout of  $0.27 \text{ g m}^{-3}$  that is based on a long-term mean annual precipitation of  $320 \text{ mm}$ . In this study, Cl concentrations in precipitation and dry fallout were measured approximately monthly for only 2 years and resulted in a precipitation-weighted average Cl concentration of  $0.14 \pm 0.03 \text{ g m}^{-3}$  (equal to Cl deposition flux of  $45 \text{ mg m}^{-2} \text{ yr}^{-1}$ ), which is about half that estimated from the  $^{36}\text{Cl}$  data ( $0.27 \text{ g m}^{-3}$ ). The Cl input estimated from the  $^{36}\text{Cl}$  data is considered more valid for this study than direct measurements of Cl in precipitation and dry fallout because it represents a long time period.

Because sediments in the Eagle Flat basin are alluvial and eolian in origin, it is unlikely that there are any sources of Cl in the subsurface. Cl concentrations in pore water are much lower than those at which halite would precipitate from a saline brine ( $\sim 220,000 \text{ g m}^{-3}$  [Holser, 1979]); therefore it is unlikely that there is any Cl in the solid phase. Cl/Br ratios measured in samples from EF 61 in an interdrainage area (92 to 150) are similar to measured Cl/Br ratios in precipitation (24 to 167) and are typical of meteoric Cl [Davis *et al.*, 1998]. In contrast,

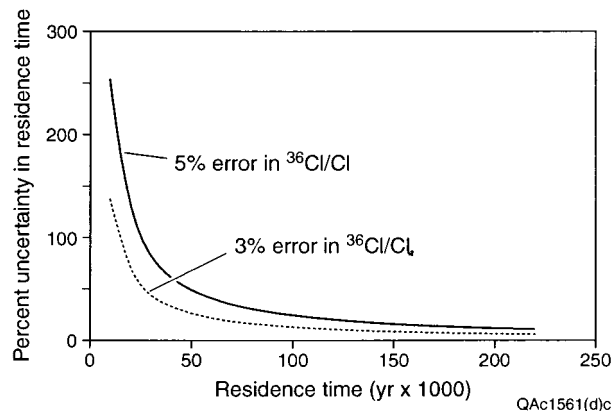


**Figure 4.** Uncertainties in pore water residence time as a result of analytical uncertainties ( $1 \sigma$ ) in  $^{36}\text{Cl}/\text{Cl}$  measurements (Appendix A).

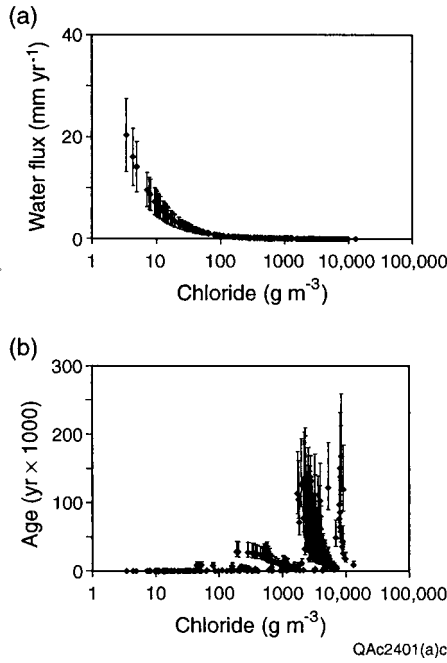


**Figure 5.** Uncertainties in (a) water flux and (b) age resulting from  $\pm 35\%$  uncertainty in Cl input in samples from profiles in drainage and fissure areas (EF 94, EF 110, EF 120, and GL 2) and interdrainage (EF 28, EF 60, EF 66, EF 91, and EF 111) areas.

Cl/Br ratios in samples affected by halite dissolution typically range from 1000 to 10,000 [Davis *et al.*, 1998]. The low Cl/Br ratios in the study area also preclude the Salt Flat playa ( $\sim 25$  km northeast of the site) as a source of airborne Cl at the site. Studies by Reheis and Kihl [1995] and Wood and Sanford [1995b] suggest that most of the salt removed by deflation of playas is deposited close to the source. The  $^{36}\text{Cl}/\text{Cl}$  ratio measured in a salt sample was  $88 \times 10^{-15}$ , which is lower than the ratios in any of the profiles in the study area ( $383$  to  $723 \times 10^{-15}$ ) and suggests negligible contribution of Cl from the Salt Flat. The Cl sample from the Salt Flat was derived partly from Permian salt, which has no  $^{36}\text{Cl}$ . The low ratio is attributed to mixing of this Permian Cl with meteoric  $^{36}\text{Cl}$  in the groundwater and in situ production near the surface because of capture of cosmogenic neutrons [Fabryka-Martin, 1988]. The low ratio is similar to  $^{36}\text{Cl}/\text{Cl}$  ratios measured in salt basins ( $< 100 \times 10^{-15}$  [Phillips *et al.*, 1995]).

Uncertainties in the Cl input were estimated from uncertainties in the atmospheric fallout of  $^{36}\text{Cl}$  and in the measured prebomb  $^{36}\text{Cl}/\text{Cl}$  ratios. Theoretical estimates of natural  $^{36}\text{Cl}$  fallout calculated by Lal and Peters [1967] are lower by a factor of 0.7 than those estimated by Bentley *et al.* [1986]. Estimates of  $^{36}\text{Cl}$  fallout are being revised by Phillips [1999] to include variations in  $^{36}\text{Cl}$  fallout with precipitation [Hainsworth *et al.*, 1994; Knies, 1995]. Although revised  $^{36}\text{Cl}$  fallout estimates differ markedly from original estimates by Bentley *et al.* [1986] in many areas, the two estimates are almost identical at our site [Phillips, 1999]. The uncertainty in  $^{36}\text{Cl}$  fallout is therefore estimated to be about 30%, which is based on the 30% difference between fallout estimated by Lal and Peters [1967] and fallout estimated by Bentley *et al.* [1986] and Phillips [1999]. Uncertainties in prebomb  $^{36}\text{Cl}/\text{Cl}$  ratios are much less than uncertainties in atmospheric fallout of  $^{36}\text{Cl}$ . The prebomb

$^{36}\text{Cl}/\text{Cl}$  ratios in widely separated profiles in Eagle Flat basin (EF 60 and EF 111,  $\sim 2$  km apart) are essentially the same ( $491 \times 10^{-15}$ ). Uncertainty in the prebomb ratio ( $\sim 5\%$ ) includes analytical uncertainty in  $^{36}\text{Cl}/\text{Cl}$  measurements ( $\sim 3\%$ ) and uncertainty around the mean value calculated for the EF 60 profile from 1.8- to 10.7-m depth ( $1\sigma = 2\%$ ). The combined effect of errors in  $^{36}\text{Cl}$  fallout (30%) and in prebomb  $^{36}\text{Cl}/\text{Cl}$  ratios (5%) results in 35% uncertainty in Cl input. The relationship between water flux and Cl input is linear (equation (1)); therefore  $\pm 35\%$  uncertainty in Cl input results in  $\pm 35\%$  uncertainty in the water flux. The inverse relationship between age and Cl input results in asymmetric error bars in age from uncertainty in Cl input that range from  $-26$  to  $54\%$  (Figure 5 and Table 1) (see Appendix B).

Uncertainties in Cl input are much greater in drainage areas because the amount of run-on and Cl concentrations in run-on are unknown. Cl concentrations in run-on are expected to be greater than those in precipitation because of leaching of Cl from surface soils. The simple CMB equation was modified by Wood and Sanford [1995a] to include the effects of run-on into playas

$$q_w = \frac{Pc_{\text{ClP}}}{c_{\text{Cluz}}} + R_{\text{on}}(A_b c_{\text{ClR}_{\text{on}}}/A_f c_{\text{Cluz}}), \quad (5)$$

where  $c_{\text{ClR}_{\text{on}}}$  is Cl concentration in run-on,  $R_{\text{on}}$  is run-on,  $A_b$  is area of the basin, and  $A_f$  is area of the playa floor. Applying (5) to Grayton Lake playa ( $R_{\text{on}} \sim 10\%$  of precipitation,  $A_b$ , 500 km<sup>2</sup>;  $A_f$  is 20 km<sup>2</sup>;  $c_{\text{ClR}_{\text{on}}}$  is  $\sim 5$  times that in precipitation ( $1.4 \text{ g m}^{-3}$ )) results in an order of magnitude increase in the water flux. Similar order-of-magnitude increases in water flux were estimated for playas in north central Texas by including run-on [Scanlon and Goldsmith, 1997]. Many of the parameters in (5) are highly uncertain, such as the amount of run-on, the area contributing run-on, and the Cl concentration in run-on. Water fluxes estimated from the simple CMB approach (equation (1)), which ignores run-on, may underestimate actual water fluxes in arid regions by an order of magnitude (Table 1). Ignoring run-on will result in overestimation of age by about an order of magnitude also, as shown in the following equation:

$$t = \int_0^z \theta c_{\text{Cluz}} dz / Pc_{\text{ClP}} + R_{\text{on}} \left( \frac{A_b c_{\text{ClR}_{\text{on}}}}{A_f c_{\text{Cluz}}} \right) c_{\text{Cluz}}, \quad (6)$$

Uncertainties in Cl output result from analytical uncertainties in Cl measurements. Cl concentrations in the supernatant of less than  $20 \text{ mg L}^{-1}$  were generally measured by ion chromatography ( $\pm 0.1 \text{ mg L}^{-1}$ ), whereas those greater than  $20 \text{ mg L}^{-1}$  were generally measured by potentiometric titration ( $\pm 2 \text{ mg L}^{-1}$ ). Uncertainties in water flux and age resulting from these uncertainties in output or Cl concentration measurements are shown in Figure 6 and derived in Appendix B. The inverse relationship between flux and Cl output (equation (1)) results in asymmetric error bars in flux when uncertainties in Cl output are large. In interdrainage areas the mean uncertainty in Cl output (3%) results in  $\pm 3\%$  uncertainty in flux. The uncertainty range of 0.5 to 10% in Cl output results in  $\pm 0.5\%$  uncertainty in flux from the lower bound (0.5%) to  $-11$  to  $9\%$  uncertainty in flux from the upper bound (10%). In interdrainage areas the uncertainty in age from uncertainties in Cl output is small (mean  $\pm 2\%$  and range 1 to 5%). In drainage areas, uncertainties in Cl output (mean  $\pm 12\%$  and range 0.5 to 83%) result in  $-11$  to  $13\%$  uncertainty in average water flux (range

**Table 1.** Uncertainties in Water Flux and Age Based on the Chloride Mass Balance (CMB) Method Resulting From Uncertainties in Cl input, Cl output, and Transport Processes for Profiles in Interdrainage (EF 28, EF 60, EF 66, EF 91, and EF 111) and Drainage and Fissure Areas (EF 94, EF 110, EF 120, and GL 2)

	Interdrainage Areas		Drainage Areas	
	Water Flux	Age	Water Flux	Age
Cl input	$\pm 35\%$	$-26$ to $54\%$	$\sim 10\times$	$\sim 0.1\times$
Cl output	$\pm 3\%$ ( $\pm 0.5$ , $-9$ to $+11\%$ )	$\pm 2\%$ ( $\pm 1$ to $\pm 5\%$ )	$-11$ to $+13\%$ ( $\pm 0.5\%$ ; $-45$ to $479\%$ )	$\pm 7\%$ ( $\pm 1$ to $\pm 20\%$ )
Combined (Cl input plus output)	$\pm 38\%$ ( $\pm 35.5\%$ ; $-44$ to $+46\%$ )	$-24$ to $56\%$ ( $-25$ to $59\%$ )		
Transport				
One Dimensional	yes	yes	yes/no*	yes/no*
Downward	yes/no†	yes/no†	yes	yes
Preferential flow	no	no	yes	yes
Diffusion	yes	yes	no	no
Overall CMB	upper bound $\pm 38\%$	lower bound $-21$ to $45\%$	lower bound $-11$ to $13\%$ ‡	upper bound $\pm 7\%$ ‡

The uncertainty in the Cl input was estimated to be 35% in interdrainage areas and an order of magnitude in the drainage areas (including the fissure). Analytical uncertainties in Cl output concentration measurements ranged from 0.5 to 10% (mean 3%) in interdrainage areas and from 0.5 to 83% (mean 12%) in drainage areas. Because Table 1 may be confusing, the following example is provided for clarity. For example, the mean error in Cl output (3%) results in  $\pm 3\%$  uncertainty in water flux. The range in error in Cl output (0.5 to 10%) results in a range in error in water flux from  $\pm 0.5\%$  to  $-9$  to  $+11\%$ . The asymmetry in the error bar is attributed to the inverse relationship between water flux and Cl. The asymmetry increases as the error increases.

\*Flow is generally 1-D beneath drainage areas; however, there is some evidence of 2-D flow (lateral flow) adjacent to drainage areas.

†Flow may be upward in the shallow zone and is assumed to be downward at greater depth ( $\geq 10$  m).

‡CMB approach underestimates water flux and overestimates age by about an order of magnitude because of neglecting Cl in run-on.

$\pm 0.5$  to  $-45$  to  $479\%$ ) and  $\pm 7\%$  uncertainty in age (range  $\pm 1$  to  $\pm 20\%$ ) (Table 1). Uncertainties in Cl output result in the CMB water fluxes being less accurate at high water fluxes because Cl concentrations are less sensitive to water fluxes at these low concentrations. Sensitivity lessens partly as a result of the inverse relationship between water flux and Cl (equation (1)), and the effect of analytical uncertainty in water flux increases as the Cl concentrations decrease. Small changes in Cl

concentration result in large changes in water flux at low Cl concentrations.

### 4.3. Uncertainties in Cl Transport Mechanisms

The CMB approach requires that Cl must be transported by 1-D, downward piston flow. Uncertainties in transport mechanisms were therefore evaluated.

**4.3.1. Flow direction.** Although the CMB approach assumes that water moves downward, water-potential data indicate that downward water movement is restricted to areas that pond water and that all other areas have upward water movement. Uniformly high water potentials beneath the fissure that plot to the right of the equilibrium line (equilibrium between water potential and gravitational potential) indicate downward water movement in the upper 10 to 20 m (Figure 1e). In contrast, water-potential data in interdrainage and shallow drainage areas indicate upward water movement (Figures 1a and 1c). Water potentials are higher (less negative) at depth and decrease toward the surface (more negative). This upward decrease in water potentials indicates an upward driving force for water movement at these locations. Water potentials plot to the left of the equilibrium line, also indicating a potential for upward water flow under steady state conditions. In the Blanca Draw drainage area, upward water-potential gradients are restricted to the upper 6 to 15 m; at greater depths, water potentials plotted to the right of the equilibrium line, indicating drainage (Figure 1c).

The timescales represented by the upward water potentials are difficult to assess. In the drainage area, upward water-potential gradients in the upper 6 to 15 m coexist with low Cl concentrations, suggesting that the upward water potentials were developed over fairly short time periods that were insufficient to accumulate significant amounts of Cl (Figures 1c and 1d). The water-potential data represent current drying conditions, whereas the Cl data represent higher water fluxes in the past that flushed out Cl. The drainage area has dense mesquite trees that have deep roots and can readily evapotranspire wa-

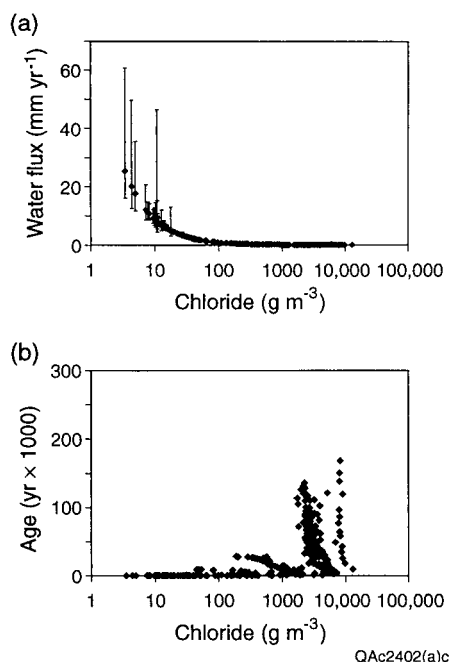


**Figure 6.** Uncertainties in (a) water flux and (b) age resulting from analytical uncertainties in Cl measurements in samples from profiles in drainage and fissure areas (EF 94, EF 110, EF 120, and GL 2) and interdrainage areas (EF 28, EF 60, EF 66, EF 91, and EF 111).

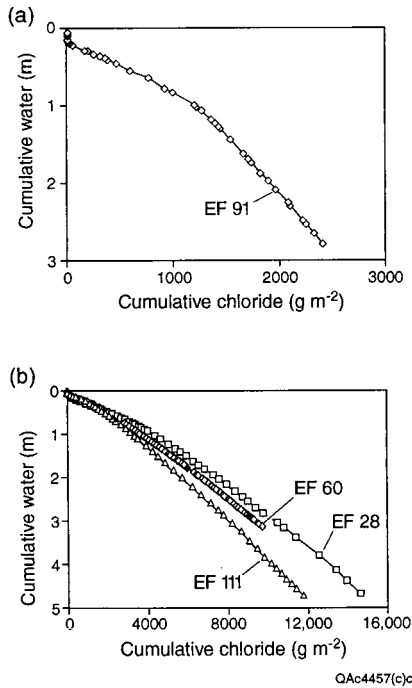


**Figure 7.** Cumulative water versus cumulative Cl for (a) EF 91 and (b) EF 28, EF 60, and EF 111 profiles in interdrainage areas.

ter from depth. Data from the drainage area therefore indicate that upward water-potential gradients are not necessarily inconsistent with long-term net downward water movement. In interdrainage areas the upward water-potential gradients may represent drying over much longer time periods and are consistent with Cl accumulation near the surface (Figure 1b). Plots of cumulative Cl versus cumulative water content (Figure 7) can be used to evaluate changing conditions over time. The plot for EF 91 shows an increase in slope (Figure 7a) that corresponds to a CMB age of about 11,000 years, similar to some other profiles in the eolian sheet [Scanlon *et al.*, 1999a, b]. Higher water fluxes prior to that time correspond to Pleistocene time. The reduced slope in the Holocene may reflect reduced water flux or change in flux direction from downward (Pleistocene) to upward (Holocene). The other profiles in the

interdrainage area do not show any response to Pleistocene climate change (Figure 7b) and represent very long time periods. It is unlikely that upward water fluxes have persisted for the entire time period represented by these Cl profiles (such as 136,000 years for EF 111 profile). If they did, we would not expect to see radioactive decay of  $^{36}\text{Cl}/\text{Cl}$ , which is found in those profiles. The time period represented by the upward water potential profiles is therefore estimated to be less than  $\sim 10,000$  years, or Holocene age.

The subsurface distributions of  $\delta^2\text{H}$  and  $\delta^{18}\text{O}$  were also used to evaluate the direction of water movement. Data from beneath and adjacent to Grayton Lake playa plot parallel to the local meteoric water line (slope 6.3), indicating no recent evaporation (Figure 8a). The profile beneath the fissure (EF 92) also shows no enrichment in  $\delta^{18}\text{O}$  relative to  $\delta^2\text{H}$  except at the shallowest depth. The stable isotope data adjacent to the fissure are similar to those in other interdrainage areas. Interdrainage profiles show enrichment of  $\delta^{18}\text{O}$  relative to  $\delta^2\text{H}$  that is described by  $\delta^2\text{H} = 3.1 \delta^{18}\text{O} - 38$  (Figure 8b). This low slope is consistent with evaporation of pore water in the unsaturated zone, similar to slopes determined by Allison [1982] for evaporation from dry soils. This evaporation line intersects the local meteoric water line at a position more depleted than that of the mean modern precipitation or mean winter precipitation, suggesting downward water flux during a cooler, wetter climate (Pleistocene times). This situation is consistent with that of the Cl data just discussed. Vertical profiles of  $\delta^2\text{H}$  and  $\delta^{18}\text{O}$  generally show the most isotopic enrichment near the surface (Figures 9a and 9b).

The stable isotope data were used to calculate subsurface evaporation rates in interdrainage areas (1) from the position of the isotopic peak and (2) from “the decay length method in the liquid transport region” [Barnes and Allison, 1983, 1988]. The depths of the isotopic peaks were similar for  $\delta^2\text{H}$  and  $\delta^{18}\text{O}$  in EF 64 (3.2 m) and in EF 91 (3.0 m). Evaporation rates calculated according to the position of the isotopic peak ranged from 0.3 to 0.4  $\text{mm yr}^{-1}$  (Appendix C). The “decay length method” assumes equilibrium between upward advection of isotopically depleted water and downward diffusion of enriched water for each isotope, resulting in exponential profiles. Evaporation rates based on this method ranged from 0.2  $\text{mm yr}^{-1}$  (EF 64) to 0.3 to 0.5  $\text{mm yr}^{-1}$  (EF 91). The calculated

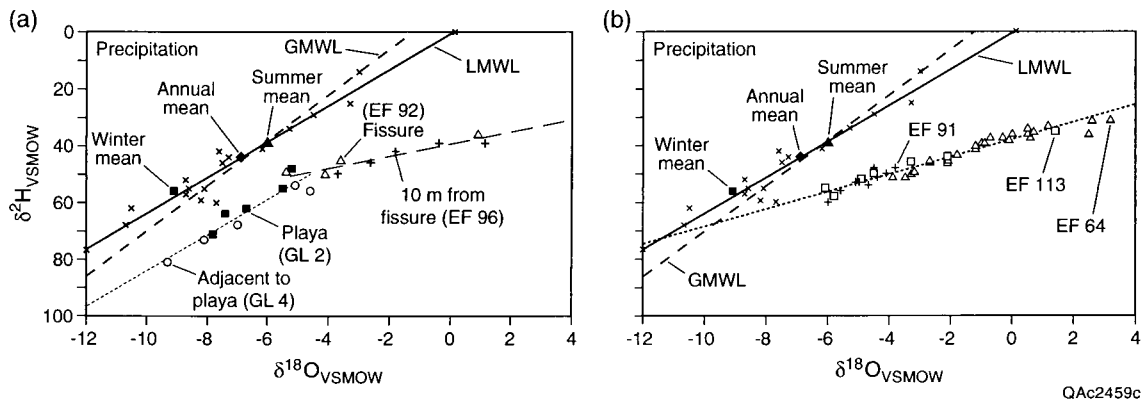


**Figure 8.** The  $\delta^2\text{H}$  versus  $\delta^{18}\text{O}$  plot including data from (a) beneath and adjacent to the fissure (EF 92 and EF 96) and beneath and adjacent to Grayton Lake playa (GL 2 and GL 4) and (b) interdrainage profiles (EF 64, EF 91, and EF 113). The local meteoric water line (LMWL) was calculated from precipitation data collected  $\sim$ monthly for 2 years. The standard error for  $\delta^2\text{H}$  analyses is  $\pm 1\text{‰}$  and for  $\delta^{18}\text{O}$  analyses is  $\pm 0.2\text{‰}$ .



upward water fluxes are high and may primarily reflect evaporation of water in the near-surface root zone.

These stable isotope data indicate that the sediments are drying and are consistent with the upward water-potential gradients. Upward movement of water in the liquid phase would reduce CMB ages because of the additional source of Cl in the denominator of equation (2). The upward water flux can also be used to explain the high Cl concentrations in the shallow subsurface and the decrease in Cl concentrations at greater depths. Cl is accumulating in the near surface because of drying of the profile and addition of Cl at the surface, which is substantiated by the cumulative Cl versus water plots and the stable isotope data. Therefore the CMB approach should not be used in the shallow zone where Cl is accumulating and where concentration gradients are steep but rather should be restricted to the deeper zones of the profiles ( $\sim \geq 10$  m).

**4.3.2. One-dimensional flow.** Because the topography of the Eagle Flat basin is fairly flat, subsurface lateral flow as a result of surface topographic variations is expected to be minimal. However, water may move laterally through layered or heterogeneous sediments. Cl profiles in interdrainage areas do not provide any indication of lateral flow, nor do calcic soil horizons seem to affect water movement. Geologic data indicate that they are fractured and consist of stage III carbonate [Jackson *et al.*, 1993; Langford, 1993].

The only evidence of lateral flow was found in areas of ponded water, such as the fissure. The steepness of the Cl and water-potential fronts at a depth of about 10 m beneath the fissure (EF 35) is attributed to the natural capillary barrier effect of layered sediments (Figures 1e and 1f) [Scanlon *et al.*, 1997a]. Dilution of Cl in the profile 10 m from the fissure (EF 36) by about 30% at approximately the depth of the Cl front in the profile beneath the fissure is attributed to lateral flow. Lateral flow was also shown in a dye-tracing experiment in

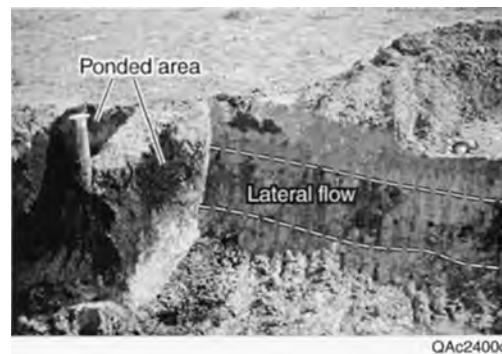


**Figure 10.** Lateral flow beneath the Eagle Flat fissure, shown by dye-tracing experiment.

which a 2-m<sup>2</sup> area was ponded for 8 hours by water containing FD&C blue dye [Scanlon *et al.*, 1999a]. Excavation beneath and adjacent to the ponded area revealed dye at distances of  $\sim 5$  m from the ponded area (Figure 10). These data suggest that the no-lateral-flow assumption may not be valid in areas where water ponds. Subsurface lateral flow should not affect the calculated CMB water flux beneath the ponded area because Cl concentrations in pore water are not affected, but it would affect the calculated water flux adjacent to the ponded areas; therefore one should use caution when calculating water fluxes in areas adjacent to ponded regions.

**4.3.3. Preferential flow.** Pulse-type tracers such as bomb  $^3\text{H}$  and bomb  $^{36}\text{Cl}$  are generally used to evaluate whether water is moving preferentially. In an interdrainage profile (EF 79), high  $^3\text{H}$  concentrations in the upper 5 m probably reflect the tail of the bomb pulse (Figure 11a), and  $^3\text{H}$  levels below this zone were low (EF 79 and EF 117 with range  $0.14 \pm 0.24$  to  $1.71 \pm 0.44$  TU ( $\pm 2\sigma$ )). In some cases the  $^3\text{H}$  levels were less than the  $2\sigma$  error, indicating no  $^3\text{H}$ . The  $^3\text{H}$  level in a procedural blank ( $0.98 \pm 0.5$  TU,  $^3\text{H}$ -free water added to an oven-dried sample) was similar to  $^3\text{H}$  levels found in EF 79 and EF 117 profiles at depth and indicates no  $^3\text{H}$  in these settings. The lack of  $^3\text{H}$  is consistent with measured high Cl concentrations and estimated low water fluxes for these sediments and indicates that there is no preferential flow in these interdrainage profiles or else that  $^3\text{H}$  is not a good tracer for such flow in these settings. In contrast, high  $^3\text{H}$  levels beneath and adjacent to the fissure (7 to 33 TU) and beneath Grayton Lake playa (5 to 12 TU) indicate preferential flow (Figure 11a). Preferential flow is expected beneath Grayton Lake playa because large desiccation cracks develop during dry periods.

In contrast to the  $^3\text{H}$  data, measured  $^{36}\text{Cl}/\text{Cl}$  ratios beneath the fissure and beneath Grayton Lake playa are low ( $290$  to  $530 \times 10^{-15}$ ) and do not provide evidence of preferential flow (Figure 11b). Typical bomb-pulse  $^{36}\text{Cl}/\text{Cl}$  ratios are about an order of magnitude higher [Phillips *et al.*, 1988; Scanlon, 1992]. Because  $^{36}\text{Cl}/\text{Cl}$  ratios are measured in core samples that contain a component of preferentially moving water and water in the matrix, mixing of water moving preferentially and in the matrix may account for the low  $^{36}\text{Cl}/\text{Cl}$  ratios. The measured  $^{36}\text{Cl}/\text{Cl}$  ratio in a mixed sample (subscript mix) can be calculated as follows:

$$^{36}\text{Cl}/\text{Cl}_{\text{mix}} = \frac{V_p \text{Cl}_p ^{36}\text{Cl}/\text{Cl}_p + V_m \text{Cl}_m ^{36}\text{Cl}/\text{Cl}_m}{V_p \text{Cl}_p + V_m \text{Cl}_m} \quad (7)$$

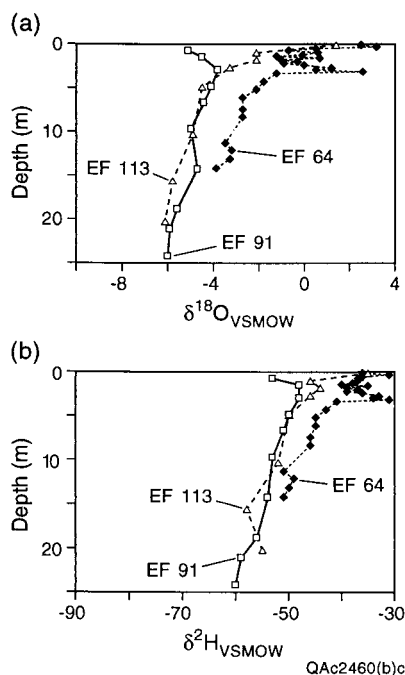


**Figure 9.** Depth profiles in (a)  $\delta^{18}\text{O}$  and (b)  $\delta^2\text{H}$  in pore water samples from boreholes EF 64, EF 91, and EF 113 in interdrainage areas.

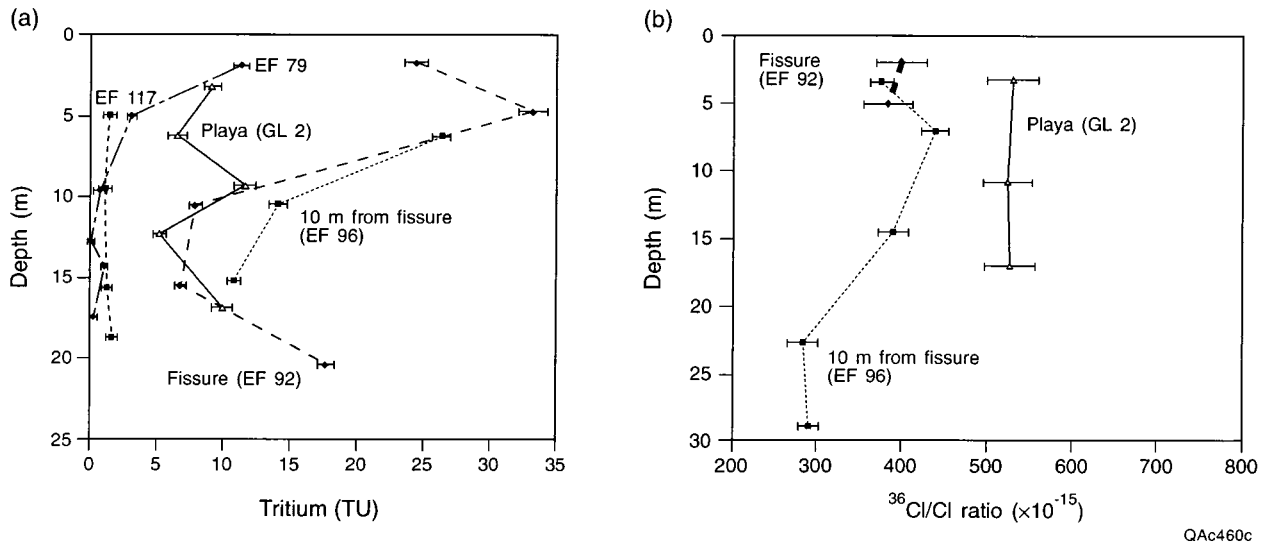


**Figure 11.** Vertical profiles in (a) tritium concentrations in interdrainage areas (EF 79 and EF 117), beneath (EF 92) and 10 m from the fissure (EF 96) and beneath Grayton Lake (GL 2) and (b)  $^{36}\text{Cl}/\text{Cl}$  ratios beneath (EF 92) and 10 m from the fissure (EF 96) and beneath Grayton Lake (GL 2).

where  $V_p$  and  $V_m$  are the fractional volumes of water moving preferentially or in the matrix water, respectively, and sum to 1, and  $\text{Cl}_p$ ,  $^{36}\text{Cl}/\text{Cl}_p$ ,  $\text{Cl}_m$ , and  $^{36}\text{Cl}/\text{Cl}_m$  refer to concentrations or ratios in water moving preferentially or in the matrix, respectively [Liu *et al.*, 1995]. The resultant  $^{36}\text{Cl}/\text{Cl}$  ratios in a mixture of water moving preferentially and through the matrix were estimated by mixing 10% preferentially moving water with a bomb-pulse  $^{36}\text{Cl}/\text{Cl}$  ratio of  $5000 \times 10^{-15}$  and Cl concentrations of 1, 10, and  $100 \text{ g m}^{-3}$  with 90% matrix water with a prebomb  $^{36}\text{Cl}/\text{Cl}$  ratio of  $500 \times 10^{-15}$  and Cl concentrations ranging from 0.1 to  $10,000 \text{ g m}^{-3}$  (Figure 12). Results indicate that the contribution of bomb-pulse  $^{36}\text{Cl}/\text{Cl}$  in preferentially moving water is damped when Cl concentrations in the matrix exceed 10 to  $100 \text{ g m}^{-3}$ , as is found beneath the playa and fissure. Therefore  $^{36}\text{Cl}/\text{Cl}$  ratios cannot be used to evaluate preferential flow when Cl concentrations in the matrix exceed 10 to  $100 \text{ g m}^{-3}$ . The  $^{36}\text{Cl}/\text{Cl}$  ratios in the mixture decrease sharply as the Cl concentrations in the matrix increase. Uncer-

tainties in  $^{36}\text{Cl}/\text{Cl}$  ratios in preferentially moving water are not critical because  $^{36}\text{Cl}/\text{Cl}$  ratios in the mixture are not very sensitive to these. Variations in the proportion of water moving preferentially from 1 to 30% resulted in only as much as 3% variation in the  $^{36}\text{Cl}/\text{Cl}$  ratio of the mixture. In this arid setting (i.e., with high Cl concentrations), bomb-pulse  $^3\text{H}$  is not as affected by mixing as are  $^{36}\text{Cl}/\text{Cl}$  ratios because the short half-life of  $^3\text{H}$  results in  $^3\text{H}$ -free matrix water. For example, mixing 10% preferentially moving water that has bomb-pulse  $^3\text{H}$  (estimated 100 TU) with 90% matrix water that has no  $^3\text{H}$  results in 10 TU in the mixture. The absence of bomb-pulse  $^{36}\text{Cl}/\text{Cl}$  ratios beneath the fissure and playa is therefore not inconsistent with preferential flow in these settings, as indicated by the  $^3\text{H}$  data.

**4.3.4. Diffusion.** The simple CMB (1) ignores diffusion; however, Cl can be transported by advection and diffusion as shown by the following steady state equation:

$$J_{\text{Cl}} = \pm q_w c_{\text{Cluz}} - D_e \frac{\partial c_{\text{Cluz}}}{\partial z}, \quad (8)$$

where  $J_{\text{Cl}}$  is the Cl mass flux or Cl input at the surface ( $M L^{-2} T^{-1}$ ) and  $D_e$  is the effective molecular diffusion coefficient ( $L^2 T^{-1}$ ). The first term on the right represents the advective Cl flux (positive for upward and negative for downward), and the second term represents diffusive Cl flux. The effective molecular diffusion coefficient for Cl is calculated by multiplying the molecular diffusion coefficient in water ( $0.064 \text{ m}^2 \text{ yr}^{-1}$  [Kemper, 1986]) by the volumetric water content and the tortuosity (function of water content). Bracketing values for  $D_e$  were based on tortuosity functions developed by Conca and Wright [1992] and by Millington and Quirk [1961].

The diffusive Cl flux was calculated from  $D_e$  times the Cl concentration gradient (equation (8)). In most profiles the downward diffusive Cl flux was high in the zone of steep Cl concentration gradients below the peak (Figures 1b and 13). Below this zone, diffusive Cl fluxes are much lower. Diffusive Cl fluxes are not as great where Cl concentration gradients are less steep, as in EF 91 (Figures 1b and 13b). These calculations indicate that Cl can be transported by downward diffusion

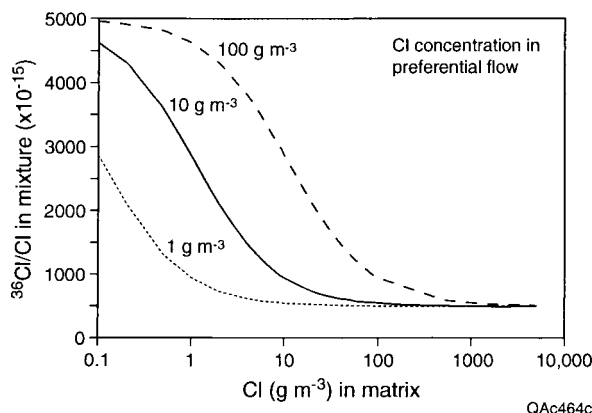


**Figure 12.** Damping of  $^{36}\text{Cl}/\text{Cl}$  ratios in preferentially moving water (10% by volume, initial  $^{36}\text{Cl}/\text{Cl}$  ratio  $5000 \times 10^{-15}$ , and Cl concentrations 1, 10, and  $100 \text{ g m}^{-3}$ ) as a result of mixing with matrix water (90% by volume,  $^{36}\text{Cl}/\text{Cl}$  ratio  $500 \times 10^{-15}$ , and Cl concentration 0.1 to  $10,000 \text{ g m}^{-3}$ ).

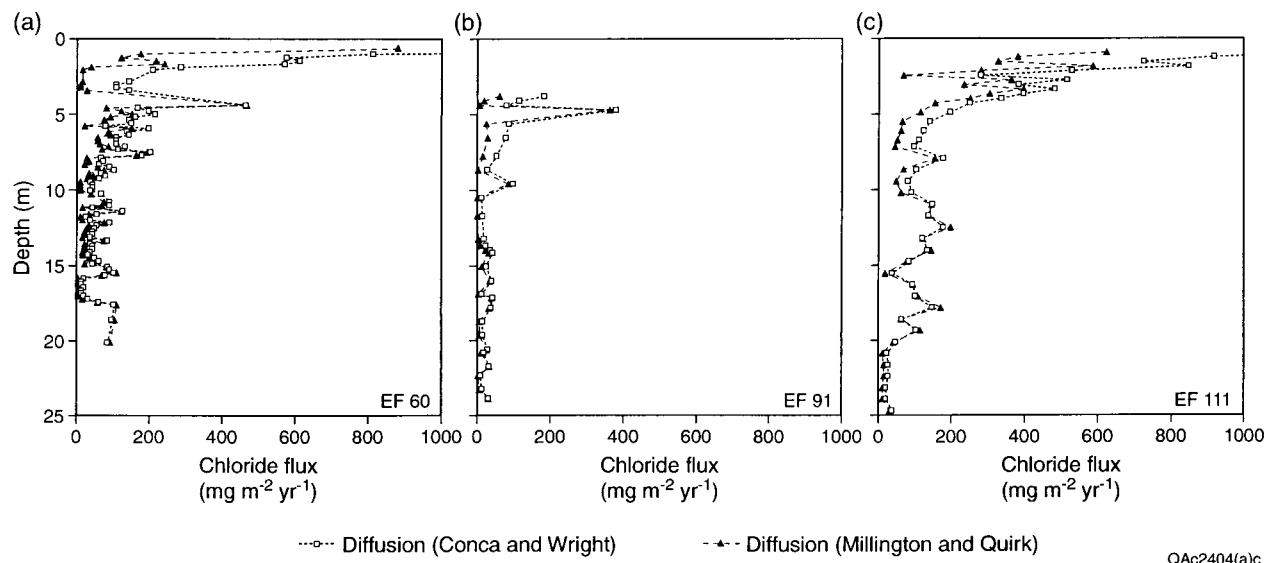


**Figure 13.** Diffusive Cl fluxes for (a) EF 60, (b) EF 91, and (c) EF 111 calculated using effective diffusivities from *Conca and Wright* [1992] and from *Millington and Quirk* [1961].

against an upward advective water flux; however, these diffusive Cl fluxes become negligible below the zone of steep concentration gradients. The diffusive Cl fluxes are based on current Cl profiles; however, diffusive fluxes may have been higher at depth if steep Cl concentration gradients occurred there in the past. Including diffusion at depth would reduce the CMB water flux slightly because some of the downward transport of Cl is by diffusion and is not moving with the water. Therefore CMB water fluxes that ignore diffusion represent upper bounds on actual water flux. Including diffusion should increase the age because the diffusive term would be in the denominator of (2) and would be negative because the Cl concentration gradients are negative. However, the present zone of steep Cl concentrations where diffusion is important is limited in vertical extent.

**4.3.5. Anion exclusion.** Because most soils outside the eolian sheet in the study area have fairly high clay content ( $\sim 50\%$ ), anion exclusion may be important. Neglecting anion exclusion, as in the CMB approach, will result in overestimation of the water flux (equation (1)) because the Cl concentration in unsaturated-zone pore water will be underestimated, and Cl moves faster than water because it is restricted to the exclusion zone [Slavich and Petterson, 1993]. Underestimation of Cl concentration in pore water results from dividing the Cl concentration in the supernatant by the total water content calculated by oven drying the sample instead of the water content in the exclusion zone. In addition, the water flux needs to be corrected for more rapid transport of Cl in the exclusion zone

$$q_w = q_{wa}(1/1 - \alpha), \quad (9)$$

where  $q_w$  is the water flux ( $L T^{-1}$ ),  $q_{wa}$  is the apparent water flux ignoring exclusion, and  $\alpha$  is the ratio of excluded water content to total water content [Slavich and Petterson, 1993]. The two effects are multiplicative. Studies by Slavich and Petterson [1993] at a site in Australia indicate that ignoring anion exclusion in the clay-rich soil at their site resulted in overestimation of water flux from 1.25 to 1.64 times and underestimation of age by a similar amount, although a smaller

effect would be expected in the coarser-grained Eagle Flat basin sediments in this study.

#### 4.4. Combined Effects of Uncertainties

Uncertainties in calculated CMB water fluxes and ages result from uncertainties in Cl transport processes, input, and output. Although the CMB approach assumes 1-D, downward piston flow, upward water-potential gradients and stable isotope data suggest net upward water movement in interdrainage areas. Cumulative Cl versus cumulative water plots and stable isotope data suggest probably downward water fluxes during the Pleistocene and drying since that time. Therefore water fluxes were calculated for the deeper zone ( $\geq 10$  m), where fluxes are expected to be downward. There is no evidence of preferential flow in interdrainage areas. Although we assume that Cl is transported with water, Cl may be transported independently of water by diffusion, or it may be transported faster than the average water by anion exclusion. If water fluxes are calculated only for the deeper sections of the profiles ( $\geq 10$  m), the effects of errors related to upward flow should be negligible. Although it is difficult to quantify the uncertainties resulting from these transport processes (diffusion and anion exclusion), they act in concert, that is, decrease the apparent CMB water flux and increase the CMB age. Ignoring all these transport processes, as is done in the simple CMB approach, results in overestimation of water flux and underestimation of age. Apparent water fluxes calculated by the CMB approach therefore constitute upper bounds and apparent ages constitute lower bounds to the extent that underlying assumptions are not met.

In **interdrainage** areas, for example, water fluxes calculated for the deeper sections of the profiles ( $\geq 10$  m depth) ranged from **0.03 to 0.17 mm yr<sup>-1</sup>** (mean 0.06 mm yr<sup>-1</sup>) using a Cl input of 87 mg m<sup>-2</sup> yr<sup>-1</sup>. Because these downward water fluxes represent older time periods, they are out of phase with current drying of the profiles. Water fluxes were calculated below the zone of steep Cl concentration gradients. Anion exclusion could reduce the apparent CMB water fluxes in clay-rich sediments. Therefore the CMB water fluxes represent an upper



bound on actual water fluxes in the interdrainage area. The low water fluxes in interdrainage settings are substantiated by thick calcic horizons (stage III) at several depths in these profiles, which imply significant evaporation of infiltrating water [Jackson *et al.*, 1993]. The estimated uncertainty in Cl input of 35% and in Cl output of  $\pm 3\%$  (0.5 to 10%) results in  $\pm 38\%$  uncertainty in calculated CMB water flux at depths  $\geq 10$  m (Table 1). The uncertainties in Cl input and output are considered error bars on the upper bounding estimate that results from uncertainties in transport mechanisms.

Residence times of Cl in interdrainage areas ranged from 27,515 years for EF 91 to 136,000 years for EF 111 at 25-m depth. Uncertainties in transport mechanisms, such as diffusion and anion exclusion, result in the calculated CMB residence times being lower bounds on actual residence times. All these transport processes act in concert and increase the residence time of Cl. The general correspondence of the CMB ages and ages based on radioactive decay of  $^{36}\text{Cl}$  indicates that overestimation of water residence time by the CMB approach is probably not greater than a factor of 2 or 3. The estimated uncertainty in Cl input of  $\pm 35\%$  and Cl output of  $\pm 3\%$  (0.5 to 10%) results in asymmetric errors ( $-24$  to  $56\%$ ) in the CMB calculated average residence time because of the inverse relationship between residence time and chloride output (Table 1).

In drainage areas or areas where surface water ponds, the CMB approach is much more difficult to apply because of (1) uncertainties in transport mechanisms (preferential flow), (2) large uncertainties in Cl input because of Cl in run-on, (3) reduced sensitivity of Cl to changes in water flux at low Cl concentrations, and (4) analytical uncertainty in Cl concentration measurements at low concentrations.

Preferential flow, as shown by  $^3\text{H}$  data beneath the fissure and playa, should affect CMB water flux. Because the CMB approach does not account for preferential flow, it therefore underestimates water flux in these areas. However, uncertainty in Cl input or run-on may be much greater than that of preferential flow. Cl provided in run-on is estimated to result in about an order of magnitude uncertainty in Cl input. Mean Cl concentrations ranged from  $92 \text{ g m}^{-3}$  beneath Blanca Draw (EF 110) to  $21 \text{ g m}^{-3}$  beneath the fissure (top 7.5 m of EF 120). Downward water fluxes calculated by the CMB approach ranged from  $0.2$  to  $20 \text{ mm yr}^{-1}$  (EF 110) beneath Blanca Draw and from  $0$  to  $25 \text{ mm yr}^{-1}$  (EF 120) beneath the fissure. Ignoring preferential flow and run-on results in underestimation of water flux by about an order of magnitude. Average uncertainties in water flux resulting from uncertainties in Cl output or analytical uncertainties in Cl measurements ( $\pm 12\%$ ) ranged from  $-11$  to  $13\%$  in drainage and fissure profiles (Figure 6a and Table 1) (Appendix B). Uncertainties in water flux can be as high as  $479\%$ . Analytical uncertainties increase as Cl concentrations decrease.

The process of estimating uncertainties in water flux and age from environmental tracers described in this study is generally applicable to systems characterized by porous media in semi-arid and arid regions. Chloride profiles described in this study are similar to those in other desert basins [Tyler *et al.*, 1996; Prudic, 1994]; therefore the findings from this study should be generally applicable to those regions. Uncertainties in Cl input and output should be similar to those used in this study also. However, specific analysis of uncertainties should be conducted at each site using both soil physics and a variety of environmental tracers as shown in this study. Although we have not specifically addressed fractured media in this work,

fractured systems would be somewhat similar to the playa setting where desiccation cracks are found in the clay sediments. Preferential flow is an important issue in fractured media and should result in underestimation of water flux by the CMB approach. Analysis of Cl in perched aquifers or shallow water tables would provide a much better integrated estimate of water flux in fractured media.

#### 4.5. Example Application of Uncertainty Analysis

In interdrainage areas, for example, using data from the EF 111 profile, the average water flux at depths  $\geq 10$  m is  $0.04 \text{ mm yr}^{-1}$ , and the CMB age at the base of the profile (25 m) is 136,000 years. Uncertainties in transport mechanisms result in these estimates of water flux being upper bounds on actual water fluxes and estimates of age being lower bounds on actual ages. Uncertainties in these bounding estimates result from uncertainty in the Cl input ( $\sim \pm 35\%$ ), which results in  $\pm 35\%$  uncertainty in water flux and  $-26$  to  $54\%$  uncertainty in age, and from analytical uncertainties in Cl measurements, which result in  $\pm 3\%$  uncertainty in water flux and  $\pm 2\%$  uncertainty in age. The combined effect of uncertainties in Cl input and Cl output measurements results in  $\pm 38\%$  uncertainty in water flux ( $0.02 \text{ mm yr}^{-1}$ ) and  $-24$  to  $56\%$  uncertainty in age (103,360 to 212,160 years).

In drainage areas, for example, using data from the EF 110 profile, the average water flux is  $\sim 3 \text{ mm yr}^{-1}$  ( $0.2$  to  $20 \text{ mm yr}^{-1}$ ), and the CMB age at the base of the profile (26 m) is 8500 years. Preferential flow and uncertainty in Cl input from run-on ( $\sim$  order of magnitude) result in the calculated CMB water fluxes representing lower bounds, and actual water fluxes could be an order of magnitude higher. Uncertainties in Cl output from analytical uncertainties in Cl measurements in this profile are about  $\pm 12\%$  and result in an uncertainty range of  $-11$  to  $13\%$  in the lower bounding estimate of water flux. Although it is difficult or impossible to quantify all sources of uncertainty, the uncertainty analysis in this study shows that calculated water fluxes and ages based on the CMB approach can generally provide bounding estimates on actual water fluxes and ages.

## 5. Conclusions

The long residence times suggested by the Cl data in interdrainage areas (55,000 to 105,000 years) were generally corroborated by residence times estimated from radioactive decay of  $^{36}\text{Cl}$  ( $39,000 \pm 13,000$  to  $59,000 \pm 14,400$  years). The various sources of uncertainty with the use of the CMB approach include uncertainties in transport processes, Cl input, and Cl output. Uncertainties in transport processes were evaluated using physical data and information from other tracers. In interdrainage areas, water-potential and stable isotope data indicate net upward water movement. Cl and stable isotope data suggest that this drying trend may have persisted through the Holocene and that water movement was probably downward in the Pleistocene. Although Cl is generally assumed to be transported with water, diffusion and anion exclusion could result in faster transport of Cl relative to water. Diffusion is important in the zone of steep concentration gradients near the surface. Because of upward flow and diffusion, the CMB approach was applied only to older, deeper sections of the profiles ( $\geq 10$  m) to calculate water flux. By ignoring these processes, such as diffusion and anion exclusion, the CMB approach provides an upper bound on actual water flux and a

lower bound on actual age because these processes decrease water flux and increase age. Water fluxes estimated for deeper sections of profiles ( $\geq 10$  m) in interdrainage areas are low (0.03 to 0.2 mm yr<sup>-1</sup>, mean 0.06 mm yr<sup>-1</sup>). Error bars on these bounding estimates were evaluated on the basis of uncertainty in CI input ( $\sim \pm 35\%$ ) and in CI output ( $\pm 3\%$ ) that result in  $\pm 38\%$  uncertainty in water flux and  $-24$  to  $56\%$  uncertainty in water age in interdrainage areas.

In drainage areas the CMB approach is much more difficult to apply because of (1) uncertainties in transport mechanisms (preferential flow as shown by <sup>3</sup>H), (2) large uncertainties in CI input because of CI in run-on (order of magnitude uncertainty), (3) reduced sensitivity of CI to changes in water flux at low CI concentrations, and (4) analytical uncertainty in CI concentration measurements at these low levels. The CMB water fluxes therefore constitute a lower bound on the actual water flux, and the CMB ages constitute an upper bound on the actual age. Calculated water fluxes ranged from 0.02 to 25 mm yr<sup>-1</sup> (mean 3 mm yr<sup>-1</sup>). Inclusion of CI in run on would increase these water flux estimates by about an order of magnitude. Error bars on this lower bounding estimate ( $-11$  to  $13\%$ ) result from uncertainties in CI output (mean  $\pm 12\%$ ).

The results of this study have important implications for waste disposal in arid regions characterized by porous media because they suggest that water fluxes estimated using the CMB approach are conservatively high in interdrainage areas where disposal facilities are generally located. Comprehensive uncertainty analysis requires information from other tracer and physical techniques to provide greater confidence than that provided by a single tracer.

## Appendix A

Uncertainties in age ( $1\sigma$ ) calculated from radioactive decay of <sup>36</sup>Cl (equation (3)) were evaluated according to the following equations [Bevington and Robinson, 1992, pp. 42–43]:

$$\sigma_t = \left[ \left( \frac{\partial t}{\partial R} \right)^2 \sigma_R^2 + \left( \frac{\partial t}{\partial R_0} \right)^2 \sigma_{R_0}^2 + \left( \frac{\partial t}{\partial R_{se}} \right)^2 \sigma_{R_{se}}^2 \right]^{0.5} \quad (A1)$$

$$\sigma_t = \left\{ \left( \frac{\sigma_R}{\lambda_{36}(R - R_{se})} \right)^2 + \left( \frac{\sigma_{R_0}}{\lambda_{36}(R_0 - R_{se})} \right)^2 + \left[ \frac{1}{\lambda_{36}} \left( \frac{1}{R_0 - R_{se}} - \frac{1}{R - R_{se}} \right) \right]^2 \sigma_{R_{se}}^2 \right\}^{0.5}, \quad (A2)$$

where  $\sigma_t$  is the uncertainty in the age,  $\lambda_{36}$  is the decay constant for <sup>36</sup>Cl ( $2.30 \times 10^{-6}$  yr<sup>-1</sup>),  $R$  is the measured <sup>36</sup>Cl/Cl ratio,  $R_{se}$  is the secular equilibrium <sup>36</sup>Cl/Cl ratio ( $\sim 10 \times 10^{-15}$ ) [Bentley et al., 1986],  $R_0$  is the initial <sup>36</sup>Cl/Cl ratio (e.g.,  $491 \times 10^{-15}$  at 10.7 m depth for the EF 60 profile),  $\sigma_R$  is the uncertainty in the <sup>36</sup>Cl/Cl ratio measurements,  $\sigma_{R_{se}}$  is the estimated uncertainty in the secular equilibrium <sup>36</sup>Cl/Cl ratio ( $0.5 \times 10^{-15}$ ), and  $\sigma_{R_0}$  is the measured uncertainty in the initial <sup>36</sup>Cl/Cl ratio (e.g.,  $11 \times 10^{-15}$  at 10.7 m depth for the EF 60 profile) (J. T. Fabryka-Martin, personal communication, 1998).

## Appendix B

Uncertainty in water flux ( $q$ ) resulting from uncertainty in CI concentrations ( $\varepsilon_{c_{Cluz}}$ ) in unsaturated zone pore water was calculated from (1) as follows:

$$q = \frac{J_{Cl}}{c_{Cluz}} = \frac{k}{c_{Cluz}} \quad q^+ = \frac{k}{(1 + \varepsilon_{c_{Cluz}})c_{Cluz}} \quad (B1)$$

$$q^- = \frac{k}{(1 - \varepsilon_{c_{Cluz}})c_{Cluz}}$$

$$\varepsilon_{fq^+} = \frac{q^+ - q}{q} = \frac{\frac{k}{(1 + \varepsilon_{c_{Cluz}})c_{Cluz}} - \frac{k}{c_{Cluz}}}{\frac{k}{c_{Cluz}}} = \frac{1}{1 + \varepsilon_{c_{Cluz}}} - 1 \quad (B2)$$

$$\varepsilon_{fq^-} = \frac{q - q^-}{q} = \frac{1}{1 - \varepsilon_{c_{Cluz}}} - 1, \quad (B3)$$

where  $J_{Cl}$  is the CI input (treated as constant ( $k$ )),  $q^+$  ( $q^-$ ) is the  $q$  resulting from an increase (decrease) in  $c_{Cluz}$  by the error in  $c_{Cluz}$  ( $\varepsilon_{c_{Cluz}}$ ). Fractional uncertainty in age resulting from uncertainty in CI input was calculated from (2) as follows:

$$t = \frac{\int_0^z \theta c_{Cluz} dz}{J_{Cl}} = \frac{k}{J_{Cl}} \quad t^+ = \frac{k}{(1 + \varepsilon_{J_{Cl}})J_{Cl}} \quad (B4)$$

$$t^- = \frac{k}{(1 - \varepsilon_{J_{Cl}})J_{Cl}}$$

$$\varepsilon_{ft^+} = \frac{t^+ - t}{t} = \frac{\frac{k}{(1 + \varepsilon_{J_{Cl}})J_{Cl}} - \frac{k}{J_{Cl}}}{\frac{k}{J_{Cl}}} = \frac{1}{1 + \varepsilon_{J_{Cl}}} - 1 \quad (B5)$$

$$\varepsilon_{ft^-} = \frac{t - t^-}{t} = \frac{1}{1 - \varepsilon_{J_{Cl}}} - 1. \quad (B6)$$

Because  $\varepsilon_{J_{Cl}}$  is 0.35,

$$\varepsilon_{ft^+} = \frac{1}{1 + \varepsilon_{J_{Cl}}} - 1 = \frac{1}{1 + 0.35} - 1 = -0.26 \quad (B7)$$

$$\varepsilon_{ft^-} = \frac{1}{1 - \varepsilon_{J_{Cl}}} - 1 = \frac{1}{1 - 0.35} - 1 = 0.54.$$

Uncertainty in age resulting from uncertainty in CI concentrations in pore water was calculated from (2) as follows:

$$\varepsilon_{ft_i} = \frac{\varepsilon_{t_i}}{t_i} = \frac{\varepsilon_{ft_{i-1}} + \Delta t_i \frac{\varepsilon_{c_{Cluz}}}{c_{Cluz}}}{t_{i-1} + \Delta t_i} \quad (B8)$$

$$\frac{\varepsilon_{t_i}}{t_i} = \frac{\varepsilon_{c_{Cluz}}}{c_{Cluz}} \quad i = 1, \quad t_{i-1} = 0, \quad \varepsilon_{t_{i-1}} = 0. \quad (B9)$$

## Appendix C

The isotopic data were used to calculate subsurface evaporation rates in the interdrainage areas (1) from the position of the isotopic peak and (2) from “the decay length method in the liquid transport region” [Barnes and Allison, 1983, 1988]. The isotopic maximum (point 1) in the profiles was used to estimate the evaporation rate as follows:

$$E = N_{sat} D^{v*} (1 - h_a) / \rho z_{ef}, \quad (C1)$$

where  $E$  is the evaporation rate ( $L\ T^{-1}$ ),  $N_{\text{sat}}$  is water vapor concentration at saturation ( $M\ L^{-3}$ ),  $D^{v*}$  is the effective vapor diffusivity ( $L^2\ T^{-1}$ ),  $h_a$  is the relative humidity of the atmosphere (mean annual  $\sim 0.5$ ),  $\rho_l$  is the liquid water density ( $M\ L^{-3}$ ), and  $z_{ef}$  is the depth of the evaporation front [Barnes and Allison, 1983]. The evaporation rate was also estimated from the decay length (point 2):

$$\frac{\delta_i - \delta_i^{\text{res}}}{\delta_i^{\text{ef}} - \delta_i^{\text{res}}} = \exp(-f(z)/\hat{z}_i), \quad (\text{C2})$$

where  $\delta$  refers to the isotopic ratio relative to VSMOW,  $\delta_i$  is the  $\delta$  value at each depth,  $\delta_i^{\text{res}}$  is the  $\delta$  value at the base of the profile (reservoir),  $\delta_i^{\text{ef}}$  is the  $\delta$  value at the evaporation front,  $f(z)$  is a depth function [Barnes and Allison, 1984], and  $\hat{z}_i$  is the decay length ( $L$ , the isotopic value at the evaporation front divided by  $e$ ) [Barnes and Allison, 1983]. The decay length ( $\hat{z}_i$ ) is calculated from this equation and is used to estimate the evaporation rate:

$$E = D_{l+v}^* / \hat{z}_i, \quad (\text{C3})$$

where  $D_{l+v}^*$  is the combined effective liquid and vapor diffusion coefficients ( $L^2\ T^{-1}$ ).

**Acknowledgments.** This research was funded by the Texas Low-Level Radioactive Waste Disposal Authority. Jinhua Liang assisted with data reduction. The author is grateful for the chemical analyses of rainwater conducted at Los Alamos National Laboratory by Laura Wolfsberg under the direction of June Fabryka-Martin. The author greatly appreciates helpful discussions with Jenny Chapman and Scott Tyler (Desert Research Institute), June Fabryka-Martin (Los Alamos National Laboratory), Glendon Gee (Pacific Northwest National Laboratory), Jim Jennings (Bureau of Economic Geology), Mitch Plummer and Fred Phillips (New Mexico Tech), and an anonymous reviewer. The author would like to acknowledge reviews by Peter Cook (CSIRO), June Fabryka-Martin (LANL), Fred Phillips (New Mexico Tech), and Eric Sonnenthal (Lawrence Berkeley National Laboratory), whose comments greatly improved the quality of the manuscript. Publication is authorized by the Director, Bureau of Economic Geology, University of Texas at Austin.

## References

- Allison, G. B., The relationship between  $^{18}\text{O}$  and deuterium in water in sand columns undergoing evaporation, *J. Hydrol.*, **55**, 163–169, 1982.
- Allison, G. B., and M. W. Hughes, The use of environmental chloride and tritium to estimate total recharge to an unconfined aquifer, *Aust. J. Soil Res.*, **16**, 181–195, 1978.
- Allison, G. B., G. W. Gee, and S. W. Tyler, Vadose zone techniques for estimating groundwater recharge in arid and semiarid regions, *Soil Sci. Soc. Am. J.*, **58**, 6–14, 1994.
- Barnes, C. J., and G. B. Allison, The distribution of deuterium and oxygen-18 in dry soils, I, Theory, *J. Hydrol.*, **60**, 141–156, 1983.
- Barnes, C. J., and G. B. Allison, Distribution of deuterium and oxygen-18 in dry soils, 3, Theory for nonisothermal water movement, *J. Hydrol.*, **74**, 119–135, 1984.
- Barnes, C. J., and G. B. Allison, Tracing of water movement in the unsaturated zone using stable isotopes of hydrogen and oxygen, *J. Hydrol.*, **100**, 143–176, 1988.
- Bentley, H. W., F. M. Phillips, and S. N. Davis,  $^{36}\text{Cl}$  in the terrestrial environment, in *Handbook of Environmental Isotope Geochemistry*, vol. 2b, edited by P. Fritz and J.-C. Fontes, pp. 422–475, Elsevier Sci., New York, 1986.
- Bevington, P. R., and D. K. Robinson, *Data Reduction and Error Analysis for the Physical Sciences*, 328 pp., McGraw-Hill, New York, 1992.
- Conca, J. L., and J. V. Wright, Diffusion and flow in gravel, soil, and whole rock, *Appl. Hydrogeol.*, **1**, 5–24, 1992.
- Cook, P. G., W. M. Edmunds, and C. B. Gaye, Estimating paleorecharge and paleoclimate from unsaturated zone profiles, *Water Resour. Res.*, **28**, 2721–2731, 1992.
- Davis, S. N., D. O. Whittemore, and J. Fabryka-Martin, Uses of chloride/bromide ratios in studies of potable water, *Ground Water*, **36**, 338–350, 1998.
- Elmore, D., B. R. Fulton, M. R. Clover, J. R. Marsden, H. E. Gove, H. Naylor, K. H. Purser, L. R. Kilius, R. P. Beukens, and A. E. Litherland, Analysis of  $^{36}\text{Cl}$  in environmental water samples using an electrostatic accelerator, *Nature*, **227**, 22–25, 1979.
- Elmore, D., N. J. Conard, P. W. Kubik, and J. Fabryka-Martin, Computer controlled isotope ratio measurements and data analysis, *Nucl. Instrum. Methods Phys. Res.*, **B5**, 233–237, 1984.
- Fabryka-Martin, J. T., Production of radionuclides in the Earth and their hydrogeologic significance, with emphasis on chlorine-36 and iodine-129, Ph.D. dissertation, 400 pp., Univ. of Ariz., Tucson, 1988.
- Fabryka-Martin, J. T., S. J. Wightman, W. J. Murphy, M. P. Wickham, M. W. Caffee, G. J. Nimz, J. R. Southon, and P. Sharma, Distribution of chlorine-36 in the unsaturated zone at Yucca Mountain: An indicator of fast transport paths, in *Focus '93: Site Characterization and Model Validation*, pp. 58–68, Am. Nucl. Soc., La Grange Park, Ill., 1993.
- Fabryka-Martin, J. T., A. V. Wolfsberg, S. S. Levy, J. L. Roach, S. T. Winters, L. E. Wolfsberg, D. Elmore, and P. Sharma, Distribution of fast hydrologic paths in the unsaturated zone at Yucca Mountain, in *Proceedings of the 8th Annual International High-Level Radioactive Waste Management Conference*, pp. 93–96, Am. Nucl. Soc., La Grange Park, Ill., 1998.
- Ginn, T. R., and E. M. Murphy, A transient flux model for convective infiltration: Forward and inverse solutions for chloride mass balance studies, *Water Resour. Res.*, **33**, 2065–2079, 1997.
- Guyodo, Y., and J.-P. Valet, Relative variations in geomagnetic intensity from sedimentary records: The past 200,000 years, *Earth Planet. Sci. Lett.*, **143**, 23–26, 1996.
- Hainsworth, L. J., A. C. Mignerey, G. R. Helz, P. Sharma, and P. W. Kubik, Modern chlorine-36 deposition in southern Maryland, U.S.A., *Nucl. Instrum. Methods Phys. Res.*, **B92**, 345–359, 1994.
- Holser, W. T., Mineralogy of evaporites, in *Marine Minerals*, vol. 6, edited by R. G. Burns, pp. 211–294, Mineral. Soc. of Am., Washington, D. C., 1979.
- Ingraham, N. L., and C. Shadel, A comparison of the toluene distillation and vacuum/heat methods for extracting soil water for stable isotopic analysis, *J. Hydrol.*, **140**, 371–387, 1992.
- International Atomic Energy Agency, Isotope techniques in the hydrogeological assessment of potential sites for the disposal of high-level radioactive wastes, *IAEA Tech. Rep. Ser.* 228, chap. 7, pp. 57–61, Vienna, 1983.
- Jackson, M. L. W., R. P. Langford, and M. J. Whitelaw, Basin-fill stratigraphy, quaternary history, and paleomagnetism of the Eagle Flat study area, southern Hudspeth County, Texas, 137 pp., final contract report, Bur. of Econ. Geol., Univ. of Tex. at Austin, 1993.
- Kemper, W. D., Solute diffusivity, in *Methods of Soil Analysis*, Part 2, *Chemical and Microbiological Methods*, *Agron. Monogr.*, vol. 9, edited by A. Klute, pp. 1007–1024, Am. Soc. of Agron., Madison, Wis., 1986.
- Knies, D. L.,  $^7\text{Be}$ ,  $^{10}\text{Be}$ , and  $^{36}\text{Cl}$  in Precipitation: Ph.D. dissertation, Purdue Univ., 114 pp., West Lafayette, Indiana, 1995.
- Lal, D., and B. Peters, Cosmic ray produced radioactivity on the Earth, in *Handbuch der Physik* 46/2, edited by S. Kitte, pp. 551–612, Springer-Verlag, New York, 1967.
- Langford, R. P., Landscape evolution of Eagle Flat and Red Light Draw Basins, Chihuahuan Desert, south-central Trans-Pecos Texas, final contract report prepared for the Texas Low-Level Radioactive Waste Disposal Authority, 153 pp., Bur. Econ. Geol., Univ. of Tex. at Austin, 1993.
- Larkin, T. J., and G. W. Bomar, *Climatic Atlas of Texas*, map LP-192, Tex. Dep. Water Resour., Austin, Tex., 1983.
- Liu, B., J. Fabryka-Martin, A. Wolfsberg, B. Robinson, and P. Sharma, Significance of apparent discrepancies in water ages derived from atmospheric radionuclides at Yucca Mountain, Nevada, in *Water Resources at Risk*, edited by W. R. Hotchkiss, J. S. Downey, E. D. Gutentag, and J. E. Moore, pp. NH52–NH62, Am. Inst. of Hydrol., Minneapolis, Minn., 1995.
- Mattick, J. L., T. A. Duval, and F. M. Phillips, Quantification of groundwater recharge rates in New Mexico using bomb  $^{36}\text{Cl}$ , bomb  $^3\text{H}$  and chloride as soil-water tracers, *Rep. 220*, 184 pp., N. M. Water Resour. Res. Inst., Las Cruces, 1987.



- Millington, R. J., and J. P. Quirk, Permeability of porous solids, *Trans. Faraday Soc.*, 57(7), 1200–1207, 1961.
- Murphy, E. M., T. R. Ginn, and J. L. Phillips, Geochemical estimates of recharge in the Pasco basin: Evaluation of the chloride mass balance technique, *Water Resour. Res.*, 32, 2853–2868, 1996.
- Nativ, R., E. Adar, O. Dahan, and M. Geyh, Water recharge and solute transport through the vadose zone of fractured chalk under desert conditions, *Water Resour. Res.*, 31, 253–261, 1995.
- Peck, A. J., C. D. Johnston, and D. R. Williamson, Analyses of solute distributions in deeply weathered soils, *Agric. Water Manage.*, 4, 83–102, 1981.
- Phillips, F. M., Environmental tracers for water movement in desert soils of the American southwest, *Soil Sci. Soc. Am. J.*, 58, 14–24, 1994.
- Phillips, F. M., Chlorine-36 in subsurface hydrology, in *Environmental Tracers in Subsurface Hydrology*, edited by P. G. Cook and A. L. Herczeg, Kluwer Acad., Norwell, Mass., 1999.
- Phillips, F. M., J. L. Mattick, and T. A. Duval, Chlorine-36 and tritium from nuclear weapons fallout as tracers for long-term liquid movement in desert soils, *Water Resour. Res.*, 24, 1877–1891, 1988.
- Phillips, F. M., D. B. Rogers, S. J. Dreiss, N. O. Jannik, and D. Elmore, Chlorine 36 in Great Basin waters: Revisited, *Water Resour. Res.*, 31, 3195–3204, 1995.
- Plummer, M. A., F. M. Phillips, J. Fabryka-Martin, H. J. Turin, P. E. Wigand, and P. Sharma, Chlorine-36 in fossil rat urine: An archive of cosmogenic nuclide deposition during the past 40,000 years, *Science*, 277, 538–541, 1997.
- Prudic, D. E., Estimates of percolation rates and ages of water in unsaturated sediments at two Mojave Desert sites, California-Nevada, *U.S. Geol. Surv. Water Resour. Invest. Rep.*, 94-4160, 19 pp., 1994.
- Reheis, M. C., and R. Kihl, Dust deposition in southern Nevada and California, 1984–1989: Relations to climate, source area, and source lithology, *J. Geophys. Res.*, 100, 8893–8918, 1995.
- Scanlon, B. R., Evaluation of liquid and vapor flow in desert soils based on chlorine-36 and tritium tracers and nonisothermal flow simulations, *Water Resour. Res.*, 28, 285–297, 1992.
- Scanlon, B. R., and R. S. Goldsmith, Field study of spatial variability in unsaturated flow beneath and adjacent to playas, *Water Resour. Res.*, 33, 2239–2252, 1997.
- Scanlon, B. R., R. S. Goldsmith, and J. P. Paine, Analysis of unsaturated flow beneath fissures in the Chihuahuan Desert, Texas, USA, *J. Hydrol.*, 203, 58–78, 1997a.
- Scanlon, B. R., S. W. Tyler, and P. J. Wierenga, Hydrologic issues in arid systems and implications for contaminant transport, *Rev. Geophys.*, 35(4), 461–490, 1997b.
- Scanlon, B. R., R. S. Goldsmith, and R. S. Langford, *Geomorphic Controls on Subsurface Flow in an Arid Setting: Case Study in the Chihuahuan Desert, Texas*, investigation report, Bur. of Econ. Geol., Univ. of Tex. at Austin, 1999a.
- Scanlon, B. R., R. P. Langford, and R. S. Goldsmith, Relationship between geomorphic settings and unsaturated flow in an arid setting, *Water Resour. Res.*, 35, 983–999, 1999b.
- Slavich, P. G., and G. H. Petterson, Anion exclusion effects on estimates of soil chloride and deep percolation, *Aust. J. Soil Res.*, 31, 455–463, 1993.
- Taylor, J. R., *An Introduction to Error Analysis, The Studies of Uncertainties in Physical Measurements*, 270 pp., Oxford Univ. Press, New York, 1982.
- Tyler, S. W., J. B. Chapman, S. H. Conrad, D. P. Hammermeister, D. O. Blout, J. J. Miller, M. J. Sully, and J. M. Ginanni, Soil-water flux in the southern Great Basin, United States: Temporal and spatial variations over the last 120,000 years, *Water Resour. Res.*, 32, 1481–1499, 1996.
- Wood, W. W., and W. E. Sanford, Chemical and isotopic methods for quantifying ground-water recharge in a regional, semiarid environment, *Ground Water*, 33, 458–468, 1995a.
- Wood, W. W., and W. E. Sanford, Eolian transport, saline lake basins, and groundwater solutes, *Water Resour. Res.*, 31, 3121–3129, 1995b.
- Yang, I. C., G. W. Rattray, and P. Yu, Interpretations of chemical and isotopic data from boreholes in the unsaturated zone at Yucca Mountain, Nevada, in *U.S. Geol. Surv. Water Resour. Invest. Rep.*, WRIR 96-4058, 1996.

B. Scanlon, Bureau of Economic Geology, University of Texas at Austin, J. J. Pickle Research Campus, Building 130, 10100 Burnet Road, Austin, TX 78713-8924. (Bridget.Scanlon@beg.utexas.edu)

(Received January 13, 1999; revised July 1, 1999; accepted July 27, 1999.)